UNIVERSITY OF CALIFORNIA
RIVERSIDE

Site-Targeting Nanotherapeutic for Suppression of Vascular Inflammation

A Dissertation submitted in partial satisfaction
of the requirements for the degree of

Doctor of Philosophy

in

Bioengineering

by

Soroush Ardekani

March 2016

Dissertation Committee:
Dr. Kaustabh Ghosh, Chairperson
Dr. Prue Talbot
Dr. Declan McCole

The Dissertation of Soroush Ardekani is approved:

_____

_____

_____

Committee Chairperson

University of California, Riverside

ACKNOWLEDGEMENTS

I would like to express the deepest appreciation to my committee chairperson, Professor Kaustabh Ghosh, whom served as my Ph.D. advisor and importantly, as a mentor and role model since the beginning of my graduate studies. He has truly molded me into the independent researcher I have become today. I would also like to thank my committee members, Professor Declan McCole and Professor Prue Talbot for their guidance and constructive criticism throughout my graduate career.

Further, I would like to acknowledge the invaluable contributions of my research findings detailed in this dissertation to my long-time lab colleagues and close friends: Dr. Harry Scott, Dr. Xiao Yang, Shane Eum, and the support from the Department of Bioengineering.

Finally, I would like to acknowledge that Chapter 2 has been previously published in the journal *Scientific Reports.*

DEDICATION

This dissertation is dedicated to my mother and uncle whose continuous love and support made me the person I am today and all of this possible.

ABSTRACT OF THE DISSERTATION

Site-Targeting Nanotherapeutic for Suppression of Chronic Vascular Inflammation

by

Soroush Ardekani

Doctor of Philosophy, Graduate Program in Bioengineering
University of California, Riverside, March 2016
Dr. Kaustabh Ghosh, Chairperson

The goal of this research was to develop a site-targeting nanotherapeutic drug delivery platform for suppression of chronic vascular inflammation and regression associated with debilitating conditions such as pulmonary arterial hypertension (PAH) and diabetic retinopathy (DR). Importantly, loss of endothelium-derived nitric oxide (NO), an endogenous anti-inflammatory and pro-vasculogenic factor that prevents leukocyte-endothelial cell (EC) adhesion and capillary regression, is strongly implicated in chronic inflammation associated with these conditions. Thus, restoring NO levels represents a viable approach for anti-inflammatory therapies. Nitroglycerin (NTG) markedly enhances nitric oxide (NO) bioavailability. However, its ability to mimic the anti-inflammatory and pro-vasculogenic properties of NO remains unknown. Here, the overarching goal was to examine whether (1) NTG can suppress vascular inflammation and regression, (2) a nanotechnological drug delivery approach can be leveraged to

simultaneously amplify its anti-inflammatory effects and ameliorate adverse effects associated with conventional high-dose NTG administration, and finally (3) NTG nanoformulation can be modified to selectively deliver NTG to inflamed ICAM-1-expressing vessels. My findings reveal that NTG significantly inhibits monocyte adhesion to inflamed ECs and prevents EC capillary regression *in vitro* through an increase in endothelial NO and decrease in endothelial ICAM-1 clustering. More importantly, nanoliposomal NTG (NTG-NL) produced an approximately 70-fold increase in NTG drug efficacy when compared with free NTG while preventing excessive mitochondrial superoxide production and loss of arterial vasorelaxation associated with high NTG doses. Finally, to facilitate targeting of NTG-NL to inflamed ICAM-1-expressing vessels, whole ICAM-1 IgG and non-immunogenic anti-ICAM-1 scFv fragment were tethered to the surface of NTG-NL. As a proof-of-concept study whole ICAM-1 IgG-modified NLs demonstrated preferential targeting to inflamed vessel, *in vivo*. Importantly, however, the translational potential of these NLs lies with the non-immunogenic scFv fragment. The following *in vitro* studies reveal that NTG-NL modified with anti-ICAM-1 scFv exhibits 6-fold greater binding to inflamed (ICAM-1-expressing) ECs than to normal ECs and achieves superior anti-inflammatory effects. Thus, these findings provide the rationale to examine this novel site-targeting NTG nanotherapeutic as a potentially superior therapy for various vascular inflammation-mediated conditions. Addressing these critical issues related to potential NTG-based therapy forms the central theme of the following dissertation.

Table of Contents

List of Figures

List of Tables

List of Schematics

List of Abbreviations

ANG-2	Angiopoietin 2
CAM	Cell adhesion molecules
DR	Diabetic retinopathy
DLS	Dynamic Light Scattering
EC	Endothelial cell
eNOS	Endothelial nitric oxide synthase
HG	High glucose
ICAM-1	Intercellular cell adhesion molecule 1
IL-1	Interleukin 1
iNO	Inhaled Nitric Oxide
mtALDH-2	Mitochondrial Aldehyde Dehydrogenase-2
Nf-kB	Nuclear factor kappa B
NP	Nanoparticle
NL	Nanoliposome
NO	Nitric oxide
NTG	Nitroglycerin
NTG-NL	Nanoliposomal Nitroglycerin
PAH	Pulmonary Arterial Hypertension
SMC	Smooth Muscle Cell
TNF-α	Tumor necrosis factor-α
VEGF	Vascular endothelial growth factor

Chapter 1:

Introduction

Preface

This Chapter discusses the role of nitric oxide (NO) in vascular inflammation-mediated conditions and advocates the use of NO-enhancing therapies for treatment of these conditions. The global aim of this doctoral research is to develop and characterize a site-targeting Nitroglycerin (NTG) nanotherapeutic system to enhance NO bioavailability and suppress chronic vascular inflammation and regression associated with intractable conditions such as pulmonary arterial hypertension (PAH) and diabetic retinopathy (DR).

The Role of Nitric Oxide in Chronic Vascular Inflammation

Under physiological conditions, vascular inflammation involves the rapid recruitment of circulating leukocytes (i.e. neutrophils, lymphocytes, and monocytes) to the site of tissue defect where leukocytes bind to the activated endothelium via surface cell adhesion molecules (CAMs) and extravasate to the site of injury. Once arriving at the site of injury/defect these cells either kill invading pathogens or clean up debris thereby resolving inflammation. However, if this process persists, chronic buildup of inflammatory cells and pro-inflammatory cytokines released by these cells (i.e. tumor necrosis factor-α (TNF-α) and interleukin-1 (IL-1)) create a toxic microenvironment for surrounding tissue causing cell death.[1] Importantly, chronic vascular inflammation is a key characteristic of many debilitating diseases.

The above-mentioned release of pro-inflammatory cytokines leads to the activation of transcription factors activating protein 1 (AP1), and nuclear factor kappa beta (NF-κB), the master inflammatory switch during endothelial cell activation. Specifically, when inactive, NF-κB is located in the EC cytoplasm bound to inhibitory protein IκBα. However, once activated (via TNF-α/IL-1 receptor-mediated stimulation), phosphorylation of IκBα by IκB kinase results in disassociation of IκBα from NF-κB allowing it to translocate into the nucleus and begin protein synthesis.[1] Importantly, NF-κB leads to expression of pro-inflammatory proteins known as endothelial CAMs including E-selectin, vascular cell-adhesion molecule 1 (VCAM-1), and to a large extent, the intracellular cell adhesion molecule 1 (ICAM-1), which are responsible for leukocyte binding to the endothelium.

Importantly, this rate-limiting step during vascular inflammation is suppressed by nitric oxide (NO), a potent anti-inflammatory and pro-vasculogenic molecule. NO is produced predominantly by endothelial nitric oxide synthase (eNOS), which converts L-arginine to L-citrulline and releases NO as a byproduct.[1,2] Once produced, NO suppresses vascular inflammation by inhibiting nuclear translocation of NF-κB,[3] that in turn, inhibits downstream production of endothelial CAMs (i.e. ICAM-1) and leukocyte binding to the endothelium.

Chronic Vascular Inflammation in Disease

Pulmonary Arterial Hypertension (PAH)

Pulmonary arterial hypertension (PAH) is a progressive condition that is clinically diagnosed by an elevation in mean pulmonary arterial pressure above 25 mm Hg at rest[4] with risk factors including genetic predisposition, drug use, tobacco smoke, and HIV infection.[5,6] PAH is characterized by (i) extensive vascular inflammation (upregulation of endothelial ICAM-1),[4] (ii) capillary degeneration,[7] and (iii) constriction of lung arteries, resulting in a significant increase in pulmonary arterial pressure and increased cardiac workload. Over time, the elevated pulmonary arterial pressure leads to right ventricular hypertrophy and, eventually, cardiac failure and death. With mean survival at time of diagnosis ranging from only three to seven years, PAH is responsible for approximately 16,000 deaths in the United States every year.[8] What makes this condition particularly serious is that it not only affects men and women, but also affects infants and children.[9]

Individuals with PAH are classified into distinct clinical groups based on the underlying etiology: group 1 (idiopathic/heritable/toxin-induced), group 2 (left heart disease), group 3 (lung diseases and/or hypoxia), group 4 (chronic thromboembolic disease), and group 5 (unclear multifactorial mechanisms).[10] The exact pathogenesis of PAH is very complex and yet to be fully understood. However, it is now widely accepted that all PAH groups share a common feature, extensive structural remodeling of pulmonary arteries leading to severe vascular constriction.[11] This arterial remodeling is characterized by (1) reduced endothelial NO bioavailability resulting from impaired eNOS activity, (2) excessive accumulation of circulating leukocytes within and around the arterial wall, and (3) excessive smooth muscle cell (SMC) proliferation and contractility within the arterial wall.

Importantly, impaired bioavailability of nitric oxide (NO), a potent anti-inflammatory and vasodilatory factor produced predominantly by endothelial NO synthase (eNOS), is strongly implicated in PAH[12] where previous studies have demonstrated eNOS knockout mice to develop PAH.[6] Since endogenous eNOS-derived NO suppresses both leukocyte accumulation (in part by inhibition of ICAM-1 expression/clustering) and SMC proliferation/contractility, impaired eNOS/NO levels are considered to be a major determinant of pulmonary arterial remodeling seen during PAH.[4] Further, these accumulating leukocytes secrete factors such as interleukin-1-β (IL-1-β), IL-6 and IL-8 that exacerbate SMC hypertrophy and recruit additional leukocytes, thereby initiating a self-sustained positive feedback loop that drives PAH progression.[13]

Diabetic Retinopathy (DR)

Diabetic retinopathy (DR) is a major microvascular complication of diabetes. It is prevalent in approximately 35% of people with diabetes and is the leading cause of blindness in the working-age (20-64 years old) population.[14] Growing evidence indicates that retinal microvascular inflammation and regression contributes significantly to DR pathogenesis.[15,16] During inflammation, activated retinal ECs undergo NF-kB-dependent upregulation of cell adhesion molecules (CAMs) such as ICAM-1 and reduced eNOS activation/expression levels.

Notably, DR pathogenesis has been shown to be accelerated in genetic knockout mice of endothelial nitric oxide synthase (eNOS), the primary enzyme that produces endothelial NO,[17] a potent vasodilatory and anti-apoptotic factor. Additionally, studies have demonstrated reduced eNOS phosphorylation levels in ECs under high glucose (diabetic) conditions. This, in turn, leads to increased leukocyte-EC adhesion (leukostasis) and subsequent release of cytotoxic, pro-inflammatory and permeability factors that, together, cause capillary degeneration (ischemia) and breakdown of blood-retinal barrier (vascular hyperpermeability; DME).[16,18]

Current Therapies and Limitations

PAH Therapies

Current treatments for PAH consist primarily of three classes of vasodilatory drugs: prostacyclin (Pgl_2) derivatives that facilitate cAMP production (required for vasodilation), endothelin-1 (E-1) receptor antagonists that block E-1, (a potent

vasoconstrictor molecule) from binding to its receptor (ER) on the smooth muscle cell (SMC) surface, and phosphodiesterase-5 (PDE-5) inhibitors that block PDE-5 from inactivating cGMP (another vasodilatory molecule).[4] These drugs primarily target the contractility machinery in arterial smooth muscle cells (SMCs), leading to SMC relaxation and widening of constricted lung vessels, thereby restoring normal blood flow and pressure. However, these systemically-administered PAH treatments have major limitations in that they fail to suppress pulmonary arterial inflammation and cause severe non-target side effects such as liver toxicity.[19] Other drugs such as Epoprostenol (Flolan®), a prostacyclin analog, require invasive medical procedures for their administration.[20]

Since NO is a potent vasodilatory factor that is markedly impaired in PAH, inhaled NO (iNO) offers an excellent alternative treatment for PAH. Importantly, this approach delivers NO selectively to the NO-deprived lung to cause rapid vasodilation, leading to reduction in mean pulmonary arterial pressure without altering systemic arterial pressure. It is commonly used in both infants with severe persistent pulmonary hypertension and adult PAH patients.[21] Due to its lung-targeted delivery, iNO is a more effective PAH therapy than systemically administered NO donors, which cause systemic hypotension. The high therapeutic efficacy of iNO also stems from its ability to leverage the dual vasodilatory *and* anti-inflammatory properties of NO.[22]

However, despite its excellent therapeutic benefits, iNO is very expensive, requires strict patient compliance and frequent administration, and combines with hemoglobin to form methemoglobin, which exhibits poor oxygen delivery properties.[4]

Thus, NO-enhancing strategies that address these major limitations of iNO would offer a superior alternative for PAH management.

DR Therapies

Current DR therapies primarily target vascular endothelial growth factor (VEGF), a potent angiogenic and permeability factor that is overexpressed in DR and contributes to multiplication of leaky retinal capillaries (proliferative DR) and diabetic macular edema (DME). Anti-VEGF therapies are very effective in treating proliferative DR.[23,24] However, recent RIDE/RISE and DRCR Protocol I clinical trials have revealed that anti-VEGF therapies are less effective in 50% of patients with DME,[25-27] thereby indicating a likely important role of VEGF-independent pathways in DR.

Notably, potent anti-inflammatory drugs such as corticosteroids are very effective in inhibiting ICAM-1-dependent diabetic retinal microvascular inflammation and improving visual acuity in individuals with DME.[28,29] However, bolus intraocular corticosteroid injection also leads to adverse side effects such as increased ocular pressure and cataract formation, which have limited their use to second-line therapy.[28] Thus, it is highly desirable, and perhaps crucial, to develop new therapeutic approaches that can leverage the tremendous anti-inflammatory properties of steroids without eliciting their adverse effects.

Since NO is a potent anti-inflammatory, anti-apoptotic, and pro-vasculogenic molecule, therapies that enchance endogenous (eNOS-derived) NO bioavailibility would likely address key characteristics associated with DR progression. Notably, corticosteroid

treatment has been shown to exert its anti-inflammatory effects, in part, through activation of eNOS and subsequent enhancement of NO.

Nitroglycerin (NTG) as a Potential Anti-inflammatory Therapy

Nitroglycerin (NTG), an FDA-approved organic nitrate for relieving chest pain (angina pectoris) resulting from acute vasoconstriction,[30] offers a potentially superior PAH and DR therapy because it enhances NO bioavailability through *both* activation/expression of eNOS and mitochondrial aldehyde dehydrogenase-2 (mtALDH-2)-mediated spontaneous biotransformation.[31,32] Since eNOS impairment is a key determinant of PAH and DR pathogenesis, eNOS activation by NTG will thus likely "regenerate" the failing pulmonary arterial endothelium, thereby reducing long-term dependence on drug intake. At the same time, NTG is expected to undergo spontaneous mtALDH-2 dependent metabolic conversion to rapidly release NO to initiate PAH/DR therapy. Importantly, previous studies have demonstrated iNO's anti-inflammatory properties.[33] In this context, coupled with studies that have shown NTG to mimic the anti-thrombotic effects and vasodilatory effects of endogenous NO,[34] it is reasonable to hypothesize the NTG will also mimic the anti-inflammatory and pro-vasculogenic properties of NO. Another advantage of using NTG is that it is already FDA-approved for NO-dependent vasodilation.

However, despite its potential anti-inflammatory properties, NTG presents a conundrum as long-term clinical use of current NTG formulations (e.g. transdermal patches, tablets) results in excessive mitochondrial superoxide generation that leads to a loss of NTG sensitivity (tolerance) and endothelial dysfunction (cross-tolerance),[31,35,36]

thereby limiting its therapeutic efficacy. Thus, new NTG formulations are required to fully leverage the anti-inflammatory potential of NTG.

Advantages of Nanotherapeutics

The application of nanotechnological principles in medicine (nanomedicine) has led to the development of nanomaterials (i.e. liposomal and polymeric) that can greatly improve drug delivery and therapeutic efficacy by simultaneously increasing drug half-life, reducing toxic off-target side-effects, and controlling drug release kinetics.[37] Such therapeutic nanomaterials have mostly been used in the field of cancer drug delivery where leaky tumor vessels permit passive targeting of nanoparticles to tumor tissue through the enhanced permeability and retention (EPR) effect[38]. The ability of such nanomaterials to treat diverse diseases will, however, depend on their ability to selectively target the tissue of interest.[37] Development of such site-targeting nanomaterials will likely create new therapeutic opportunities for the management of intractable diseases where systemic therapies often are limited by a high risk/benefit ratio.

Further, the development of site-targeting nanotherapeutics can further improve the efficacy of encapsulated drugs by simultaneously increasing drug half-life, localizing drug delivery to sites of inflammation, and reducing undesirable off-target effects. As others have previously shown,[39,40] such site-targeting can be accomplished by tethering unique site-targeting moieties (peptides, aptamers, antibodies, and antibody fragments)[37,39] on the nanoparticle surface that can guide the nanotherapeutic selectively

to sites of vascular inflammation and facilitate local drug delivery and therapeutic effect.[41,42]

Proposed Nanotherapeutic Approach

To address the limitations associated with high clinical doses of NTG, the field of nanomedicine will be leveraged to develop and evaluate a novel ICAM-1-targeting nanotherapeutic platform. Notably, once injected into the blood stream, this nanotherapeutic will efficiently and selectively deliver NTG to inflamed vessels to achieve local anti-inflammatory and pro-vasculogenic effects without causing adverse off-target effects. Thus, taken together, the proposed therapy implicates nanoparticles as an effective NTG delivery system that has the potential to address the major issue of tolerance associated with current NTG therapy.

Chapter 2:

Nanoliposomal Nitroglycerin Exhibits Potent Anti-inflammatory Effects

Preface

Nitroglycerin (NTG) markedly enhances nitric oxide (NO) bioavailability. However, its ability to mimic the anti-inflammatory properties of NO remains unknown. This Chapter examines whether NTG can suppress vascular inflammation and whether its nanoliposomal formulation (NTG) can simultaneously amplify its anti-inflammatory effects and ameliorate adverse effects associated with high-dose NTG administration.

This Chapter has been reproduced from ***Ardekani S**. et al. *Scientific Reports*. 2015, 5, 16258. with permission from Nature Publishing Company.

*Adapted from manuscript: Figures 2.1-2.11 and Tables: 2.1-2.2

Introduction

Loss of endothelium-derived nitric oxide (NO), which prevents leukocyte-endothelial cell (EC) adhesion, is strongly implicated in chronic inflammation associated with debilitating cardiovascular conditions such as pulmonary arterial hypertension (PAH),[43] atherosclerosis,[44] and diabetes.[45] Administration of nitrates/nitrites, which rapidly produce NO, is thus being explored as anti-inflammatory therapy.[46,47] Since organic nitrates exert superior NO-dependent vasodilatory effects when compared with inorganic nitrates/nitrites,[48] they likely also exhibit more potent anti-inflammatory effects.

Of the clinically used organic nitrates, nitroglycerin (NTG) holds particular promise as an anti-inflammatory drug because, in addition to spontaneously producing NO via mitochondrial aldehyde dehydrogenase (ALDH-2),[49] it also activates endothelial NO synthase (eNOS),[32,50] the key NO-producing enzyme in ECs that is impaired in inflammatory cardiovascular conditions[45]. However, despite its potential anti-inflammatory properties, NTG presents a conundrum as long-term clinical use of current NTG formulations (e.g. transdermal patches, tablets) results in excessive mitochondrial superoxide generation that leads to a loss of NTG sensitivity (tolerance) and endothelial dysfunction (cross-tolerance),[31,35,36] thereby limiting its therapeutic efficacy. Thus, new NTG formulations are required to fully leverage the anti-inflammatory potential of NTG.

The field of nanomedicine has enabled the development of nanomaterials (liposomes and polymeric nanoparticles) that can greatly improve drug delivery and therapeutic efficacy by simultaneously increasing drug half-life, lowering effective drug

dose (IC_{50}), and reducing toxic side-effects.[37,51] For instance, our previous work has shown that encapsulation of genistein within polymeric nanoparticles improves its anti-inflammatory effect by over two orders of magnitude.[39] Thus, such a nanotherapeutic approach has the ability to amplify the potential anti-inflammatory effects of NTG as well as ameliorate the adverse effects associated with contemporary high-dose NTG administration.

Here, it was first demonstrated that NTG-derived NO effectively suppresses endothelial activation during inflammation. Further, development of a new nanoencapsulation approach for effective NTG delivery exhibited potent anti-inflammatory effects at a dose 70-fold lower than that of free NTG while preventing excessive mitochondrial superoxide production associated with high NTG doses.

Materials and Methods

Cell Culture. Human microvascular endothelial cells (HMEC-1) were purchased from the Center for Disease Control (CDC)[52] and cultured on gelatin-coated tissue culture-treated dishes in growth medium composed of MCDB-131 basal medium (VWR International, USA) supplemented with 10% FBS (Fisherbrand, USA), 2 mM L-Glutamine (Invitrogen, USA), 1x antimycotic/antibiotic mixture (Life Technologies, USA), 10 ng/ml huEGF (Millipore, USA) and 1 μg/ml Hydrocortisone (Sigma Aldrich, USA). Human U937 monocytic cells were purchased from ATCC (Manassas, VA, USA) and cultured in suspension in growth medium composed of RPMI 1640 (Fisherbrand, USA) supplemented with 2 mM L-Glutamine (Invitrogen), 10 mM HEPES (Fisherbrand,

USA), 10% FBS (Fisherbrand), antimycotic/antibiotic mixture (Life Technologies, USA), 1 mM sodium pyruvate (Life Technologies, USA) and 4.5 mg/ml glucose (Sigma Aldrich, USA).

Nanoparticle (NP) Formulation. To synthesize NTG-loaded polymeric nanoparticles (NP), block co-polymer PLGA (17 kDa)-PEG-COOH (3.4 kDa) (75:25), Advanced Polymer Materials Inc., QC, Canada) was dissolved in DMSO (Sigma Aldrich, USA) at a final concentration of 1 mg/ml[39], followed by addition of NTG at 10% w/w. NPs were obtained by dialysis using Spectra/Pore 6 dialysis membrane (1 kDa MWCO; VWR, USA) where the NTG-polymer solution was dialyzed against distilled water (5 L) at room temperature, which also removed excess NTG. To synthesize NTG-loaded nanoliposomes (NTG-NL), four lipid molecules viz. 1,2-di-(3,7,11,15-tetramethylhexadecanoyl)-sn-glycero-3-phosphocholine (DPhPC; Avanti Lipids, USA), 1-hexadecanoyl-2-(9Z-octadecenoyl)-sn-glycero-3-phosphocholine (POPC; Avanti Lipids, USA), Cholesterol (Sigma Aldrich, USA), and 1,2-dihexadecanoyl-sn-glycero-3-phosphoethanolamine-triethylammonium salt (Texas Red-DHPE; Invitrogen, USA) were dissolved in chloroform at a molar ratio of 6:2:2:0.2, respectively, and purged with Nitrogen (N_2) to evaporate the chloroform. The resulting lipid cake was placed under vacuum for at least two hours prior to rehydration in aqueous NTG (5, 10 and 25% w/w of total lipid; Cerilliant, USA) or Fluorescein (1 mM; Sigma Aldrich, USA) solution to obtain a final 1 mg/ml drug- or dye-loaded liposome suspension. To obtain NTG-NLs, these liposome suspensions underwent five freeze-thaw cycles in liquid N_2 followed by

eight extrusion cycles through a 100 nm polycarbonate membrane filter (Avanti Lipids, USA). Unincorporated NTG or fluorescein was discarded by spinning down NTG-NLs for two hours at 60,000 relative centrifugal force (rcf) using a refrigerated ultracentrifuge (Beckman Coulter, USA) and decanting the supernatant. The final NTG-NL pellet was suspended at 1 mg/ml in water and stored at 4^{o}C until use.

NTG Incorporation Efficiency. To determine NTG incorporation efficiency within polymeric NPs and NTG-NLs, pellets of polymeric NP (1 mg) or NTG-NL (200 μg) were dissolved in 100% methanol and analyzed using electron spray ionization-mass spectroscopy (ESI-MS; Agilent Technologies). NTG (MW 227.1 Da) was ionized by trifluoroacetic acid (MW: 112.9 Da) and the signature NTG mass/charge spectrum peak was detected at 339.9 mass/charge (m/z; charge z=1 coulomb). Area under the NTG peak was measured for both the initial and incorporated NTG and their ratio was calculated to determine % NTG incorporation efficiency.

Nanoliposome Size and Morphology Characterization: Blank NL and NTG-NL suspensions were prepared at 0.5 mg/ml in distilled water and size distribution was measured by dynamic light scattering (DLS) using a Delsa Nano C Particle Analyzer (Beckman Coulter, USA). Microsoft Excel and Origin Pro software were used to acquire and analyze the data. NL morphology was analyzed using scanning electron microscopy (SEM; FEI NNS450) operated in high vacuum mode. For SEM samples, NLs were fixed in 2.5% glutaraldehyde (Electron Microscopy Sciences, USA) for 2 hr at 4^{o}C. After

fixation, 10 μL of NLs were added to Poly-L-Lysine (Sigma-Aldrich, USA)-coated 12 mm glass coverslips, allowed to settle for 5 minutes, and subjected to critical-point drying in liquid CO_2 (Critical-point-dryer Balzers CPD0202). Samples were then sputter-coated with chromium for 30 sec and analyzed using the SEM instrument described above.

Nanoliposome (NL) Uptake. To determine the percent (%) of NL uptake by ECs, Texas Red®-labeled NLs were diluted in EC culture medium at 5 μg/ml and added to ECs for 5, 15, 30 or 60 min at 37°C. To quantify the extent of NL uptake at different doses, Texas Red®-labeled NLs at 5, 10, 50 or 100 μg/ml were added to EC monolayer for 30 min at 37°C. After treatment, non-internalized NLs were removed by rinsing ECs twice with PBS, following by culturing ECs in phenol-red free MEM media (Life Technologies, USA) supplemented with 2 mM L-Glutamine and 10% FBS and measurement of fluorescence intensity by Wallac 1420 Victor2 fluorescent microplate plate reader (Perkin Elmer, USA). To determine % NL uptake, fluorescence intensity of NL-treated ECs was normalized with respect to the intensity obtained from unrinsed samples. Further, to determine whether NTG-NLs were successfully endocytosed, ECs treated with fluorescein-incorporated NLs were stained with LysoTracker® Deep Red (Invitrogen, USA) to label acidic organelles (lysosomes and endosomes).

Monocyte-EC Adhesion Assay. To examine the effects of NTG on monocyte-EC adhesion, confluent EC monolayers were either serum-starved (MCDB-131, 2.5% FBS,

and 1X antibiotic/antimycotic supplement) overnight and treated with 10 ng/ml TNF-α (eBiosciences, USA) for 4 hr or treated with 5 mM L-NIO (N^5 - (1- iminoethyl)- L-ornithine; selective eNOS inhibitor; Cayman Chemical, MI, USA) ± varying doses of NTG (0, 0.07, 0.2, 1 or 5 μM; Cambridge Isotope, MA) overnight in regular medium, followed by addition of fluorescently-labeled U937 monocytic cells at a density of 130,000 cells/cm^2. To confirm that NTG-NLs can be readily uptaken by ECs and processed to release NO, some EC cultures were also treated with L-NIO ± NTG-NL for 4 hr prior to addition of fluorescently-labeled U937 cells. After 30 min of U937 cell -EC interaction at 37^{o}C, the EC monolayers were gently rinsed twice with PBS (to remove unbound U937s) prior to fixation in 1% paraformaldehyde (PFA; Electron Microscopy Sciences, USA). Fluorescent images (10 per condition) of labeled U937 cells were then acquired using a Nikon Eclipse Ti microscope (Nikon, Japan) fitted with a Nikon Digital Sight DS-Qi1Mc camera and the number of adherent U937s was counted using ImageJ software (NIH). For experiments involving NLs, ECs were incubated with 5 μg/ml of blank or 10% (w/w) NTG-loaded nanoparticles (NTG-NL) for 30 minutes at 37^{o}C, rinsed with PBS to remove excess NLs, and cultured overnight prior to addition of fluorescently-labeled U937 cells (as described above).

Determination of NTG-NL's therapeutic efficacy: The therapeutic efficacy of NTG-NL was determined by taking the ratio of the net *free* NTG dose required to exert significant anti-inflammatory effect with the net NTG dose needed to exert the same effect when delivered within NL. Significant anti-inflammatory effect was achieved at a

free NTG dose of 5 μM (1.136 μg/ml), which results in a net NTG dose of 0.284 μg per 250 μL of EC culture medium. In comparison, considering a 10% (w/w) initial NTG loading, 36.4% NTG incorporation efficiency within NLs, and a 9% intracellular uptake (greatest % uptake compared with other doses; Table 2.1), NTG-NLs exhibit similar anti-inflammatory effect at a dose of 5 μg/ml (0.182 μg/ml of NTG), which results in a net intracellular NTG dose of 0.004 μg per 250 μL of EC culture medium. The ratio of net *free* NTG dose (0.284 μg) to net NTG dose delivered via *NLs* (0.004 μg) was used to determine the fold-increase in NTG efficacy achieved with NTG-NLs.

Measurement of endothelial cell (EC)-derived NO. Two independent methods were used to measure the amount of NO produced by ECs. In the first method, ECs were treated overnight with L-NIO (5 mM) ± NTG (5 μM) or NTG-NL (10 μg/ml), followed by incubation with a NO-sensitive fluorescent dye DAF-FM diacetate (2 μM; Life Technologies, USA) for 20 minutes at 37^0C. Following dye loading, ECs were again treated with L-NIO and NTG during a recovery phase for an additional 1 hr in regular growth medium. EC culture media was then rinsed once with Krebs-Henseleit Buffer (KHB) containing 125 mM NaCl, 4.74 mM KCl, 2.5 mM $CaCl_2$, 1.2 mM KH_2PO_4 1.2 mM $MgSO_4$, 5 mM $NaHCO_3$ and 10 mM Glucose (Sigma Aldrich, USA), replaced with fresh KHB and immediately subjected to live cell fluorescence imaging using Nikon Eclipse Ti microscope. At least 30 cells per condition were analyzed for total cell fluorescence using ImageJ software (NIH). For the second method, a Nitric Oxide Analyzer (NOA; Sievers, USA) was used to measure EC-secreted NO in culture medium.

For this measurement, confluent ECs were treated overnight with either L-NIO (5 mM) ± NTG (5 μM) or NTG alone, followed by sequential 1 hr incubations with KHB without and with L-NIO ± NTG at 37^{o}C. KHB conditioned medium (4 replicates per condition) was then collected and analyzed using NOA.

Phosphorylated eNOS Western Blot. ECs were allowed to reach confluence, and treated overnight with 1 mM L-NIO and 5 μM NTG. These cells were then lysed with RIPA buffer containing protease and phosphatase inhibitors and protein supernatant was obtained by centrifugation at 4°C for 20 minutes. The protein samples were ran in 7.5% SDS-polyacrylamide gel with GAPDH as the loading control. Phosphorylated eNOS was stained using primary mouse anti-phospho-eNOS Ser1179 antibody (BD Biosciences) and FITC-conjugated DyLight anti-mouse IgG secondary antibody (Vector Labs). Protein bands were imaged using Biospectrum AC Imaging System (ultraviolet Products) and densitometric analysis was performed using ImageJ software (NIH).

ICAM-1 Clustering. ECs were grown to confluence on glass coverslips under normal growth conditions and treated with L-NIO (5 mM) ± [NTG (5 μM) or NTG-NL (5 μg/ml)] for 24 hr. Next, a monocyte adhesion assay was performed (as described earlier) and the U937 cell-EC cocultures were fixed, permeabilized with 0.1% Triton X-100, blocked with 2% bovine serum albumin (BSA; Millipore, USA), and sequentially incubated with primary anti-ICAM-1 mouse antibody (Santa Cruz Biotechnology, USA) and secondary FITC-conjugated DyLight 488 anti-mouse IgG (Vector Labs, USA). To

visualize actin microfilaments, U937 cell -EC cocultures were incubated with Alexa Fluor 594-Phalloidin (BD Biosciences, USA). Coverslips were mounted onto glass slides and fluorescence images (15 per condition) were taken using a Nikon Eclipse Ti microscope fitted with a Nikon Digital Sight DS-Qi1Mc camera. ICAM-1 clustering index was determined by measuring ICAM-1 fluorescence intensity (from $n \geq 20$ U937 cells) at the U937-EC adhesion site and normalizing it to the average 'background' intensity measured from three neighboring EC cytoplasmic sites.

ICAM-1 Expression by Flow cytometry. ECs were grown to confluence under normal growth conditions and treated with L-NIO (5 mM) ± NTG (5 μM) overnight. ECs were then detached and sequentially labeled with primary anti-ICAM-1 antibody (Santa Cruz Biotechnology, USA) for 20 min, followed by FITC-conjugated DyLight 488 anti-mouse IgG (Vector labs. USA). Next, ECs were fixed with 1% PFA, detected by a Cell Lab Quanta SC flow cytometer (Beckman Coulter, CA), and analyzed by FlowJo software (Treestar Inc, CA).

Detection of Endothelial Mitochondrial Superoxide Production. ECs were plated at sub-confluence on gelatin-coated MatTek dishes under normal culture conditions and subjected to overnight treatment with either L-NIO (3 mM) ± [NTG (5, 25, or 100 μM) or NTG-NL (5, 50 or 100 μg/ml)]. To detect mitochondrial superoxide, ECs were labeled with MitoSOX™ (Life Technologies, USA), a mitochondrial superoxide-sensitive fluorescent dye that is widely used to measure mitochondrial ROS production under

various conditions, including NTG treatment [53]. ECs were labeled with MitoSOX™ Red at a final dose of 5 μM in KHB for 10 min at 37°C, rinsed three times with KHB to remove excess dye and placed at 37°C in KHB for an additional 10 min prior to live cell imaging. Fluorescence images (six per condition) were acquired using Nikon Eclipse Ti microscope and total cell fluorescence intensity from at least 20 cells was analyzed using ImageJ software.

Pulmonary Artery Ring Preparation and Isometric Tension Measurements. All animal procedures were in accordance with the Animal Welfare Act, the Guiding Principles in the Care and Use of Animals approved by the Council of the American Physiological Society, the National Institutes of Health Guide for the Care and Use of Laboratory Animals, and Loma Linda University Institutional Animal Care and Use Committee (IACUC). Pregnant ewes were anesthetized with ketamine (10 mg/kg, IV) and midazolam (5 mg/kg, IV) and anesthesia maintained with inhalation of 1-3% isoflurane in O_2 throughout surgery as required. Ewes and Fetuses were euthanized with an overdose of Euthasol (pentobarbital sodium, 100 mg/kg) and phenytoin sodium (10 mg/kg; Virbac, Ft. Worth, TX).

To assess arterial vasorelaxation in response to NTG treatment, pulmonary arteries (4^{th}-5^{th} order) were harvested from newborn fetal sheep (gestational period between 138-141 days) obtained from Loma Linda University Animal Care Facility, dissected free of parenchyma and cut into 5 mm long rings (at least 8 per condition) in ice-cold HEPES buffer (Sigma Aldrich, USA). Rings were then preincubated in L-NIO (1

mM) ± [NTG (5 or 100 μM) or NTG-NL (5 or 100 μg/ml)] for 4 hr at 37^0C; free NTG at 100 μM has previously been reported to induce NTG tolerance of isolated arterial rings within 4 hr[31]. Following treatment, rings were mounted onto tungsten wires under 0.5 g of resting tension in organ baths containing KHB, gassed with 95% O_2 - 5% CO_2, and maintained at 37^0C. Arterial rings were rinsed once with KHB, allowed to equilibrate for at least 30 minutes, and retensioned prior to addition of 125 mM KCl (Sigma Aldrich, USA) to ensure rings were still functional. Rings were rinsed three times to remove KCl, allowed to relax, and preconstricted with 10 μM Serotonin (Tocris Bioscience, USA) to achieve 100% contraction. Rings were then exposed to increasing concentrations of free NTG (1 nM to 100 μM) and subsequent recordings of concentration-response curves were acquired using a force displacement transducer (AD Instruments, New Zealand) and analyzed using Prism (Graphpad Software Inc).

Statistics. All data were obtained from multiple replicates (as described in the appropriate sections) and expressed as mean ± standard error of mean (SEM). Statistical significance was determined using analysis of variance (ANOVA; InStat; Graphpad Software Inc.) followed by a Tukey multiple comparison post-hoc analysis. Results demonstrating significance were represented as *$p<0.05$, **$p<0.01$, or ***$p<0.001$.

Results

NTG Exerts Anti-inflammatory Effects on Activated ECs

Since NTG enhances endothelial NO bioavailability through both spontaneous biotransformation and eNOS activation,[32,49] we asked whether NTG could mimic the anti-inflammatory property of NO. To address this question, EC monolayers were treated with L-NIO (5 mM), a selective eNOS inhibitor[8], or TNF-α (10 ng/ml), which downregulates eNOS mRNA,[54] to impair endogenous endothelial NO production and thereby enhance monocyte-EC adhesion both *in vitro* and in pathological conditions *in vivo.*[43,45] Images of fluorescently-labeled adherent U937 cells and their quantification revealed that addition of NTG to L-NIO-treated ECs produces a dose-dependent inhibition of U937 cell adhesion to ECs (Fig. 2.1A, B), with the inhibition being significant ($p<0.01$) at 5 μM NTG dose where U937 cell adhesion was comparable with that on untreated ECs. Notably, NTG exerted a similar dose-dependent anti-inflammatory effect on cells activated with TNF-α (Fig. 2.1C).

NTG Enhances Endothelial NO Production

The potent and hitherto-unknown anti-inflammatory effect of NTG expectedly resulted from an increase in endothelial NO production, as confirmed by two independent approaches. Measurement of released (extracellular) NO by nitric oxide analyzer (NOA) revealed that addition of NTG to L-NIO-treated ECs prevented the loss of NO by L-NIO (Fig. 2.2A). These findings were independently confirmed by measurement of intracellular NO using a fluorescent NO-sensitive DAF-FM diacetate dye where

quantification of fluorescence intensities revealed that NTG causes a significant (79%; $p<0.001$) recovery of NO (Fig. 2.2B), in part, by recovery of phosphorylated eNOS expression levels (Fig. 2.2C).

NO is known to suppress leukocyte-EC adhesion by inhibiting the clustering and/or expression of endothelial cell adhesion molecules (CAMs).[3,55] Our flow cytometry measurement revealed that neither inhibition of NO (using L-NIO) nor its enhancement (using NTG) altered ICAM-1 expression (Fig. 2.3). However, quantitative analysis of fluorescent images of U937 cell-EC co-cultures labeled with anti-ICAM-1 antibody and phalloidin (which stains actin cytoskeleton) revealed that NTG prevents the significant increase (1.6-fold; $p<0.001$) in ICAM-1 clustering seen on NO-deficient (L-NIO-treated) ECs (Fig. 2.2D).

Synthesis and Physicochemical Characterization of Nanoliposomal NTG (NTG-NL)

Currently available NTG formulations that aim to treat severe vasoconstriction (angina pectoris) commonly yield a cumulative plasma NTG concentration of ~90 μM (20 mg/L).[56-58] Such high NTG doses result in excessive mitochondrial superoxide production that, in turn, leads to impaired NTG sensitivity (tolerance) and endothelial dysfunction.[31,35,36] Thus to successfully leverage the important therapeutic implications of the anti-inflammatory effects of NTG, we employed the principles of nanotechnology to incorporate NTG within nanoparticles (NPs) as they are known to significantly improve drug efficacy.[37,39] NPs were made either from an amphiphilic block copolymer poly(D,L-lactide-co-glycolide)-block-poly(ethylene glycol) (PLGA-b-PEG) or from a combination

of four lipids (DPhPC, POPC, Cholesterol, and DHPE-Texas Red). The two distinct building blocks were chosen because the NTG molecule contains both hydrophilic and hydrophobic residues (Fig. 2.4A). Thus, we reasoned that if NTG exhibits predominantly hydrophobic characteristics, it would preferentially incorporate within the hydrophobic PLGA core of the PLGA-b-PEG nanoparticle; if it exhibits greater hydrophilicity, it would incorporate within the hydrophilic core of the lipid nanoparticle (nanoliposomes; NL) (Fig. 2.4B).

Analysis of electrospray ionization-mass spectroscopy (ESI-MS) peaks revealed differences in NTG uptake into nanoliposomes (NLs) vs. polymeric NPs. While NLs demonstrated a dose-dependent increase in NTG loading (Fig. 2.4C and Table 2.1), polymeric NPs failed to incorporate NTG (Fig. 3D). These findings, which represent the first attempt to encapsulate NTG within a nanocarrier, identify NLs as the preferred vehicle for NTG packaging and delivery. Interestingly, although NTG incorporation within NLs understandably increased with increasing loading, the incorporation efficiency was highest (~37% of initial NTG added) at an intermediate NTG loading of 10% (w/w) (Table 2.1). Based on these findings, 10% (w/w) NTG-NL was chosen as the preferred nanoformulation for subsequent cell functional studies.

The size distribution profile of NLs, obtained using dynamic light scattering (DLS), revealed an average diameter of 157 ± 36 nm and 154 ± 33 nm for blank and NTG-NL, respectively (Fig. 2.4E), which was independently confirmed by scanning electron microscopy (Fig. 2.4F).

Cellular Uptake of Nanoliposomes

Following NL synthesis, we examined their uptake by cultured ECs. Fluorescein-loaded NLs (5 μg/ml) were added to ECs for 5, 15, 30, or 60 min prior to fixation and imaging. Quantification of intracellular fluorescence intensity measurements revealed that nanoliposomal uptake peaked at approximately 30 min, followed by a plateau between 30-60 min (Fig. 2.5A). These internalized NLs expectedly localized within the acidic endocytic organelles viz. lysosomes and endosomes that line the perinuclear region (Fig. 2.5B). Notably, although the amount of internalized NLs increased at higher NL doses, the percent internalization was highest (9%) at 5 μg/ml (Table 2.2). Based on these observations of nanoliposomal uptake, all subsequent *in vitro* cell functional studies were performed following 30 min treatment with a 5 μg/ml dose of NL.

NTG-NL Exerts Superior Anti-inflammatory Effects

For NTG-NL to be truly effective as an anti-inflammatory therapy, it is essential that blank NLs exert no inflammatory effects. To confirm this, we analyzed U937 cell adhesion to ECs treated with blank NLs. Quantification of adherent U937 cells revealed that U937 cell adhesion to blank NL-treated ECs is comparable to that seen on untreated ECs (Fig. 2.6A). Further, treatment of ECs with blank NLs failed to suppress L-NIO-induced increase in U937 cell-EC adhesion (Fig. 2.6A). These data clearly indicate that blank NLs are totally inert to ECs.

Nanoliposomes are known to enhance drug efficacy (i.e. reduce effective drug dose) by simultaneously increasing drug half-life and facilitating rapid cellular

uptake.[37,39,51] Thus, we asked whether the internalized NTG-NLs could improve the anti-inflammatory effect of incorporated NTG. Our studies indicate that addition of NTG-NL at 5 μg/ml to L-NIO-treated ECs produced a significant (52%; $p<0.001$) prevention of U937 cell adhesion to ECs, with the number of adherent U937s returning to the levels seen on untreated ECs (Fig. 2.6B). This reduction in U937 cell-EC adhesion by NTG-NL was comparable to the anti-inflammatory effect produced by a 5 μM (0.284 μg total) dose of free NTG. Determination of the total amount of NTG delivered intracellularly through nanoliposomal formulation revealed that NTG-NL produced its potent anti-inflammatory effect at an equivalent NTG dose of 0.07 μM (0.004 μg total), which is 70-fold less than the effective dose of free NTG (5 μM) (refer to Materials and Methods). In other words, NTG-NL was found to be 70-fold more effective than free NTG in suppressing endothelial activation. That this remarkable increase in therapeutic efficacy resulted primarily from nanoformulation of NTG was confirmed by the observation that an equivalent amount (0.07 μM) of free NTG failed to produce a significant anti-inflammatory effect (Fig. 2.6B). NTG-NLs stored at 4°C and 37°C for 24 hr exerted similar anti-inflammatory effects (Fig. 2.7), thereby confirming past findings that nanoliposomes act as stable drug carriers.[59] Moreover, similar to free NTG, the anti-inflammatory effects of NTG-NL correlated strongly with its ability to enhance endothelial NO production (Fig. 2.8A, B) and suppress ICAM-1 clustering (Fig. 2.8C).

NTG-NL Prevents Endothelial Superoxide Formation Associated with High NTG Dose

High plasma concentrations of NTG that result from the use of conventional NTG formulations (e.g. transdermal patches and tablets) are known to cause significant increase in mitochondrial superoxide formation that, in turn, leads to impaired NTG bioconversion to NO (tolerance) and endothelial dysfunction.[31,35,36] Consistent with these observations, treatment of ECs with a 100 μM dose of free NTG, which is comparable to the high doses used in NTG therapies, caused a 2-fold ($p<0.001$) increase in mitochondrial superoxide formation (Fig. 2.9A, B), as determined by quantitative analysis of cells labeled with MitoSOX™, a fluorescent mitochondrial superoxide-sensitive dye that is widely used to measure mitochondrial reactive oxygen specie (ROS) production in response to high-dose NTG treatment.[53] Notably, as shown in Fig. 2.10, this difference in MitoSOX™ fluorescence intensity is a true reflection of the differences in mitochondrial superoxide production and not an artifact resulting from varying cell density or spreading.

Since NTG-NL exhibited potent anti-inflammatory effects at a dose 70-fold lower than that of free NTG, we next asked whether a similar 20-fold increase in NTG-NL dose would ameliorate the adverse effects associated with high-dose NTG therapies. Indeed, we found that NTG-NL did not elicit any increase in mitochondrial superoxide production when used at the 20-fold higher dose of 100 μg/ml (Fig. 2.9A, B).

Consistent with the view that excessive mitochondrial superoxide production at high NTG doses inhibits ALDH-2 activity and, thus, NTG bioconversion to NO, we

observed a drastic loss (~2-fold decrease; $p<0.001$) in the anti-inflammatory effects of free NTG at 100 μM (Fig. 2.9C). In contrast, NTG-NL retained its potent immunosuppressive effects (84% inhibition; $p<0.001$) when used at a 20-fold higher dose of 100 μg/ml (Fig. 2.9D). We further confirmed NTG-NL's ability to prevent loss of NTG sensitivity at high doses using an *ex vivo* arterial vasorelaxation assay. This assay, which is widely used to evaluate NTG tolerance,[35,60] demonstrated that while arteries pretreated with 100 μM free NTG exhibited a significant loss of NTG sensitivity (IC_{50} increasing from 0.2 to 15 μM), those treated with NTG-NL at an equivalent 20-fold higher dose maintained their normal vasodilatory responsiveness (Fig. 2.11).

Discussion

This study demonstrates a proof-of-principle for a new nanoliposomal NTG formulation that amplifies the newly-identified anti-inflammatory properties of NTG while significantly ameliorating the adverse effects associated with high NTG doses. NTG is one of the most commonly used organic nitrates in the clinic where it is intended to mimic the vasodilatory effects of endothelium-derived NO.[56] When compared with inorganic nitrites/nitrates, NTG produces a significantly greater and rapid yield of NO,[48] which explains its superior vasodilatory properties. Since endothelial NO also exhibits potent anti-inflammatory effects, here we asked whether NTG can suppress leukocyte-EC adhesion.

Our findings reveal that NTG significantly inhibits U937 cell adhesion to NO-deficient ECs. This anti-inflammatory effect of NTG occurred in a dose-dependent

manner, with significance achieved at a dose of 5 μM. That a higher NTG dose is required to achieve significant anti-inflammatory effect than is required for vasodilation (IC_{50} = 0.2 μM) may be attributed to the fact that these different therapeutic effects of NTG involve different target cell types with potentially distinct NTG sensitivity. For instance, NTG exerts its anti-inflammatory effect on luminal ECs that undergo activation to promote monocyte adhesion[1] while its vasodilatory effects are targeted towards abluminal smooth muscle cells that exhibit excessive vasoconstriction.[43] Thus, it is plausible that smooth muscle cells are more sensitive to NTG than ECs, and thereby require lower doses to exhibit NTG-dependent vasodilation. It should, however, be noted the effective anti-inflammatory NTG dose of 5 μM still lies within the dose range (0.09-90 μM) that is widely used for current NTG therapies.[56-58]

Further, consistent with past findings that suppression of monocyte-EC adhesion by NO results from inhibition of endothelial CAM clustering,[55] NTG treatment produced significant inhibition of ICAM-1 clustering on EC surface. ICAM-1 is a key EC surface membrane protein (trafficked via membrane-bound endosomes) that facilitates leukocyte-EC adhesion by undergoing clustering, which results in the formation of an ICAM-1 binding pocket for firm leukocyte docking and adhesion.[61] Past studies have indicated that the ability of NO to inhibit ICAM-1 clustering likely results from suppression of Rho/ROCK-dependent actin cytoskeletal reorganization at the site of monocyte-EC adhesion.[62,63]

Although inorganic nitrites have been shown to exert anti-inflammatory effects,[46] to our knowledge, this is the first report indicating that NTG also exhibits similar

properties. Coupled with previous findings that (1) NTG activates eNOS,[32,50] the major NO-producing enzyme in ECs that is impaired in inflammatory conditions such as PAH[43] and diabetes,[45] and (2) NTG mimics the anti-coagulating properties of NO to prevent inflammation-associated hypercoagulopathy,[64] the current findings provide further rationale for investigating the use of NTG for anti-inflammatory therapies.

NTG undergoes rapid (within 15-30 min) clearance from bloodstream.[65] To address this issue, current NTG formulations are commonly administered at high doses (up to 90 μM).[56-58] It is, therefore, likely that similar high NTG doses may be necessary to achieve its potent anti-inflammatory effects. However, this approach poses a limitation in that such high NTG doses lead to excessive mitochondrial superoxide production, which greatly limit NTG's therapeutic efficacy.[31,35] Mitochondrial superoxide, a ROS that is formed as a byproduct during NTG bioconversion to NO, inhibits the activity of mitochondrial aldehyde dehydrogenase (ALDH-2),[31,35] the chief enzyme responsible for NTG bioconversion. Thus, excessive amounts of mitochondrial superoxide generated in response to high NTG doses significantly impairs ALDH-2 activity and, as a consequence, NTG bioconversion and sensitivity.[31] Indeed, our studies confirmed that raising the dose of free NTG from 5 μM to 100 μM led to a significant increase in mitochondrial superoxide production that, in turn, correlated with a significant loss in the anti-inflammatory effects of NTG.

To improve the benefit/risk profile of NTG therapy, we leveraged the principles of nanotechnology to develop a new nanoliposomal NTG formulation (NTG-NL) that undergoes rapid intracellular uptake via the conventional clathrin-mediated pathway[66]

and demonstrates a remarkable 70-fold increase in drug efficacy. Such a tremendous increase in drug efficacy is the hallmark of nanocarrier-mediated drug delivery, which is known to enhance drug half-life and promote rapid cellular uptake and bioavailability of encapsulated drugs.[37,39] Importantly, the significant enhancement in NTG-NL bioactivity and resultant lowering of the effective therapeutic dose meant that, unlike free NTG, NTG-NL did not elicit an increase in mitochondrial superoxide production even at very high (20-fold greater) dose. This observation is supported by findings that, in contrast to free NTG, NTG-NL treatment at a high dose did not exhibit any loss of anti-inflammatory effect *in vitro* or loss of vasorelaxation response in isolated pulmonary arteries. Taken together, these findings implicate NLs as an effective NTG delivery system that has the potential to amplify the newly-identified anti-inflammatory effects while addressing the adverse effects associated with high NTG doses.

Conclusions

The *in vitro* and *ex vivo* studies performed here are widely used to examine the effects of NTG on the vasculature.[31,53] However, to fully establish the translational potential of nanoliposomal NTG, the current proof-of-concept studies need to be validated in appropriate animal models of vascular inflammation. NTG-NL are expected to be biocompatible as the lipids used to synthesize these nanoliposomes are found in cell membranes.[67] This excellent biocompatibility is an important reason why liposomes are widely used as drug carriers in pharmaceutical industry.[37,67] Further, the size (~150 nm dia.) of NTG-NL is suitable to achieve a long circulation time.[37,68] Thus, the

proof-of-concept studies described here set the stage for the development of *site-targeting* NTG nanotherapeutics that can further improve the efficacy of nanoliposomal NTG by simultaneously increasing drug half-life, localizing drug delivery to sites of inflammation, and reducing undesirable off-target effects. As we and others have previously shown,[39,40] such site-targeting can be accomplished by tethering unique site-targeting moieties (peptides, aptamers or antibodies)[37,39] on the nanoparticle surface that can guide the nanotherapeutic selectively to desired vascular sites and facilitate local drug delivery and therapeutic effects. Thus, by simultaneously leveraging the newly-identified anti-inflammatory and well-known vasodilatory properties of NTG, such smart nanomedicine approaches may provide a superior therapeutic strategy for effective management of PAH that is characterized by both chronic pulmonary arterial inflammation and vasoconstriction[69].

Figures

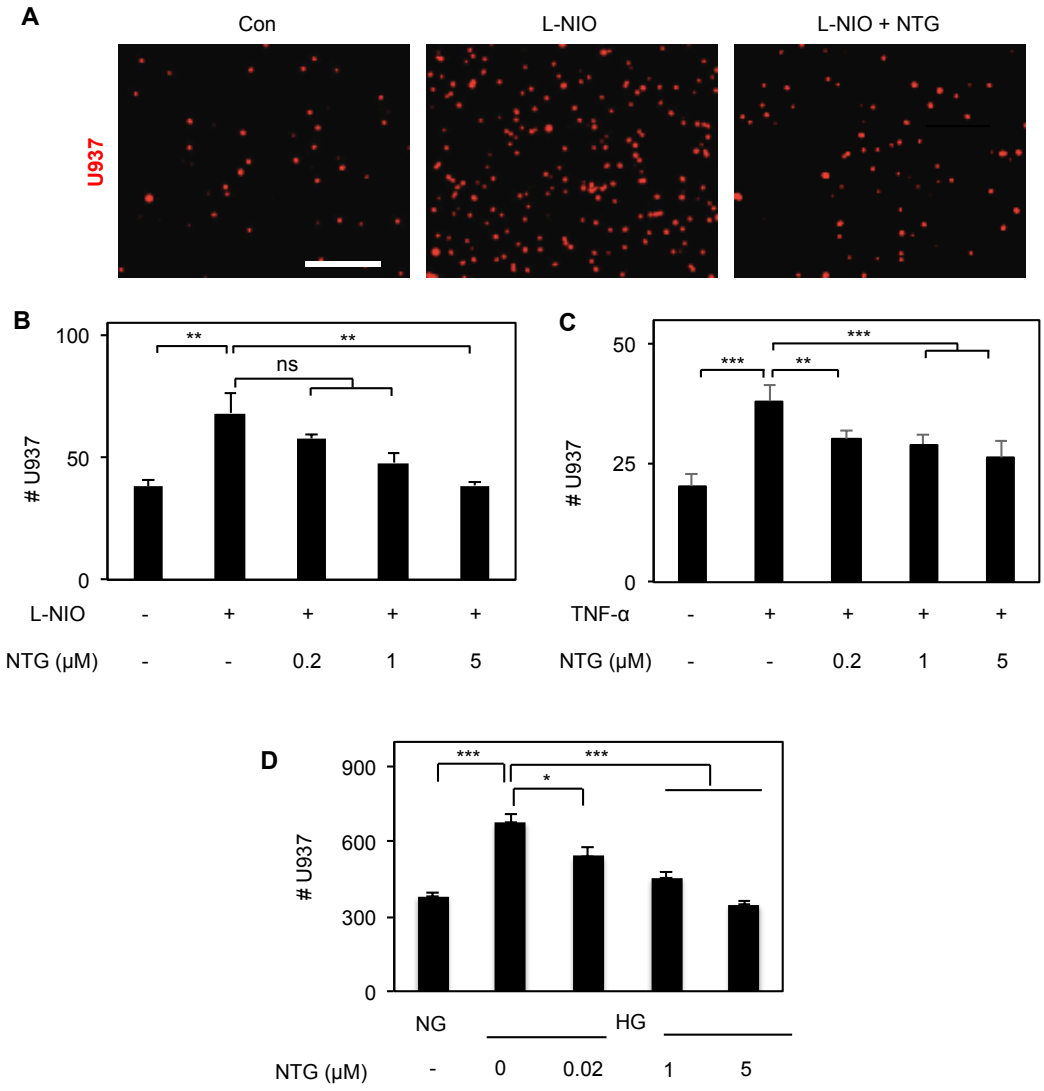
A
Con
L-NIO
L-NIO + NTG
U937
B
U937
100
50
0
**
**
ns
L-NIO - + + + +
NTG (μM) - - 0.2 1 5
C
U937
50
25
0
***
***
**
TNF-α - + + + +
NTG (μM) - - 0.2 1 5
D
U937
900
600
300
0
***
***
*
NG
HG
NTG (μM) - 0 0.02 1 5

Fig. 2.1. NTG Exerts Anti-inflammatory Effects on Activated ECs.

NTG produces dose-dependent inhibition of U937 monocytic cell adhesion to L-NIO-treated (5 mM; overnight) ECs, with significant inhibition observed at 5 μM NTG dose and not lower (0.2 μM and 1 μM doses), as shown in (**A**) the fluorescence images and (**B**) quantified in the bar graph (n = 10 fields of view). **, $p<0.01$; ns, no significance. **(C)** Similar anti-inflammatory effect of NTG was observed on TNFα-treated ECs and (D) ECs treated with high glucose (HG; 15 mM; Diabetic blood glucose levels)(n = 10 fields of view). **, $p<0.01$; ***, $p<0.001$. Data are expressed as mean ± SEM. Scale bar: 200 μm.

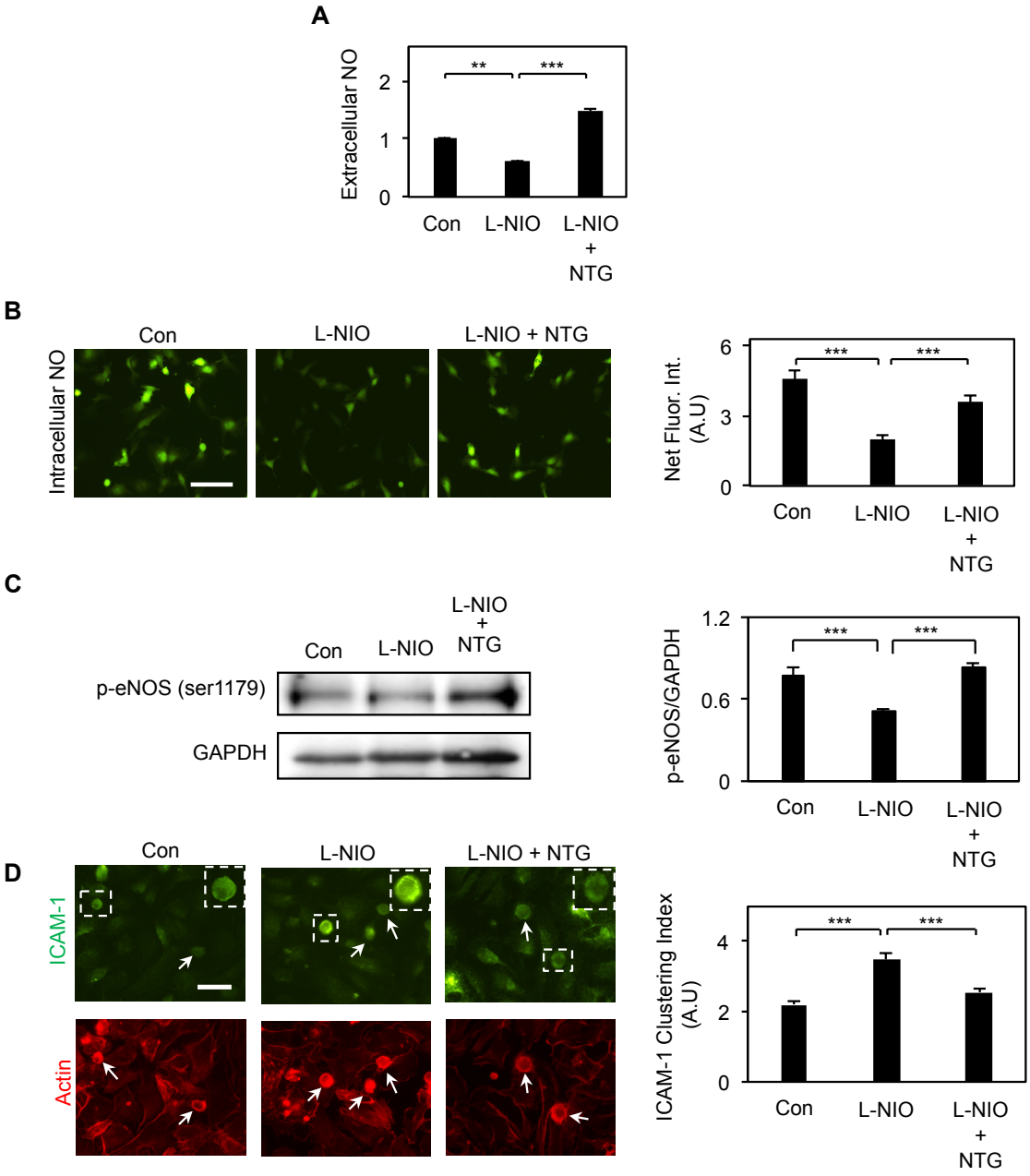
A
Extracellular NO
2
1
0
**
***
Con
L-NIO
L-NIO + NTG
B
Con
L-NIO
L-NIO + NTG
Intracellular NO
Net Fluor. Int. (A.U)
6
3
0
***
***
Con
L-NIO
L-NIO + NTG
C
Con
L-NIO
L-NIO + NTG
p-eNOS (ser1179)
GAPDH
p-eNOS/GAPDH
1.2
0.6
0
***
***
Con
L-NIO
L-NIO + NTG
D
Con
L-NIO
L-NIO + NTG
ICAM-1
Actin
ICAM-1 Clustering Index (A.U)
4
2
0
***
***
Con
L-NIO
L-NIO + NTG

Fig. 2.2 NTG Enhances Endothelial NO Production.

(**A**) Addition of NTG (5 μM) to L-NIO-treated ECs prevents the loss of endothelial NO production by L-NIO, as determined by NOA measurement of extracellular NO (n = 4 replicates per condition). Data normalized with respect to untreated control condition (con). **, $p<0.01$; ***, $p<0.001$. (**B**) Fluorescent images of ECs labeled with NO-sensitive dye (DAF-FM diacetate) and subsequent image analysis (bar graph; n = at least 30 cells) confirms that NTG-mediated increase in NO results from greater endothelial NO synthesis. *Scale bar:* 25 μm. ***, $p<0.001$. (**C**) Representative western blot bands and their Densitometric analyses (bar graphs) together reveal that the levels of phosphorylated-eNOS is significantly higher (***, $p<0.001$) after NTG-treatment. Bar graphs indicate average ± SEM. Phospho-eNOS levels were normalized with respect to the corresponding levels of GAPDH (loading control) Staining of U937 cell-EC co-cultures with anti-ICAM-1 and phalloidin (to label actin) and subsequent image analysis (bar graph; $n \geq 30$ cells), as described in Materials and Methods, indicates that the anti-inflammatory effect of NTG (5 μM) correlates strongly with its ability to prevent ICAM-1 clustering induced by NO deficiency (L-NIO treatment). ***, $p<0.001$. *Scale bar:* 25 μm. Data are expressed as mean ± SEM.

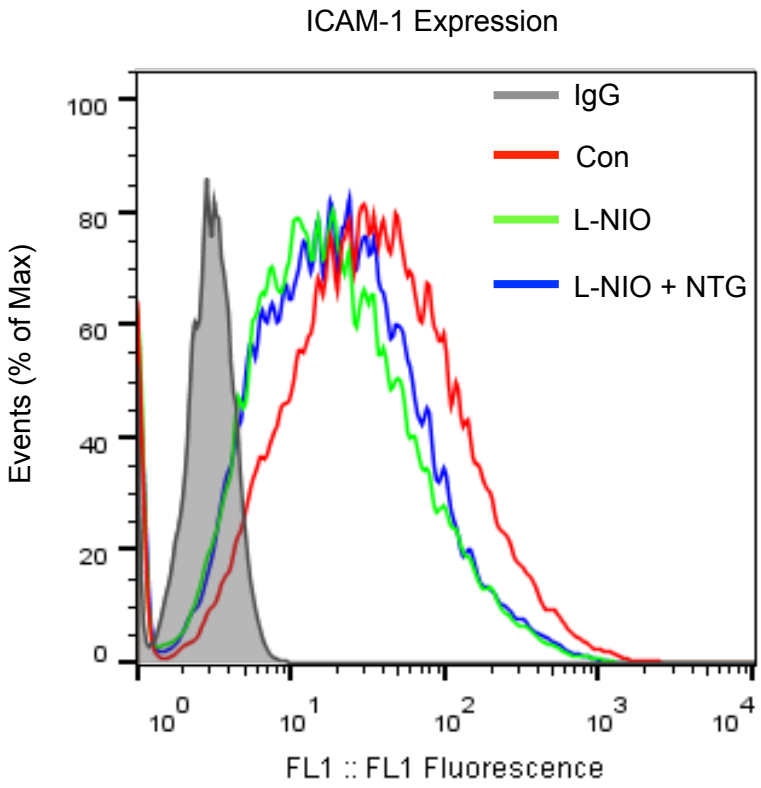

Fig. 2.3. ICAM-1 Expression is Not Altered by L-NIO or NTG Treatment.

ECs were treated overnight with L-NIO (5 mM) ± NTG (5 μM) and surface expression of endothelial ICAM-1 was determined by flow cytometry. Quantitative analysis of fluorescence vs. size (electronic volume) histogram indicates that neither L-NIO nor NTG treatment alters ICAM-1 expression in ECs.

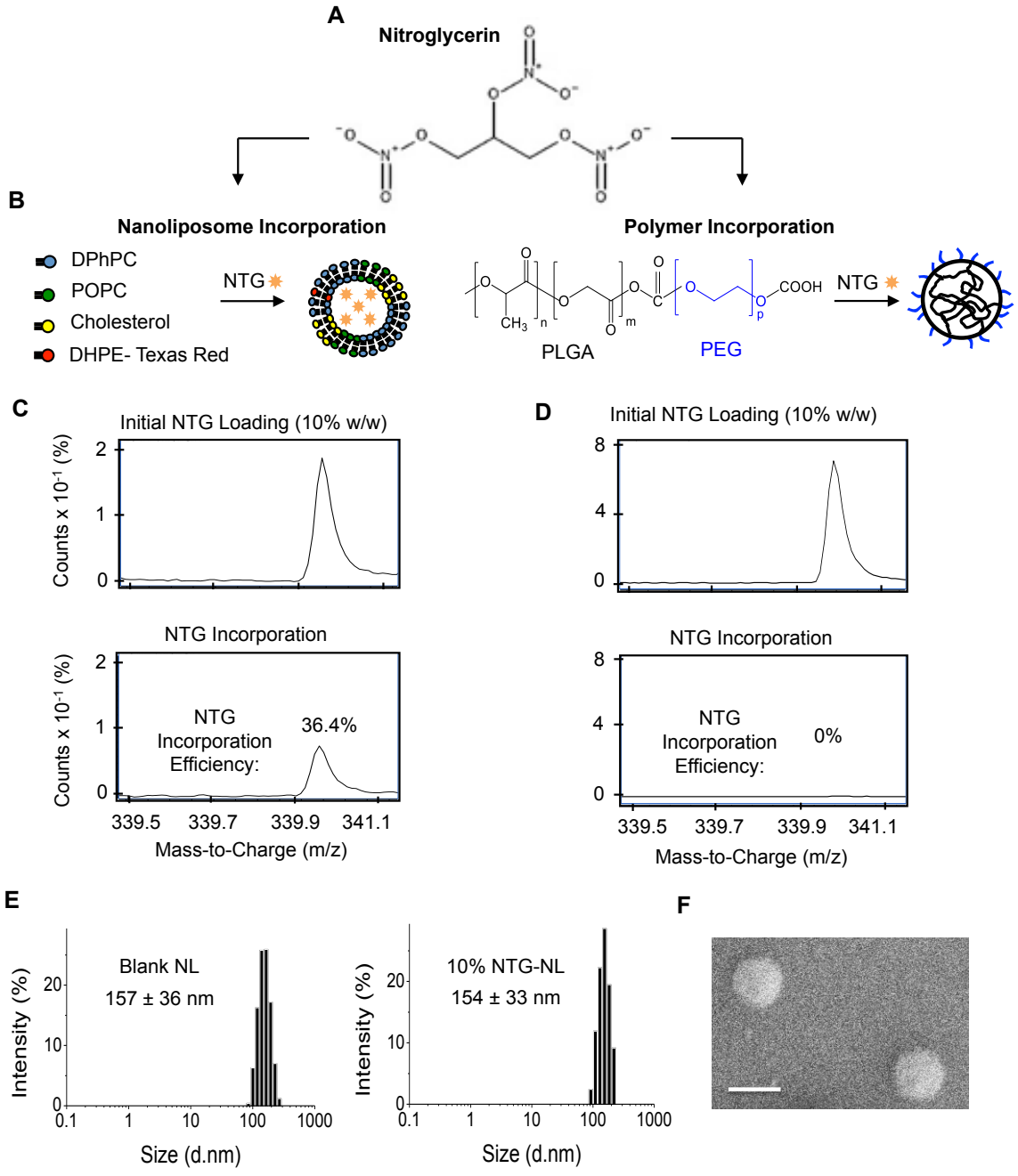
A
Nitroglycerin
B
Nanoliposome Incorporation
DPhPC
POPC
Cholesterol
DHPE- Texas Red
NTG
Polymer Incorporation
COOH
NTG
PLGA
PEG
C
Initial NTG Loading (10% w/w)
Counts x 10-1 (%)
NTG Incorporation
NTG Incorporation Efficiency:
36.4%
339.5 339.7 339.9 341.1
Mass-to-Charge (m/z)
D
Initial NTG Loading (10% w/w)
NTG Incorporation
NTG Incorporation Efficiency:
0%
339.5 339.7 339.9 341.1
Mass-to-Charge (m/z)
E
Blank NL
157 ± 36 nm
Intensity (%)
Size (d.nm)
10% NTG-NL
154 ± 33 nm
Intensity (%)
Size (d.nm)
F

Fig. 2.4. Synthesis and Physicochemical Characterization of Nanoliposomal NTG (NTG-NL).

(**A**) Schematic of NTG molecule depicting the hydrophobic (-CH_2-CH_2-) and hydrophilic ($ONOO^-$) groups. (**B**) For incorporation within nanoliposomes (NLs), NTG was mixed with four lipids viz. DPhPC, POPC, Cholesterol, and DHPE-Texas Red, which self-assemble to form nanoliposomes in an aqueous solution. For incorporation within polymeric NPs, NTG was mixed with an amphiphilic PLGA-b-PEG block copolymer that spontaneously self-assembles in aqueous solution to form NPs with a hydrophobic PLGA core and hydrophilic PEG surface. ESI-Mass Spec. measurements reveal that at 10% w/w initial NTG loading, **(C)** NLs exhibit successful incorporation (~37% incorporation efficiency), while (**D**) polymeric NPs failed to incorporate NTG. (**E**) Dynamic Light Scattering **(**DLS) analysis reveals that both blank and NTG-loaded NLs exhibit similar diameter (~155 nm). (**F**) Size distribution of NL was independently confirmed using scanning electron microscope (SEM). *Scale bar:* 200 nm. Data are expressed as mean ± Std Dev.

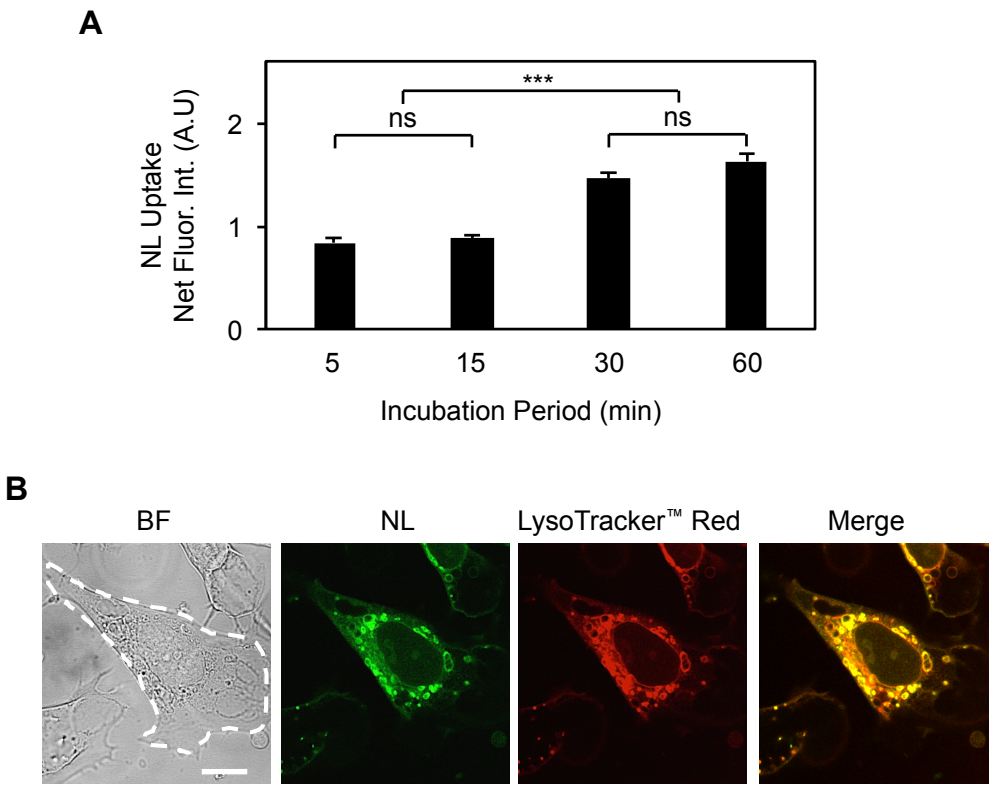

Fig. 2.5. Cellular Uptake of Nanoliposomes.

(**A**) Spectrophotometer measurements of internalized fluorescently-labeled nanoliposomes (NL) reveal time-dependent uptake of NLs by cultured ECs (n = 5 replicates per condition). ***, $p<0.001$; ns, no significance. (**B**) Fluorescent images of internalized NLs indicate strong colocalization with LysoTracker Red™-labeled endocytic vesicles (lysosomes and endosomes). *Scale bar:* 10 µm. Data are expressed as mean ± SEM.

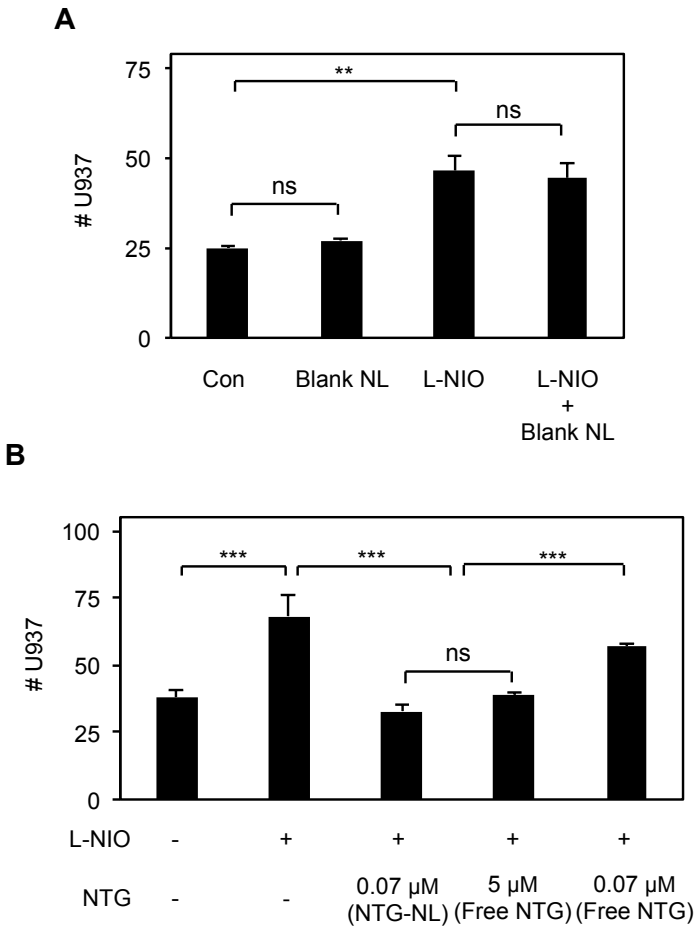

Fig. 2.6. NTG-NL Exerts Superior Anti-inflammatory Effects.

(**A**) Blank NLs are inert to ECs as cells treated with blank NLs exhibit neither an increase in U937 cell adhesion (with respect to control) nor a decrease in LNIO-induced U937 cell adhesion (n = 10 fields of view). **, $p<0.01$; ns, no significance. (**B**) Addition of 5 μg/ml NTG-NL (≡ 0.07 μM NTG) to L-NIO-treated ECs significantly inhibits U937 cell-EC adhesion, which is comparable to the inhibition produced by a 70-fold greater dose of free NTG (5 μM). Free NTG dose of 0.07 μM does not produce a significant anti-inflammatory effect. (n = 10 fields of view). ***, $p<0.001$; ns, no significance. Data are expressed as mean ± SEM.

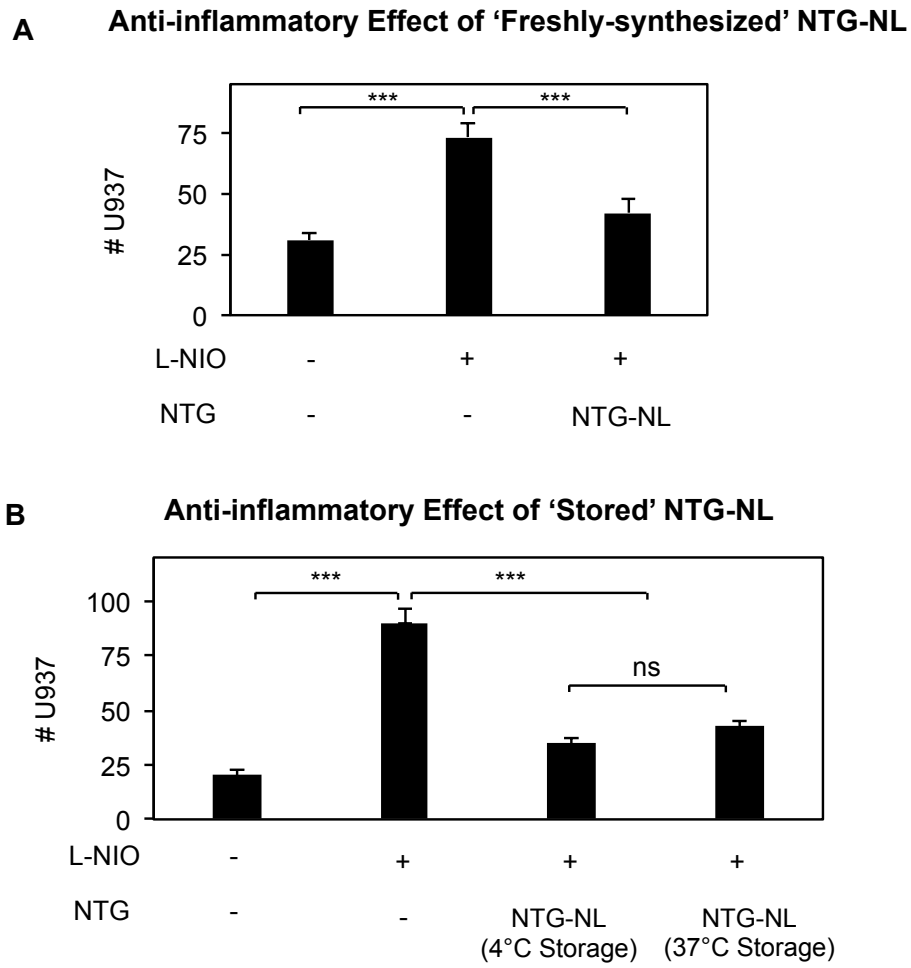

Fig. 2.7. Anti-inflammatory Effects of Freshly-prepared and Stored NTG-NL.

EC monolayers were treated with L-NIO ± NTG-NL (100 μg/ml) that were either (**A**) freshly synthesized or **(B)** stored at 4°C or 37°C for 24 hr prior to use. Quantification of adherent U937 cells (per mm^2) on EC monolayers (n = 10 fields of view) reveals significant inhibition in U937 cell-EC adhesion following treatment with NTG-NLs that were stored for 24 hr, indicating stable retention of NTG within the lipid core of nanoliposomes. ***, $p<0.001$; ns, no significance.

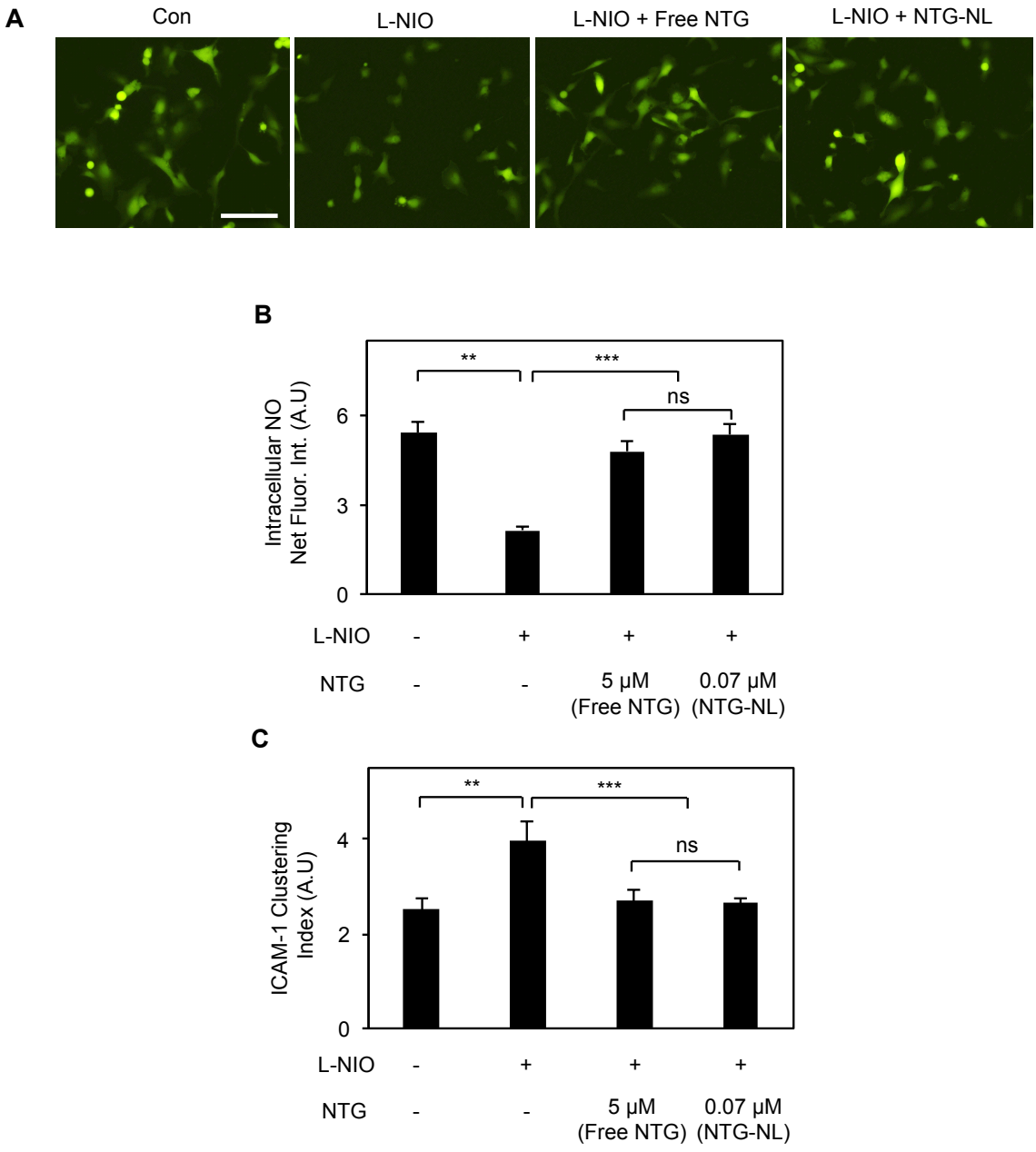
A
Con
L-NIO
L-NIO + Free NTG
L-NIO + NTG-NL
B
Intracellular NO
Net Fluor. Int. (A.U)
0
3
6
**
***
ns
L-NIO - + + +
NTG - - 5 μM (Free NTG) 0.07 μM (NTG-NL)
C
ICAM-1 Clustering
Index (A.U)
0
2
4
**
***
ns
L-NIO - + + +
NTG - - 5 μM (Free NTG) 0.07 μM (NTG-NL)

Fig. 2.8. NTG-NL Enhances Endothelial NO Production.

(**A**) Immunofluorescent staining of ECs labeled with NO-sensitive dye (DAF-FM diacetate) and (**B**) subsequent image analysis (bar graph; n = at least 30 cells) confirms that, like free NTG, NTG-NL enhances NO production in L-NIO-treated cells. *Scale bar:* 25 μm. **, $p<0.01$; ***, $p<0.001$; ns, no significance. (**C**) Immunofluorescent staining of U937 cell-EC co-cultures for ICAM-1 and subsequent fluorescent intensity measurement (bar graph; n = at least 20 cells) reveals that, like free NTG (5 μM), NTG-NL (5 μg/ml) suppresses ICAM-1 clustering induced by NO deficiency (L-NIO treatment). **, $p<0.01$; ***, $p<0.001$; ns, no significance. Data are expressed as mean ± SEM.

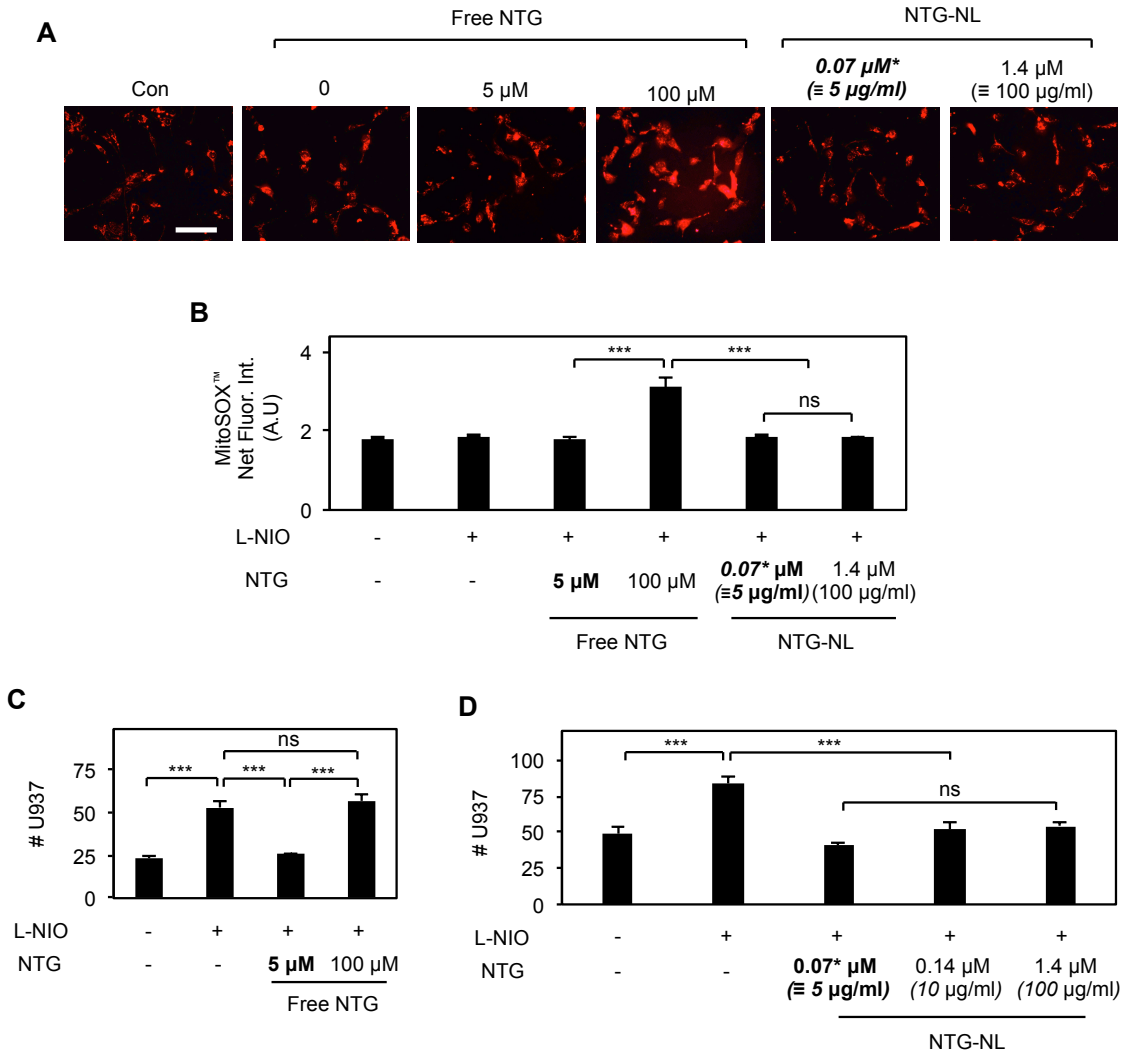
A
Free NTG
NTG-NL
Con
0
5 µM
100 µM
0.07 µM*
(≡ 5 µg/ml)
1.4 µM
(≡ 100 µg/ml)
B
MitoSOX™
Net Fluor. Int.
(A.U)
4
2
0
***
***
ns
L-NIO
NTG
5 µM
100 µM
0.07* µM
(≡5 µg/ml)
1.4 µM
(100 µg/ml)
Free NTG
NTG-NL
C
U937
75
50
25
0
ns
***
***
***
L-NIO
NTG
5 µM
100 µM
Free NTG
D
U937
100
75
50
25
0
***
***
ns
L-NIO
NTG
0.07* µM
(≡ 5 µg/ml)
0.14 µM
(10 µg/ml)
1.4 µM
(100 µg/ml)
NTG-NL

Fig. 2.9. NTG-NL Prevents Endothelial Superoxide Formation Associated with High NTG Dose.

(**A**) Representative fluorescent images of MitoSOX™-labeled ECs and (**B**) subsequent quantification (bar graph; n ≥ 30 cells) indicate that addition of 20-fold higher dose (100 μM) of free NTG to L-NIO-treated ECs significantly increases mitochondrial superoxide formation while similar increase in NTG-NL dose (0.07 μM to 1.4 μM) produces no effect. *Scale bar:* 100 μm. ***, $p<0.001$; ns, no significance. (**C**) The high dose (100 μM) of free NTG fails to suppress U937 monocytic cell adhesion to L-NIO-treated ECs (n = 10 fields of view). ***, $p<0.001$; ns, no significance. (**D**) Unlike free NTG, NTG-NL continues to exert potent anti-inflammatory effects on L-NIO-treated ECs even at a 20-fold higher dose (n = 10 fields of view) with all NTG-NL doses demonstrating similar inhibition of U937 adhesion. Therapeutic dose is indicated ***in bold.*** ***, $p<0.001$; ns, no significance. Data are expressed as mean ± SEM.

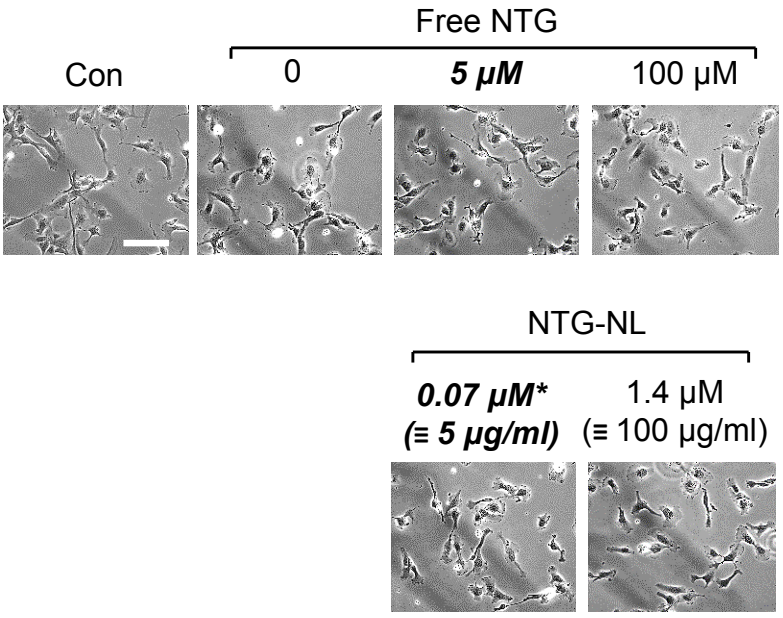

Fig. 2.10. EC Density And Spreading Are Similar Across Various Treatment Conditions.

Phase images of ECs treated without or with L-NIO ± NTG or NTG-NL show that cell spreading is similar across all treatment conditions. Therefore, the difference in MitoSox® fluorescence intensity seen in Figure 2.9A reflects the actual difference in mitochondrial superoxide production. The effective therapeutic NTG dose is indicated *in bold*. Scale bar = 100 μm.

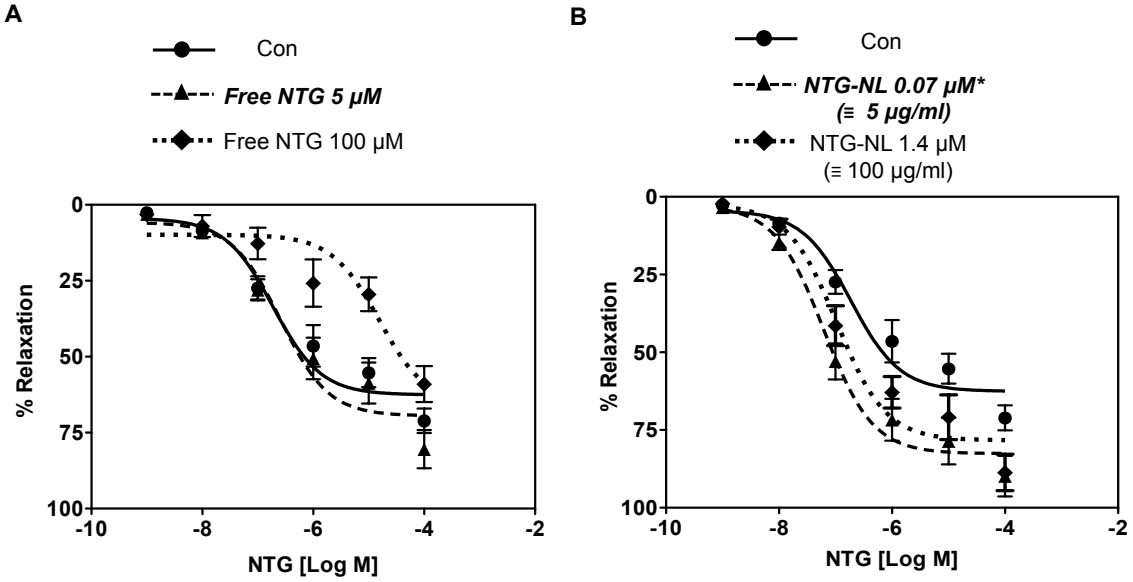

C

	-Log IC_{50} (Mean $IC_{50,}$ µM)		Maximal Relaxation (%)
Con	6.73 ± 0.14	(0.19)	63 ± 3
Free NTG 5 µM	**6.60 ± 0.18**	**(0.25)**	**69 ± 4***
Free NTG 100 µM	4.81 ± 0.24***	(15.5)	66 ± 9
NTG-NL 0.07 µM (5 µg/ml)	**7.21 ± 0.15**	**(0.07)**	**83 ± 3**
NTG-NL *1.4 µM* (100 µg/ml)	6.98 ± 0.15	(0.10)	78 ± 4

D

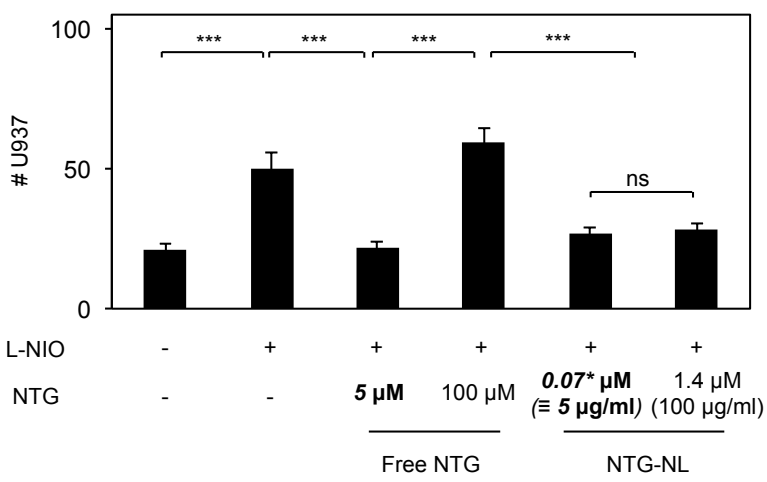

Fig. 2.11. Effects of Free NTG and NTG-NL Treatment on IC50 and Maximal Vasorelaxation of Isolated Pulmonary Sheep Arteries.

(**A**) Pulmonary arterial rings pretreated with 100 μM free NTG exhibit impaired responsiveness to acute NTG treatment, as indicated by a significant rightward shift in NTG dose-relaxation curve (n ≥ eight arterial rings). (**B**) In contrast, arterial rings pretreated with a similar 20-fold higher NTG-NL dose exhibit normal relaxation response to acute NTG treatment. (**C**) Pulmonary sheep arteries pretreated with the effective (anti-inflammatory) free NTG dose of 5 μM exhibit normal NTG dose-relaxation profile similar to untreated controls. In contrast, arteries pretreated with a 20-fold higher free NTG dose (100 μM) demonstrate a significant increase in mean IC50 values. Remarkably, pretreatment with NTG-NL at both 5 and 100 μg/ml doses exhibit no evidence of NTG tolerance. IC50 are concentrations that produced 50% relaxation in response to NTG stimulation. The maximal relaxation response was, however, similar in the control and both free NTG-treated arteries while the NTG-NL-treated arteries exhibited marginally improved maximal relaxation response. The precise reason for this improvement in maximal relaxation by NTG-NL remains unclear. (D) Demonstration of intracellular NTG-NL uptake and bioavailability following 4h treatment. EC monolayers were treated with L-NIO ± NTG or NTG-NL for 4 hr prior to addition of fluorescently-labeled U937 monocytic cells. Quantification of adherent U937 cells (per mm^2) on EC monolayers (n = 10 fields of view) show that both NTG at 5 μM and NTG-NL at 5 μg/ml produce significant inhibition of U937 cell-EC adhesion within 4 hr of treatment. Further, while free NTG loses its therapeutic effect at a 20-fold higher dose of 100 μM, NTG-NL

retains its immunosuppressive effects at a similar 20-fold greater dose (100 μg/mL). Thus, the anti-inflammatory effects of free NTG and NTG-NL observed after 4 hr of treatment are consistent with those seen following overnight treatment. **, $p<0.01$; ***, $p<0.001$; ns, no significance. Therapeutic dose is highlighted *in bold*. Data are expressed as mean ± SEM.

Tables

Initial NTG Loading (% w/w)	Incorporated NTG (Peak Area)	NTG Incorporation Efficiency (%)
5	3039	15.6
10	14307	36.4
25	28653	23.4

Table 2.1. ESI-MS Analysis of NTG Incorporation Efficiency within NLs.

NTG incorporation within NLs increased with increasing loading (5, 10, and 25% wt. NTG/wt. NLs), although the maximum incorporation efficiency was observed at the intermediate NTG loading of 10% w/w (~37% incorporation efficiency). This trend is consistent with drug loading within nanoparticles, as previously reported.

NL Conc. (μg/ml)	NL Uptake Net Fluor. Int. (A.U)	% NL Uptake
5	72	9.0
10	163	5.1
50	579	2.0
100	1580	0.8

Table 2.2. NL Uptake by Cultured ECs.

When added to cultured ECs, fluorescently-labeled nanoliposomes undergo dose-dependent uptake by ECs, with the net internalized amount increasing with increasing NL dose. However, this dose-dependent increase in net NL uptake is inversely proportional to *percent* uptake by ECs, which is the highest at 5 μg/ml dose and decreases progressively with increasing NL dose.

Chapter 3:

Nanoliposomal Nitroglycerin Prevents Endothelial Cell Capillary Regression

Preface

Nitric Oxide (NO) is known to exert both anti-inflammatory and pro-vasculogenic effects. In Chapter 2, I demonstrated that NTG exerts anti-inflammatory effects through enhancement of NO production. In this Chapter, I investigated whether NTG also exhibited pro-vasculogenic properties via NO production. Specifically, I examined whether: (i) NTG could also mimic the pro-vasculogenic effects of NO to prevent EC capillary regression; and (ii) leveraging the previously developed NTG nanoformulation (NTG-NL) would amplify its pro-vasculogenic effects.

Original contribution:	Data for Figures 3.1, 3.5-3.6
In collaboration:	Data for Figures 3.2-3.4, 3,7

Introduction

Impaired endothelium-derived nitric oxide (NO), a potent vasculogenic/angiogenic molecule, is strongly implicated in vascular degeneration associated with PAH[12] and DR.[18] Thus, administration of nitrates/nitrites, which rapidly enhances NO bioavailability, is being explored to promote vessel growth and regeneration.[70] Since organic nitrates exert potent vasodilatory effects compared with inorganic nitrate/nitrites,[48] they are likely to also exhibit superior neovascularization effects.

Importantly, Nitroglycerin (NTG) holds promise for pro-vasculogenic/pro-angiogenic therapies due to its ability to enhance eNOS/NO bioavailability as previously demonstrated in Chapter 2. Therefore, it was likely that similar NO-mediated therapeutic effects would be observed with free NTG with an increase in NTG therapeutic efficacy with NTG nanoformulation.

Here we first hypothesized that NTG-derived NO can prevent regression of a 2D endothelial cell (EC) capillary network and this effect may be mediated by key physical determinants of capillary formation (i.e. adhesion, spreading, and elongation). Further, by utilizing the principles of nanotechnology, a nanoliposomal NTG formulation (NTG-NL) was developed, that *in vitro* studies indicate, demonstrates a 35-fold greater pro-vasculogenic effect compared with free NTG. Thus, these findings implicate NTG nanotherapeutic as a new and improved NO-dependent approach that may lead to superior clinical management of various diseases that are marked by chronic vascular regression and dysfunction.

Materials and Methods

Cell Culture. Human microvascular endothelial cells (HMEC-1) were purchased from the Center for Disease Control (CDC)[52] and plated on gelatin-coated tissue culture dishes in growth medium composed of MCDB-131 (VWR International, USA), 10% FBS (Fisherbrand, USA), 1x antimycotic/antibiotic mixture (Life Technologies, USA), 2 mM L-Glutamine (Invitrogen, USA), 1 μg/ml Hydrocortisone (Sigma Aldrich, USA), and 10 ng/ml huEGF (Millipore, USA).

Nanoliposome (NL) Formulation. NTG-loaded nanoliposomes (NTG-NL) were synthesized as previously described in Materials and Methods section of Chapter 2 (pg. 14).

NL Size and Morphology Characterization. Dynamic light scattering (DLS) measurements and scanning electron microscopy images were obtained as previously described in Materials and Methods section of Chapter 2 (pg. 15).

Vasculogenesis Assay. To examine whether NTG could exhibit therapeutic effects and prevent EC capillary regression, ECs were treated with 1 mM N^5-(1-iminoethyl)-L-ornithine (L-NIO; Cayman Chemical, USA) ± 5 μM Nitroglycerin (NTG: Cambridge Isotope, MA) or 10 μg/ml NTG-NL 0.12 μM NTG on Matrigel (BD Bioscience, USA). Briefly, Matrigel was formed in 48-well plates, incubated at 37^0C for 30 min prior to the addition of ECs at a cell density of 25,000 cells/cm^2 per well and observed over 18 hr. To

examine whether NTG could also exhibit a long-term effect, ECs were cultured on gelatin-coated well plates, treated with L-NIO ± 5 μM NTG for 18 hr, detached, rinsed twice with PBS, and re-plated onto Matrigel without factors and observed over 18 hr. For time-lapse imaging, 10x images were taken every 0.5, 1, 2, and 4 hr with a Nikon Eclipse Ti microscope. At least 4 images per condition were analyzed for total cord length measurements using ImageJ software (NIH).

Measurement of Endothelial cell-derived NO. Measurement of EC-derived NO production was performed as previously described in Material and Methods section of Chapter 2 (pg. 18).

EC Adhesion, Spreading, and Elongation. To evaluate EC adhesion, cells were pretreated overnight with 1 mM L-NIO ± 5 μM NTG. Cells were then detached and re-plated on gelatin-coated tissue culture plastic in regular medium at a cell density of 90k cells/cm^2. After 30 min, cells were gently rinsed twice with PBS (to remove non-adhered ECs) and fixed with 1% PFA. Phase images (at least 8 per condition) were then taken using a Nikon Eclipse TI microscope.

Next, to evaluate cell spreading, ECs plated on Matrigel for Vasculogenesis assay (as described above) were imaged 0.5 hr post-plating at and 10x phase images were acquired using a Nikon Eclipse TI microscope. Cell area was quantified from at least 40 cells per condition using ImageJ software.

Further, to determine EC elongation cell aspect ratio, ECs from the same Vasculogenesis Assay were imaged at 1, 2, and 4 hr post-plating. 10x phase images were acquired and subsequent analysis of cell aspect ratio was determined by dividing major axis by minor axis of the cells.

EC Cytoskeletal Organization. To evaluate cytoskeletal organization, ECs were cultured on gelatin-coated glass cover slips and after 1.5 hr cells were treated with 1 mM L-NIO ± 5 μM NTG. 6 hr post-plating, cells were fixed with 1% PFA, permeabilized with 0.2% Triton X-100 (Sigma Aldrich, USA), and stained with Alexa Fluor-488 phalloidin (Invitrogen) and DAPI (Invitrogen) for visualization of actin microfilaments and nuclei, respectively. Fluorescent images were obtained using Nikon Eclipse TI fluorescence microscope and the number of actin filaments were quantified using ImageJ.

Statistics. All data were obtained from multiple replicate experiments (as described in the appropriate sections) and shown as mean ± standard error mean (SEM). Statistical significance was determined using analysis of variance (ANOVA; InStat; Graphpad Software Inc.) followed by a Tukey-Kramer method. Significance of the results were represented as *$p<0.05$, **$p<0.01$, or ***$p<0.001$.

Results

NTG Prevents Capillary Regression in NO-deficient ECs.

NTG has been shown to enhance NO bioavailability through both EC metabolic conversion and eNOS activation[32,71] so we first asked whether NTG could recapitulate the pro-vasculogenic properties of NO. When NTG was added to ECs treated with L-NIO (1 mM), a selective eNOS inhibitor that causes significant regression ($p<0.01$) in total EC cord formation, it recovered the loss of 2D endothelial capillary networks (Fig. 3.1).

Additionally, similar to previous findings in Chapter 2, NTG's pro-vasculogenic effects resulted from a significant (*$p<0.05$) increase in NO production in L-NIO-treated ECs (Fig. 3.2).

NTG Normalizes Key Physical Determinants of EC Capillary Formation: Adhesion, Spreading, and Elongation.

Since NTG prevented the collapse of a NO-dependent capillary network, we asked whether this effect was due to the effect of NTG on various key physical determinants of capillary formation including EC adhesion, spreading/cytoskeleton, and (elongation) aspect ratio, where previous studies have shown the effect of NO on cell mechanics to be strongly implicated.[72] To observe the effects of NTG-derived NO on these functional responses, time-lapse images were taken at 0.5, 1, 2, and 4 hr time-points during an *in vitro* vasculogenesis assay. First, NTG treatment demonstrated a significant (***$p<0.001$) recovery effect on adhesion of L-NIO-treated ECs (Fig. 3.3A). Next, NTG treatment exerted similar recovery effects on EC spreading after 0.5 hr (Fig. 3.3B) as

quantified in the bar graph as cell area (Fig. 3.3C), and EC elongation over 4 hr (Fig. 3D), quantified in the bar graph as cell aspect ratio (Fig. 3.3E). Notably, these functional recovery effects of NTG correlated strongly with the restoration of actin cytoskeletal organization in NTG-treated ECs (Fig. 3.4).

Synthesis and Physicochemical Characterization of NTG Nanotherapeutic (NTG-NL).

As previously demonstrated in Chapter 2, NLs were made from a combination of four lipids (DPhPC, POPC, Cholesterol, and DHPE-Texas Red) (Fig. 3.5A). Additionally, DLS and SEM imaging revealed an average diameter of 155 ± 32 nm and 153 ± 32 nm for blank and NTG-NL, respectively (Fig. 3.5B). This finding was independently confirmed using SEM (Fig. 3.5C).

NTG-NL Exerts Superior Pro-vasculogenic Effects on NO-deficient ECs.

Nanoliposomes are known to enhance drug efficacy as previously demonstrated in Chapter 2. Thus, we asked whether NTG-NL could enhance the pro-vasculogenic effects of encapsulated NTG. These studies indicate that addition of NTG-NL (10 μg/ml) to L-NIO-treated ECs produced a significant ($p<0.05$) recovery in EC total cord network formation (Fig. 3.6A). This recovery in cord formation by NTG-NL was comparable to the recovery caused by a 5 μM dose of free NTG. Determination of the total amount of NTG delivered through the nanoliposomal formulation revealed that NTG-NL produced its pro-vasculogenic effect at an equivalent NTG dose of 0.14 μM, which is 35-fold less

than the effective pro-vasculogenic dose of free NTG. To confirm that this effect resulted primarily from nanoencapsulation of NTG we demonstrated that an equivalent amount (0.14 μM) of free NTG failed to produce a significant recovery in EC capillary formation (Fig. 3.6A).

Additionally, similar to free NTG, the preventative effect of NTG-NL was consistent with its ability to enhance EC-derived NO production (Fig. 3.6B) and normalize the key physical determinants of EC capillary cord formation, cell spreading (Fig. 3.7A) and elongation (Fig. 3.7B).

Discussion

This study reveals the proof-of-principle for a nanoliposomal NTG formulation that enhances the newly-identified pro-vasculogenic effects of NTG. NTG, a commonly used organic nitrate in the clinic, is used to mimic the vasodilatory effects of endothelium-derived NO[56]. Importantly, when compared with inorganic nitrites/nitrates, NTG produces a significantly greater and rapid yield of NO[48], which explains its potent vasodilatory effects. Since endothelial NO also exhibits superior pro-vasculogenic effects, here we asked whether NTG can prevent capillary regression in NO-deficient ECs. These findings demonstrate that NTG significantly prevents EC capillary regression. This preventative effect of NTG was observed at a dose of 5 μM.

Importantly, eNOS-derived NO promotes neovascularization while impaired eNOS activity leads to vessel regression and death. Additionally, vascular endothelial growth factor (VEGF), a potent angiogenic/vasculogenic growth factor, has been shown

to exert these effects in a NO-dependent matter. Therefore, since NTG is known to enhance endothelial NO it was likely to exert pro-vasculogenic effects as well. Notably, these findings are consistent with the ability of inorganic nitrites to protect against capillary regression associated with chronic ischema.[70,73-76] This is the first report indicating that NTG also exerts similar pro-vasculogenic effects.

Neovascularization is a physical process that is governed by a mechanical force balance, which is established by ECs when they exert their adhesions to the surrounding extracellular matrix (ECM). While contractile forces generated in the actin cytoskeleton maintain the ECM in a prestressed state, changes in ECM compliance can feed back to regulate cell tension creating a feedback system. Importantly, it is this constant change in EC-ECM force equilibrium that can produce cord-like networks during normal vessel formation.[77-81]

Importantly, these studies reveal that NTG regulates several of these key processes, which is consistent with previous studies that demonstrate the ability of NO to promote cell adhesion and spreading, and assembly of actin fibers.[82]

Together with the finding that NTG activates eNOS[32], the key NO-producing enzyme that mediates neovascularization and is impaired in conditions marked by vessel regression,[83] the current findings provide added rationale for investigating NTG as a pro-vasculogenic drug.

Further, to improve the therpaeutic effects of NTG therapy, we leveraged nanotechnological principles and developed a nanoliposomal NTG formulation (NTG-NL) that demonstrates a 35-fold increase in drug efficacy. This significant increase in

drug efficacy is a hallmark of nanotherapeutic strategies, which is known to greatly improve therapeutic efficacy by simultaneously increasing drug half-life and intracellular uptake.[37,39,51] To fully leverage the benefits of nanoparticle drug delivery, these particles must be rationally designed for long circulation times *in vivo*. When determining the optimal size of long-circulating NLs, studies have shown particles that exceed 200 nm risk being caught in the intracellular slit (IES) filtration system of the spleen, while NLs smaller than 100 nm likely increase the risk of uptake by liver hepatocytes. Thus, a size range between 120 -200 nm is ideal for this nanotherapeutic.[84] Additionally, surface modifications including addition of poly (ethylene glycol) (PEG) chains will provide "stealth" to the NLs so it can avoid capture by circulating immune cells, liver, and kidney.[85] Specifically, short-chain PEG-lipid conjugates of molecular weight 2000 kDa were used as long-chain PEG conjugates (molecular weight $\geq$ 5000 kDa) result in poor steric protection and destabilization.[84] All together, these engineering design criteria should facilitate the effectiveness of the proposed nanotherapeutic.

Conclusions

The *in vitro* studies executed have been used to examine the effects of nitrites and now NTG on EC capillary formation. Importantly, however, to fully appreciate the therapeutic potential of NTG-NL, the current in *vitro* studies should be validated in appropriate animal models of ischemia. Importantly, the proof-of-concept studies described here allow for further enhancement of this nanotherapeutic system with the development of site-targeting nanoliposomes, which have been previously shown to

simultaneously increase drug half-life, enhance circulation time *in vivo*, and reduce off-target side-effects. Specifically, these nanoliposomes can be surface modified with peptides, antibodies, antibody fragments that can guide the nanoliposomes to sites of vascular defect. Therefore, by utilizing NTG's newly-identified pro-vasculogenic properties, new approaches for treatment of capillary regression can be explored.

Figures

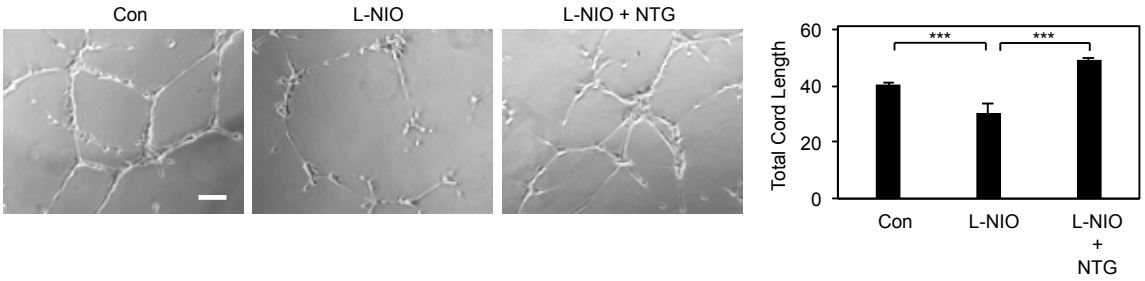

Fig. 3.1. NTG Prevents Capillary Regression in NO-deficient ECs.

Addition of NTG to L-NIO-treated microvascular ECs significantly prevents capillary regression when plated on Matrigel, as shown by phase contrast images and subsequent total cord length (μm X 10^3) /mm^2) analysis (bar graph; n = 8 fields of view). *Scale bar:* 100 μm. ***, $p<0.001$ Data are expressed as mean ± SEM.

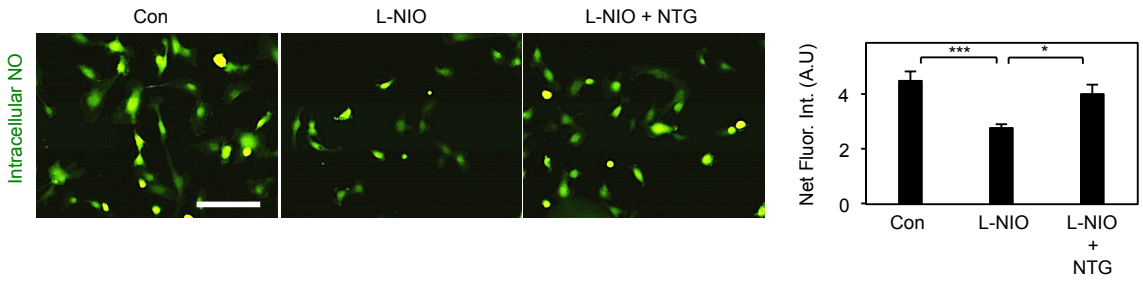

Fig. 3.2. NTG Promotes Endothelial NO Synthesis.

Images of fluorescently-labeled **(**NO-sensitive dye; DAF-FM diacetate) microvascular ECs and subsequent image analysis (bar graph; n = at least 30 cells) confirms that NTG-mediated increase in NO results from enhancement of endothelial NO production. *Scale bar: 25 μm.* ***, $p<0.001$; *, $p<0.01$. Data are expressed as mean ± SEM.

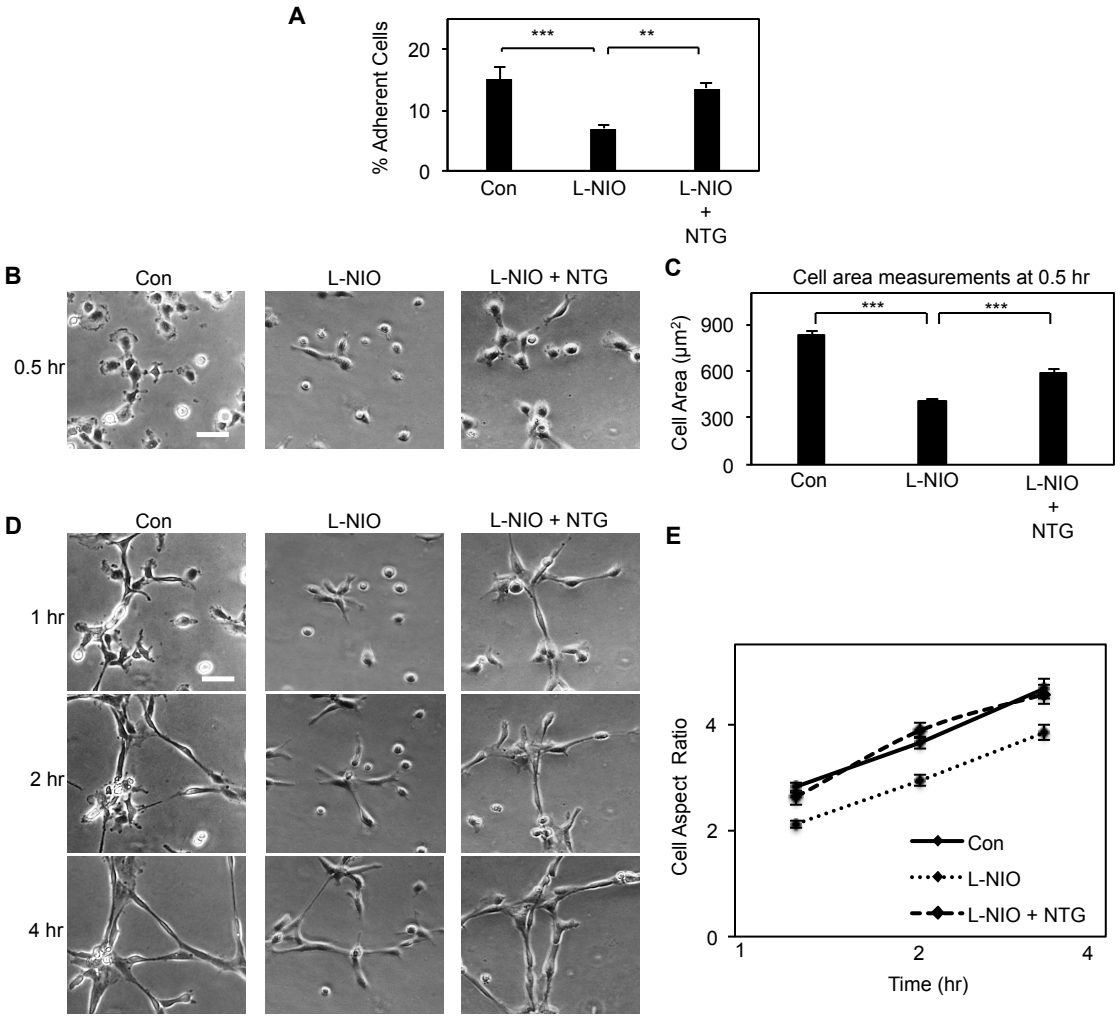

Fig. 3.3. NTG Normalizes Key Physical Determinants of EC Capillary Formation: Adhesion, Spreading, and Elongation.

(A) NTG recovers cell adhesion of L-NIO-treated ECs, as quantified in the bar graph (n = 4 fields of view). Similarly, time-lapse phase images of EC spreading after 0.5 hr and subsequent analysis of EC area **(B)** and EC elongation at 1, 2, and 4 hr post-plating and subsequent analysis of aspect ratio **(C)** show significant recovery after NTG treatment compared to control (untreated), respectively. ***, $p<0.001$. *Scale bar:* 10 μm.

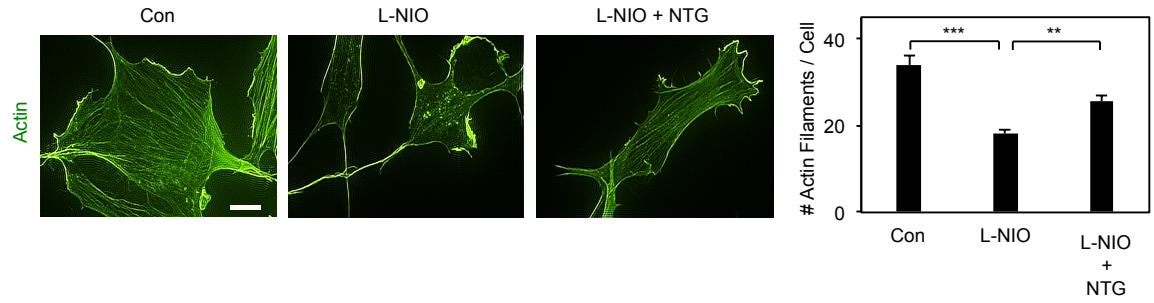

Fig. 3.4. NTG Normalizes EC Actin Cytoskeletal Organization.

Immunofluorescent images of phalloidin-stained-ECs and subsequent analysis of actin filaments show a recovery in actin filament density per cell (bar graph; n = at least 30 cells) after NTG treatment of L-NIO-treated ECs. ***, $p<0.001$; **, $p<0.01$. *Scale bar:* 25 μm. Data are expressed as mean ± SEM.

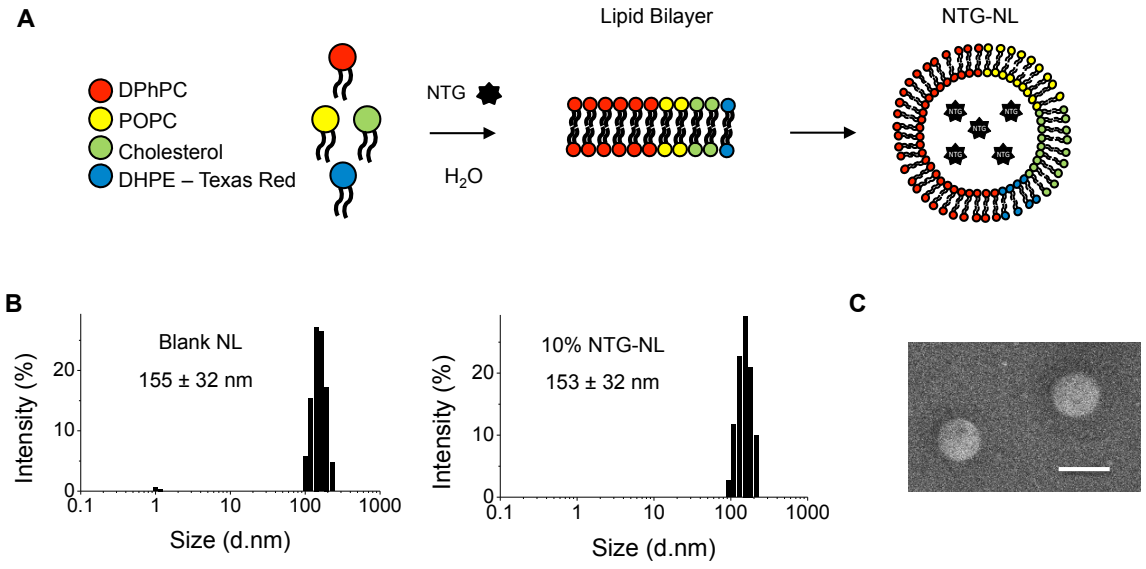

Fig. 3.5. Synthesis and Physicochemical Characterization of NTG Nanotherapeutic (NTG-NL).

(**A**) For NTG incorporation within nanoliposomes (NLs), NTG was mixed with four lipids viz. DPhPC, POPC, Cholesterol, and DHPE-Texas Red, which self-assemble to form liposomes in an aqueous solution followed by extrusion through 100 nm membrane to form NLs. (**B**) Dynamic Light Scattering **(**DLS) analysis revealed that both blank and NTG-loaded NLs exhibit similar diameter (~155 nm). **(C)** Size distribution of NLs was independently confirmed using scanning electron microscope (SEM). *Scale bar:* 200 nm. Data are expressed as mean ± Std Dev.

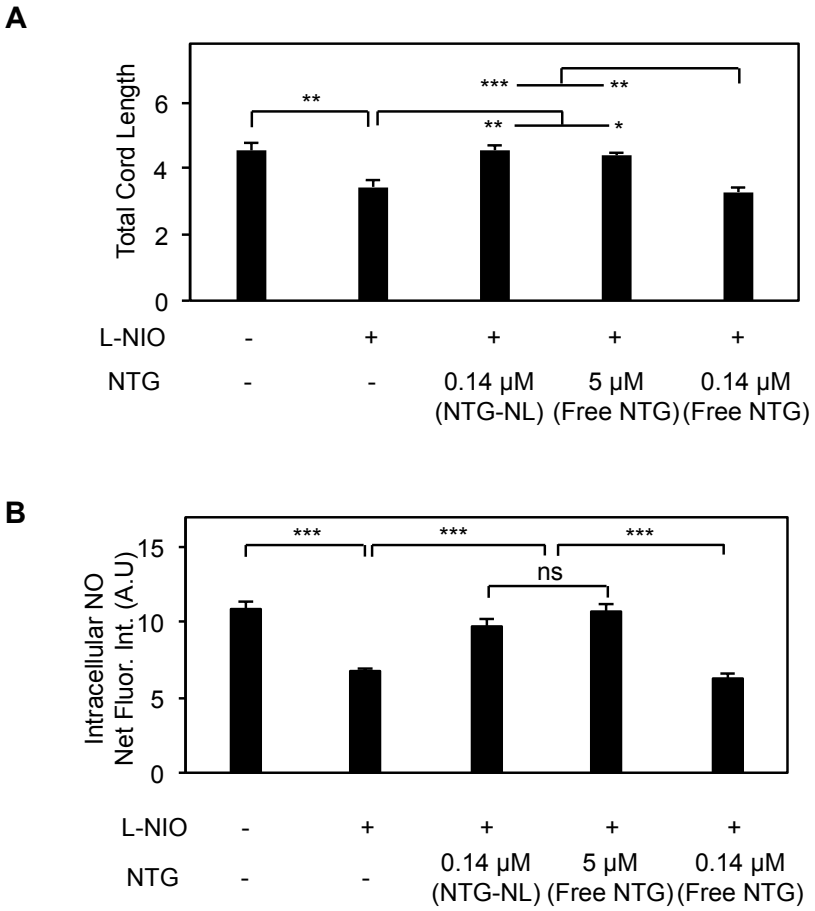

Fig. 3.6. NTG-NL Exerts Superior Pro-vasculogenic Effects on NO-deficient ECs.

(**A**) Addition of 10 µg/ml (≡ 0.14 µM NTG) NTG-NL to L-NIO-treated ECs significantly prevents capillary regression (n = 8 fields of view), which is comparable to the same effect demonstrated by a ~35-fold greater dose of free NTG (5 µM). (**B**) Quantitative analysis (bar graph; n = at least 30 cells) of fluorescent images of ECs labeled with NO-sensitive dye (DAF-FM diacetate) confirms that, like free NTG, NTG-NL also enhances NO production in L-NIO-treated cells. ***, $p<0.001$; **, $p<0.01$; *, $p<0.05$ *Scale bar:* 100 µm. Data are expressed as mean ± SEM.

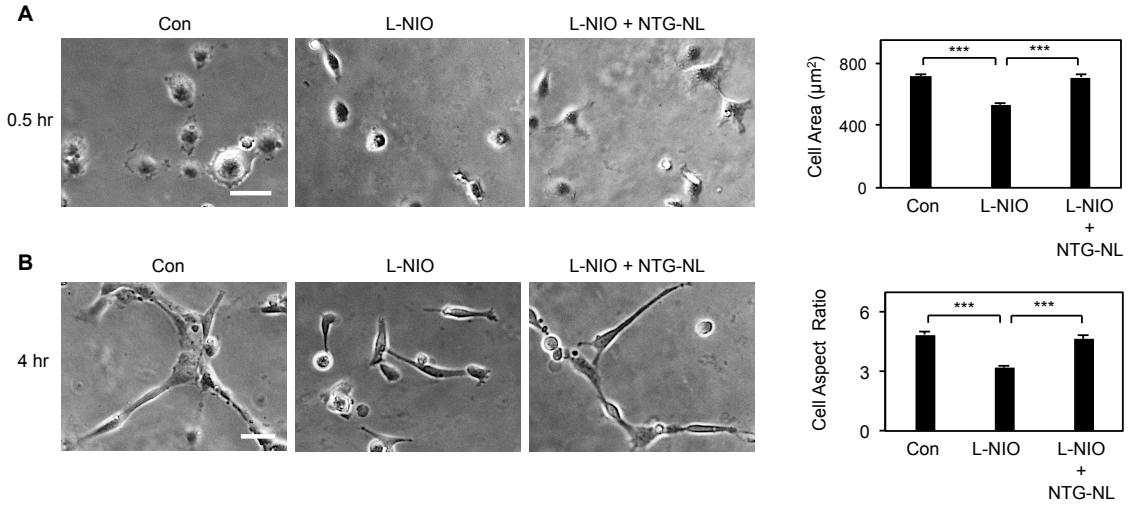

Fig. 3.7 NTG-NL Normalizes Key Physical Determinants of EC Capillary Formation: Spreading and Elongation.

Quantification of phase images of ECs for (**A**) cell spreading and (**B**) elongation confirms that like free NTG (5 μM), NTG-NL (10 μg/ml) also normalizes spreading (n = at least 4 fields of view) and elongation of LNIO-treated ECs, respectively. ***, $p<0.001$. *Scale bar:* 25 μm. Data are expressed as mean ± SEM.

Chapter 4:

Site-Targeting Anti-ICAM-1 Scfv-Modified Nanoliposome Suppresses Vascular Inflammation

Preface

This Chapter describes the surface modification of nanoliposomal NTG that will enable their site-targeted delivery to sites of chronic vascular inflammation. Since PAH and DR are inflammatory conditions marked by enhanced ICAM-1 expression, site-targeting capability was conferred to NTG-NL using ICAM-1-targeting single-chain variable fragments (scFv).

Original contribution:	Data for Figures 4.1, 4.3C-F, 4.4C, 4.6A, 4.7A
In collaboration:	Data for Figures 4.2, 4.3A-B, 4.4A-B, 4.5, 4.4B, 4.7B-C

Introduction

Many therapeutic agents do not accumulate at intended targets in the body, which lower their efficacy and causes adverse off-target effects. The field of nanomedicine has enabled the development of site-targeting nanomaterials (i.e. polymeric & liposomal nanoparticles) that can deliver drugs locally to sites of tissue defects and greatly improve their therapeutic efficacy by simultaneously increasing drug half-life and reducing toxic off-target effects.[51] Such site-targeted drug delivery can be accomplished by tethering unique site-targeting moieties (peptides, aptamers, or antibodies)[37,39] on the nanoparticle (NP) surface that can guide the nanotherapeutic selectively to desired sites in the body and facilitate local drug delivery and therapeutic effect. Although most of the site-targeting approaches have focused on localized tumor drug delivery, there is growing interest in targeting drugs selectively to sites of vascular defects.

Vascular-targeting strategies have used monoclonal antibodies due to their robust high binding affinity properties. However, despite their advantages, monoclonal antibodies lack clinical translational potential due to a resident effector domain known as the fragment crystallizable (F_C), which is known to elicit complement system activation and subsequent rapid clearance from the circulation.[86] Importantly, this disadvantage has been remedied by using NPs tethered to antibody fragments (Fab') that are void of the F_C domain allowing for enhanced circulation times and site-targeting potential, *in vivo*.[87]

More recently, even smaller antibody fragments known as single-chain variable fragments (scFv) are being explored as an alternative to conventional monoclonal antibodies or the Fab' fragments. These small antibody fragments offer several

advantages for use as site-targeting moieties on NP surfaces including lower production costs and easier handling, higher surface packing density due to lower steric hindrance, and strong binding affinity for their target antigen. Further and more importantly, scFv lacks the Fc receptor domain, which is responsible for activation of the host complement system, which if activated would result in premature clearance of any scFv-modified NP construct thereby reducing its therapeutic effects.[66,88,89]

Since ICAM-1 is overexpressed on inflamed (activated) ECs of pulmonary arteries and retinal capillaries in PAH and DR, respectively, I hypothesize that nanoliposomes (described in Chapters 2 and 3) surface-modified with anti-ICAM-1 scFv would preferentially bind to and accumulate within these inflamed ECs and deliver low doses of anti-inflammatory NTG to achieve local and potent immune suppression. Here, for the first time, I report proof-of-concept studies for the development of ICAM-1-targeting nanoliposomes (NLs) that preferentially bind to inflamed vessels *in vitro and in vivo,* and further, exhibit a significant increase in the anti-inflammatory efficacy of NTG.

Materials and Methods

NL-anti-ICAM-1 Targeting to Inflamed Retinal Vessels in Mice. To enhance ICAM-1 expression in mouse retinal vessels, anesthetized male C57BL/ (8-12 weeks old) mice were injected intravitreally with 20 μg of angiopoietin-2 (ANG-2; Sigma Aldrich, USA) in one eye. The other eye served as a control. After 4 hr, the ANG-2-treated mice were injected intravenously with mouse anti-ICAM-1 IgG-modified (BD Biosciences, USA)

and unmodified NLs (containing Texas red-modified lipids for imaging) at a dose of 5 mg/kg. 30 min post-injection, mice were sacrificed and eyes were enucleated for subsequent retinal capillary isolation and whole mount fluorescence imaging.

Retinal Capillary Isolation and Whole Mount Fluorescence Imaging. Enucleated eyes from mice were fixed in 4% PFA (Electron Microscopy Sciences, USA) overnight prior to retinal isolation. Retinas were isolated, rinsed twice in PBS, and imaged using an Sp5 confocal microscope.

Cell Culture. Primary Human Pulmonary Arterial ECs (HPAEC) and Human Monocytic cells (U937) were purchased from ATCC (Manassas, VA, USA). Human Pulmonary ECs were cultured in growth medium composed of MCDB-131 (VWR International, USA) supplemented with 10% FBS (Fisherbrand, USA), 2 mM L-Glutamine (Invitrogen, USA), 1x antimycotic/antibiotic mixture (Life Technologies, USA), 10 ng/ml huEGF (Millipore, USA) and 1 μg/ml Hydrocortisone (Sigma Aldrich, USA), 100 ng/ml Heparin Sodium Salt (Sigma Aldrich, USA), and 30 ng/ml Endothelial Cell Growth Supplement (Sigma Aldrich, USA). U937 monocytes were grown in RPMI-1640 medium (GE Healthcare, USA) supplemented with 10% FBS, 2 mM L-Glutamine, 1x antimycotic/antibiotic mixture, 1.5 mg/ml sodium bicarbonate (Life Technologies), 1 mM sodium pyruvate (Life Technologies), and 4.5 mg/ml glucose (Sigma).

Cloning, Expression, and Characterization of Anti-ICAM-1 scFv. The DNA fragment encoding the scFv light and heavy chain domain of Anti-ICAM-1 was obtained from previously reported Amino Acid Sequences [90] and amplified by real-time polymerase chain reaction (RT-PCR). The resulting DNA sequence was then inserted into the Sfi digestion site of pMopac vector. To confirm whether the scFv DNA sequence was successfully inserted into the Sfi digestion site, the vector containing the scFv insert was digested and analyzed by DNA electrophoresis. Transformed E. coli (Jude-1) were grown in enriched LB media (500 ml) supplemented with 100 μg/ml ampicillin at 37°C and allowed to reach an OD_{600} of 0.7-1, followed by addition of 0.2 mM isopropyl-b-d-thiogactopyranoside (IPTG; Sigma Aldrich, USA) to induce anti-ICAM-1 scFv expression. After induction at 37°C for 16 hr, cells were pelleted by centrifugation (4k rcf for 10 min) and resuspended in 0.1 M Tris-HCl (pH 7.4). To lyse cells, 50 mg/ml lysosome was added to cell suspension and incubated on ice for 10 min. Cells were then pelleted at 4°C at 10k relative centrifugal force (rcf) for 10 min and supernatant containing scFv was filtered on ice. To purify scFv, cell supernatant was loaded into a Ni^{2+}-NTA resin-containing affinity column (Qiagen; CA, USA) and kept at 4°C. The column was then eluted using 200 mM imidazole, transferred to a 15 ml concentration tube (3k MWCO; Millipore, USA), and centrifuged at 4°C at 4k rcf for 30 min. Typically ~1.5 mg of purified Anti-ICAM-1 scFv was obtained from a 500 ml culture. To confirm successful scFv purification, protein was loaded and run through a 10% SDS-PAGE gel.

Anti-ICAM-1 scFv Binding to ICAM-1 Expressing ECs. To determine whether the engineered scFv had binding affinity for ICAM-1-expressing ECs, EC monolayers were stimulated with TNF-α (eBiosciences, USA) for 4 hr in starvation media (2.5 % FBS), followed by incubation with primary scFv at varying (0.06, 0.3, and 1.5 μM) doses for 20 min at 4°C. Next, ECs were incubated with mouse anti-HIS antibody for 20 min at 4°C, followed by FITC-conjugated DyLight 488 anti-mouse IgG (Vector labs, USA) for an additional 20 min as previously reported.[91] ECs were fixed with 1% paraformaldehyde (PFA; Electron Microscopy Sciences, USA), detected by a Cell Lab Quanta SC flow cytometer (Beckman Coulter, CA), and analyzed by FlowJo (Treestar Inc, CA).

Nanoliposome (NL) Formulation and Conjugation to Anti-ICAM IgG and Anti-ICAM-1 scFv. NTG-loaded nanoliposomes (NTG-NL) were synthesized as previously reported.[91] Briefly, five lipid molecules viz. 1,2-di-(3,7,11,15-tetramethylhexadecanoyl)-sn-glycero-3-phosphocholine (DPhPC; Avanti Lipids, USA), 1-hexadecanoyl-2-(9Z-octadecenoyl)-sn-glycero-3-phosphocholine (POPC; Avanti Lipids, USA), Cholesterol (Sigma Aldrich, USA), 1,2-distearoyl-*sn*-glycero-3-phosphoethanolamine-N-[maleimide(polyethylene glycol)-2000] (DSPE-PEG(2000) Maleimide (Mal) or Carboxylic Acid (COOH); Avanti Lipids, USA) and 1,2-dihexadecanoyl-sn-glycero-3-phosphoethanolamine-triethylammonium salt (Texas Red-DHPE; Invitrogen, USA) were dissolved in chloroform at a molar ratio of 5:2:2:1:1:0.2, respectively and purged with N_2 to evaporate the chloroform. The resulting lipid cake was placed under vacuum and rehydrated in aqueous NTG (10% w/w of total lipid;

Cerilliant, USA) or Fluorescein (1 mg/ml; Sigma Aldrich, USA) solution to obtain a final 1 mg/ml drug- or dye-loaded liposome suspension. To obtain NTG-NL-Mal and NTG-NL-COOH, these liposome suspensions underwent freeze-thaw cycles in liquid N_2 followed by extrusion through a 100 nm polycarbonate membrane filter (Avanti Lipids, USA) where unincorporated NTG or fluorescein was discarded by ultracentrifuge (Beckman Coulter, USA) and decanting the supernatant. The final NTG-NL pellet was suspended at 1 mg/ml in water and stored at 4^{o}C until use. Next, to conjugate Anti-ICAM-1 IgG or anti-ICAM-1 scFv onto the NL surface, anti-ICAM-1 IgG at 100 μg/ml and scFv at varying doses (20, 50, 100 μg/ml corresponding to 0.76, 1.9, 3.8 μM) were added to NL suspensions containing either reactive carboxylic acid or maleimide groups (to facilitate NL surface-antibody chemical conjugation), respectively, and incubated overnight (O/N) at 4°C with rotation. After O/N incubation, free cysteine (10 μM; Sigma-Aldrich, USA) was added only to the NL-scFv suspension to quench unreacted maleimide groups for 2 hr at RT followed by 3 PBS rinses and storage at 4°C until further use.

Detection of scFv on NL Surface. To detect conjugation of anti-ICAM-1 IgG and scFv to NL surface, NL-scFv was labeled with mouse anti-HIS antibody (Life Technologies, USA) for 2 hr at room temperature (RT) followed by FITC-conjugated DyLight 488 anti-mouse IgG (Vector labs. USA) for an additional 2 hr at RT, while NL-anti-ICAM-1 was only labeled with FITC-conjugated DyLight 488 anti-mouse IgG (Vector labs. USA) for 2 hr at RT. Next, NL-scFv was transferred to a black-walled 96-well plate and detected

by a Flexstation 2 fluorescent microplate reader (n = 3 per condition) (Molecular Devices, USA).

Characterization of NL Size and Morphology. Dynamic Light Scattering (DLS) and Scanning Electron Microscopy (SEM) sample preparation and imaging was obtained using techniques we have previously reported.[91] Briefly, for DLS samples NL suspensions were prepared at 0.25 μg/ml for measurements by a Delsa Nano C Particle Analyzer (Beckman Coulter, USA). For SEM samples, NLs were fixed in 2.5% glutaraldehyde (Electron Microscopy Sciences, USA) for 2 hr at 4^{o}C, added to Poly-L-Lysine (Sigma-Aldrich, USA)-coated 12 mm glass coverslips, and subjected to critical-point drying (Critical-point-dryer Balzers CPD0202). Samples were then sputter-coated with platinum/palladium for 30 sec and imaged using an SEM (FEI NNS450).

NL Uptake. To determine whether NTG-NLs were successfully endocytosed, ECs treated with fluorescein-incorporated NLs were stained with LysoTracker® Deep Red (Invitrogen, USA) to label acidic organelles (lysosomes and endosomes). Quantitative analysis of the degree of the colocalization between green (NL) and red (acidic organelles) fluorescent images was performed using Bitplane IMARIS imaging software (Zurich, Switzerland). To quantify the extent of NL-scFv uptake at different scFv doses, EC monolayers were first treated with TNF-α (10 ng/ml) and then treated with Texas Red®-labeled NLs conjugated with scFv doses; 20 (0.76), (50) 1.9 and 100 μg/ml (3.8 μM) for 30 min at 37^{o}C. EC monolayers were then gently rinsed twice with PBS prior to

fixation in 1% PFA. Fluorescent images (8 per condition) of NL-scFv-treated ECs were then acquired using an Sp5 Confocal Microscope (Leica, Germany) and net cell fluorescent intensities quantified using ImageJ software (NIH).

Monocyte-EC Adhesion Assay. To examine the effects of NTG and NTG-NL-scFv on U937-EC adhesion, EC monolayers were either treated with TNF-α (10 ng/ml) ± NTG (5 μM) for 4 hr or with TNF-α for 4 hr prior to treatment with NTG-NL-scFv for an additional 4 hr. Next, fluorescently-labeled (DAPI) human U937s (130,000 cells/cm^2) were added for 30 min at 37^{o}C. Following two rinses with PBS, adherent U937s were fixed with 1% PFA, imaged using Nikon Eclipse Ti microscope fitted with a Nikon DS-Qi1Mc camera, and counted using ImageJ (n = ≥10 images per condition).

NTG-NL Drug Release Kinetics. To measure the release kinetics of incorporated NTG, 1 mg/ml NTG-NL was suspended in water and incubated at 37°C for pre-determined time durations (0, 6, 12, and 48 hr) (n = 3 per time point). At the end of each time point NTG-NL was pelleted by ultracentrifugation at 60k rcf for 1.5 hr and pellets dissolved in 200 μl methanol for electrospray mass spectroscopy (ESI-MS) measurement of residual NTG.

Statistics. All data were obtained from multiple replicates and expressed as mean ± standard error of mean (SEM). Statistical significance was determined using analysis of variance (ANOVA; Graphpad Instat) followed by a Tukey's post-hoc analysis. Results

were considered significant if $p<0.05$ and were represented as $*p<0.05$, $**p<0.01$, or $***p<0.001$.

Results and Discussion

In modern medicine, antibodies including whole IgG and fragmented IgG (i.e. Fab, scFv) are being explored for treatment strategies. During PAH and DR activated ECs overexpress ICAM-1 resulting in leukocyte adhesion, the initial step of the vascular inflammation cascade,[92] making ICAM-1 an excellent molecular address for site-targeting nanotherapeutics.

More recently, scFv has been pursued for benefits including increased stability, long-term storage, and low production costs.[88] Importantly, scFv DNA sequences can be readily engineered for further functionalization onto NP surfaces.

Therefore, as a proof-of-concept study prior to exploring anti-ICAM scFv fragments, the site-targeting potential of whole ICAM-1 IgG was investigated. Whole anti-ICAM-1 IgG-modified NLs were synthesized using a combination of five lipids (DSPE-PEG_{2000}–COOH, DPhPC, POPC, Cholesterol, and DHPE-Texas Red) that spontaneously self-assemble in aqueous solution to form liposomes and subsequently extruded through 100 nm membranes to form nanoliposomes (NLs) (Fig. 4.1A). Once the NLs were surface modified, surface packing of anti-ICAM-1 antibody was quantified (Fig. 4.1B).

To demonstrate proof-of-concept *in vivo* targeting of whole-ICAM-1-modified NLs, mouse retina was inflamed using a pro-inflammatory cytokine, angiopoietin-2

(ANG-2), a known enhancer of ICAM-1 expression.[93] Upon intravenous injection of both modified and unmodified NLs (containing Texas red-labeled lipids to facilitate imaging), fluorescent images reveal that anti-ICAM-1-modified NLs preferentially accumulated within ICAM-1-expressing (ANG-2-treated) retinal vessels (Fig. 4.2A). Importantly, this was not observed with unmodified NLs (Fig. 4.2B and C). Upon successful targeting of NL-anti-ICAM IgG to inflamed mouse retinal vessels, engineering of anti-ICAM-1 scFv for superior NL-targeting was explored.

To render these NLs site-targeting, anti-ICAM-1 scFv was engineered using previously established variable Light and Heavy chain amino acid sequences[90] with a conventional $(Gly_3Ser)_4$ linker, and a reactive cysteine at the heavy chain terminus that would facilitate Maleimide-thiol surface chemistries (Fig.4.3A). Successful fusion of scFv DNA sequence into a pMopac vector and expression of scFv fragments was determined by DNA electrophoresis and SDS-PAGE (~26 kDa), respectively (Fig. 4.4B and 4.4C). To demonstrate the ability of scFv to bind human ECs, we added scFv to activated (TNF-α-stimulated) ECs. Flow cytometry measurements revealed that Anti-ICAM-1 bound activated ECs in a dose-dependent manner (Fig. 4.3B and Fig. 4.5).

As a building block for these NLs, we used a combination of five lipids (DSPE-PEG_{2000}–Maleimide, DPhPC, POPC, Cholesterol, and DHPE-Texas Red) as previously described (Fig. 4.3C). Specifically, to render NLs suitable for ICAM-1 targeting, DSPE-PEG_{2000}–Maleimide was incorporated within the lipid bilayer and serves two purposes: firstly, the Maleimide (M) group will permit chemical conjugation of a ICAM-1-targeting moiety (scFv) onto NL surface,[94] and secondly, poly (ethylene glycol) (PEG) chains will

provide “stealth” to the NLs so it can avoid capture by circulating immune cells, liver, and kidney.[85] To achieve ICAM-1-targeting, an anti-ICAM-1 scFv was chemically conjugated to the NL surface. ScFv will serve as the preferred targeting moiety because ICAM-1, an endothelial transmembrane protein, is significantly overexpressed (at ~30-fold greater density) in lung vessels compared to vessels in other organs.[95]

To confirm successful NL-scFv conjugation, we employed Maleimide-Thiol chemistry to covalently conjugate DSPE-PEG-Maleimide to increasing amounts of scFv to maximize surface packing on NL surface (Fig. 4.3D). The size distribution profile of NLs obtained using dynamic light scattering (DLS) revealed an average particle diameter of 144 ± 30 nm (Fig. 4.3E), which was independently confirmed by scanning electron microscopy (Fig. 4.3F).

NLs are known to enhance drug efficacy by simultaneously increasing drug half-life and facilitating rapid cellular uptake.[37,39,91] To determine how these NLs were uptaken by ECs, we stained NL-bound ECs with lysotracker to label intracellular acidic organelles (lysosomes/endosomes). Overlay of green (fluorescein-loaded NLs) and red (lysotracker) fluorescent images revealed a ~95% co-localization of green and red (Fig. 4.6A). These data suggest these NLs are endocytosed via conventional clathrin-mediated pathway.[66]

During PAH, infiltrating leukocytes (i.e. monocytes and lymphocytes) produce various potent inflammatory cytokines including TNF-α, which further activates resident ECs and creates a self-sustaining toxic microenvironment, *in vivo*.[92] Importantly, to demonstrate the capability of NL-scFv conjugates to preferentially bind activated ECs,

we added fluorescently-labeled NL-scFv conjugates to both untreated (without TNF-α) and TNF-α-stimulated ECs. Quantitative measurement of fluorescence intensity of NL-treated ECs revealed ~6-fold greater binding of NL-scFv conjugates to stimulated ECs compared to untreated control ($p<0.001$; Fig. 4.6B), thus verifying the potent ICAM-1-targeting capability of these NLs.

To demonstrate the therapeutic potential of these ICAM-1-targeting NLs for PAH and DR treatment, we tested their ability to inhibit U937 cell adhesion to TNF-α-stimulated ECs using an *in vitro* U937 cell-EC adhesion assay. In the present study we used NTG, a potent endothelial NO enhancer, recently discovered by our lab to exhibit significant anti-inflammatory effects.[91] We first confirmed the anti-inflammatory effects of free NTG on TNF-α-stimulated ECs by showing a dose-dependent inhibition of U937 cell adhesion (Fig. 4.7A). Next, NTG was incorporated into NLs at 10% (w/w) ratio as previously reported[91], and its release kinetics were evaluated over a 48 hr time period. ESI-MS quantitative measurements revealed an initial burst release of NTG lastly approximately 12 hr followed by a steady release over 48 hr, with approximately ~90% of the incorporated NTG being released over 48 hr (Fig. 4.7B). Importantly, to both demonstrate and compare the therapeutic efficacy of NTG-loaded NLs with and without scFv functionalization, we treated ECs with TNF-α for 4 hr followed by treatment with NTG-NL or NTG-NL-scFv for an additional 4 hr and quantified the adhesion of fluorescently-labeled U937s (Fig. 4.7C). Not only did we observe inhibition of U937 adhesion ($p<0.005$) to ECs treated with NTG-NL, but observed a ~2-fold greater inhibition of U937s with NTG-NL-scFv.

Conclusions

In summary, we have demonstrated a proof-of-concept for ICAM-1-targeting NL that could potentially provide superior treatment strategies for patients with PAH and DR and other inflammation-mediated (ICAM-1 overexpressing) disease states. In addition to exhibiting a ~6-fold greater site-targeting capability to activated endothelium, these nanomaterials may overcome the limitations associated with systemic drug delivery while delivering a remarkable anti-inflammatory and pro-vasculogenic effect, *in vitro*. Importantly, however, these nanomaterials will require further evaluation in animal models of PAH and DR.

More Importantly, there are numerous inflammation-mediated conditions that are marked by overexpression of ICAM-1 (i.e. ischemia reperfusion injury (IR/I) and atherosclerosis),[15,47] where this nanoliposomal drug delivery system can be leveraged using different classes of anti-inflammatory drugs. Further, this NL platform allows for conjugation of additional targeting moieties (i.e. antibody, aptamers, peptides), offering a wide spectrum of therapeutic opportunities making this system robust in its design and application.

Figures

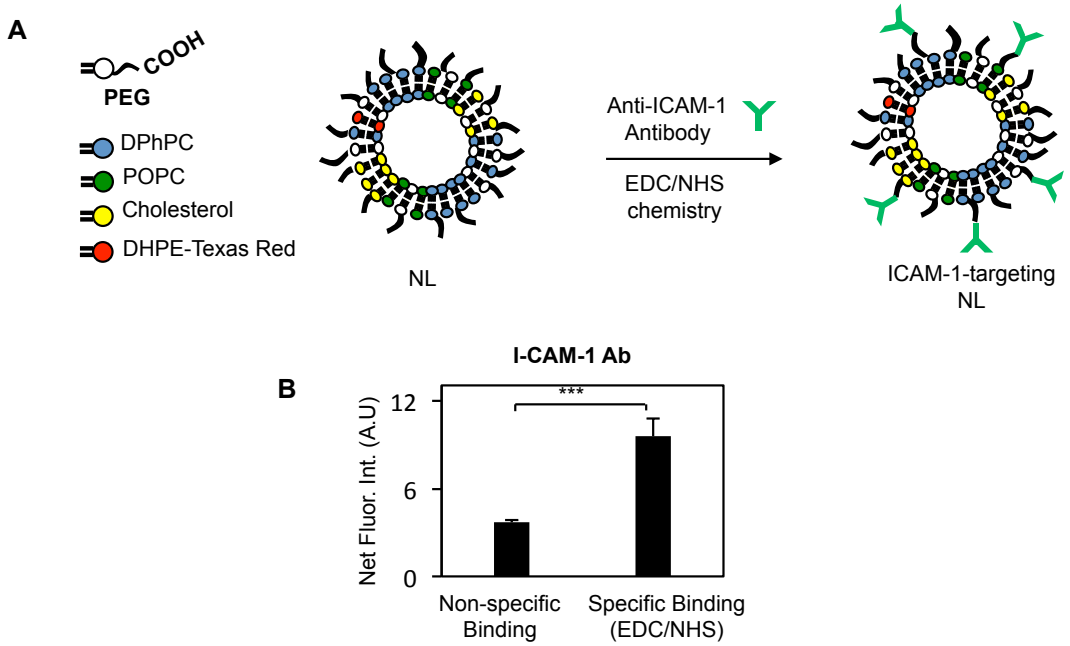

Fig. 4.1. Synthesis and Physicochemical Characterization of NL-anti-ICAM-1 IgG.

(**A**) Schematic depicting the synthesis of anti-ICAM-1 IgG modified nanoliposomes (NL-ICAM-1 IgG). Five lipids viz. DSPE-PEG-COOH, DPhPC, POPC, Cholesterol, and DHPE-Texas Red were combined to form NL in water. Anti-ICAM-1 antibody was conjugated on the surface of NL using EDC/NHS reaction chemistry to develop NL-ICAM-1. (**B**) To detect conjugation of anti-ICAM-1 to NL surface, NL-ICAM-1 was labeled with FITC-conjugated anti-mouse IgG. Anti-ICAM-1 conjugation to NL surface was quantified using a fluorescent microplate reader, which demonstrated a dose-dependent increase in scFv conjugation to the NL surface.

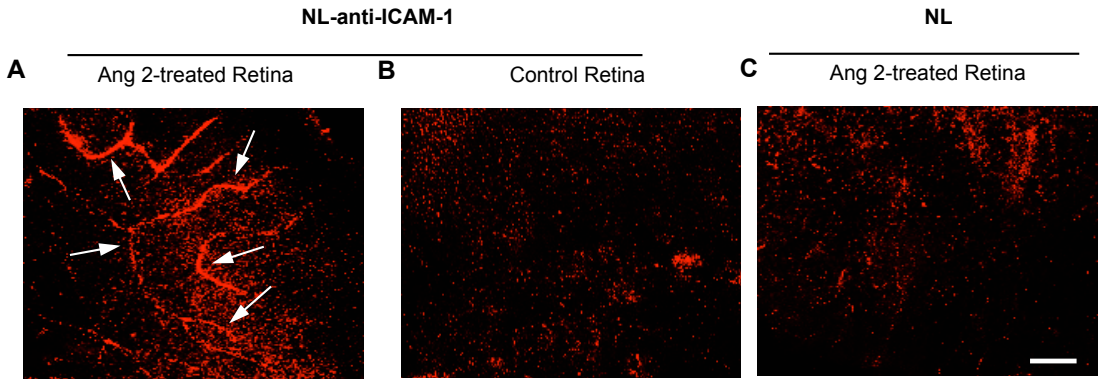

Fig. 4.2. NL-anti-ICAM-1 IgG Targets Inflamed Mouse Retinal Vessels

Demonstrates NTG-NL-anti-ICAM-1 preferential targeting to inflamed retinal vessels in vivo. To enhance ICAM1 expression in mouse retinal vessels, angiopoietin-2 (Ang-2) was injected in one eye of adult mice. Ang-2 is known to enhance ICAM-1 expression in vascular endothelial cells (ECs). The other eye that received no Ang-2 served as control. To evaluate site-targeting capability of anti-ICAM1-conjugated nanoliposomes (NL-anti-ICAM1), these or unconjugated (control) nanoliposomes were administered (I.V.) into the angiopoietin-2-treated mice. To facilitate imaging, nanoliposomes were labeled with a red fluorescent dye. As shown in the fluorescent images above, NL-anti-ICAM-1 preferentially accumulated within ICAM-1-expressing retinal vessels but not in control eyes (A, B). Importantly, this preferential targeting was not seen with unconjugated nanoliposomes (C). Scale Bar: 50 um

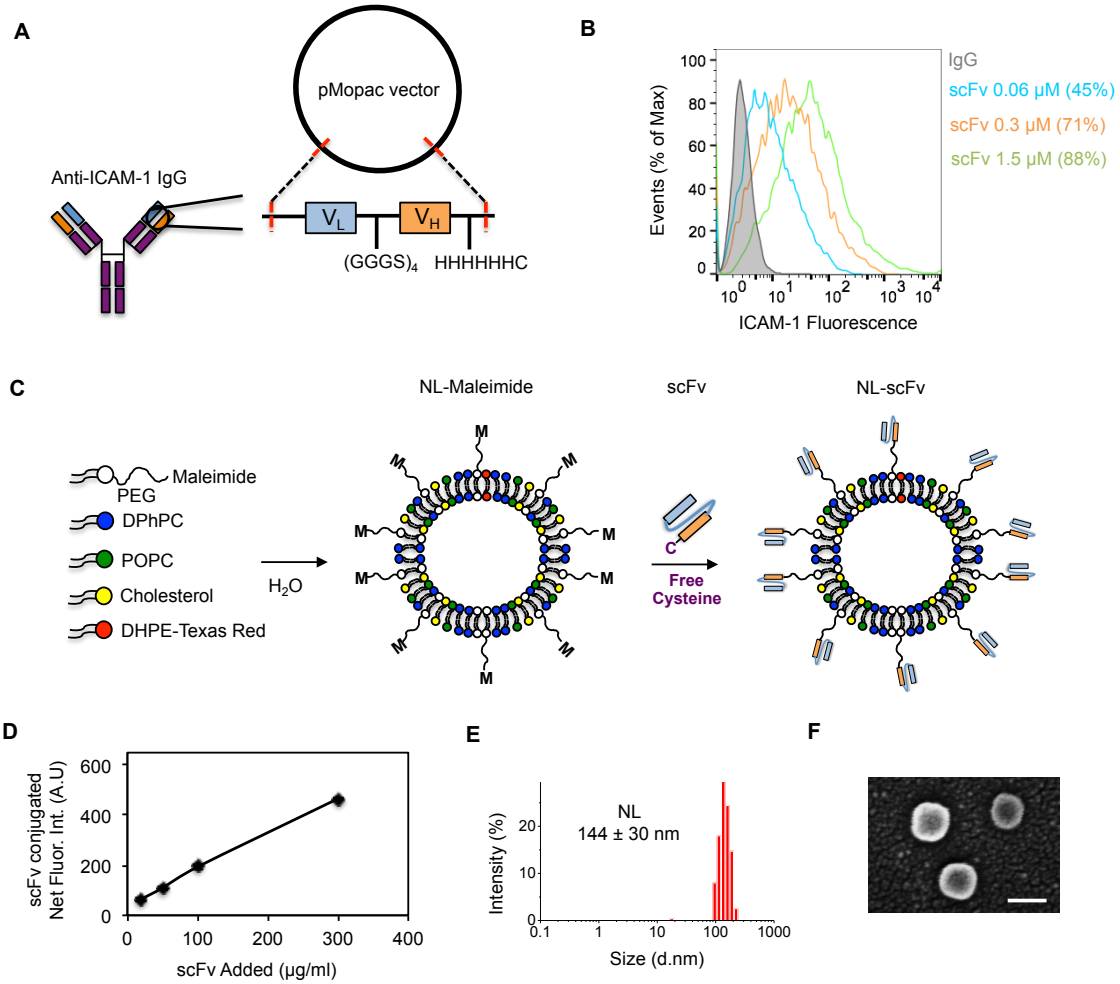
A
pMopac vector
Anti-ICAM-1 IgG
V_L
V_H
$(GGGS)_4$ HHHHHHC
B
IgG
scFv 0.06 μM (45%)
scFv 0.3 μM (71%)
scFv 1.5 μM (88%)
Events (% of Max)
ICAM-1 Fluorescence
C
NL-Maleimide
scFv
NL-scFv
Maleimide
PEG
DPhPC
POPC
Cholesterol
DHPE-Texas Red
H_2O
Free
Cysteine
D
scFv conjugated
Net Fluor. Int. (A.U)
scFv Added (μg/ml)
E
NL
144 ± 30 nm
Intensity (%)
Size (d.nm)
F

Fig. 4.3. Synthesis and Physicochemical Characterization of scFv and NL-scFv.

(**A**) Schematic diagram describing the cloning strategy for constructing scFv fragments of ICAM-1 antibody in vector. Variable domains of heavy chain (V_H) and light chain (V_L) were linked together and then fused with histidine $(HIS)_6$ tag and terminal free cysteine (C). (**B**) Flow cytometry plots indicate dose-dependent binding of scFv to ICAM-1-expressing ECs at 0.06, 0.3 and 1.5 μM. (**C**) Schematic depicting the synthesis of scFv-modified nanoliposomes (NL-scFv). Five lipids viz. DSPE-PEG-Maleimide, DPhPC, POPC, Cholesterol, and DHPE-Texas Red were combined to form NL in water. ScFv fragments were conjugated on the surface of NL using maleimide-thiol reaction chemistry to develop NL-scFv. (**D**) To detect conjugation of scFv to NL surface, NL-scFv was labeled with mouse anti-HIS antibody followed by FITC-conjugated anti-mouse IgG. ScFv conjugation to NL surface was quantified using a fluorescent microplate reader, which demonstrated a dose-dependent increase in scFv conjugation to the NL surface. (**E**) Dynamic Light Scattering (DLS) analysis reveals NL has diameter of ~144 nm. (**F**) Size distribution of NL was further confirmed using scanning electron microscope (SEM). *Scale bar:* 100 nm. Data are expressed as mean ± Std. Dev.

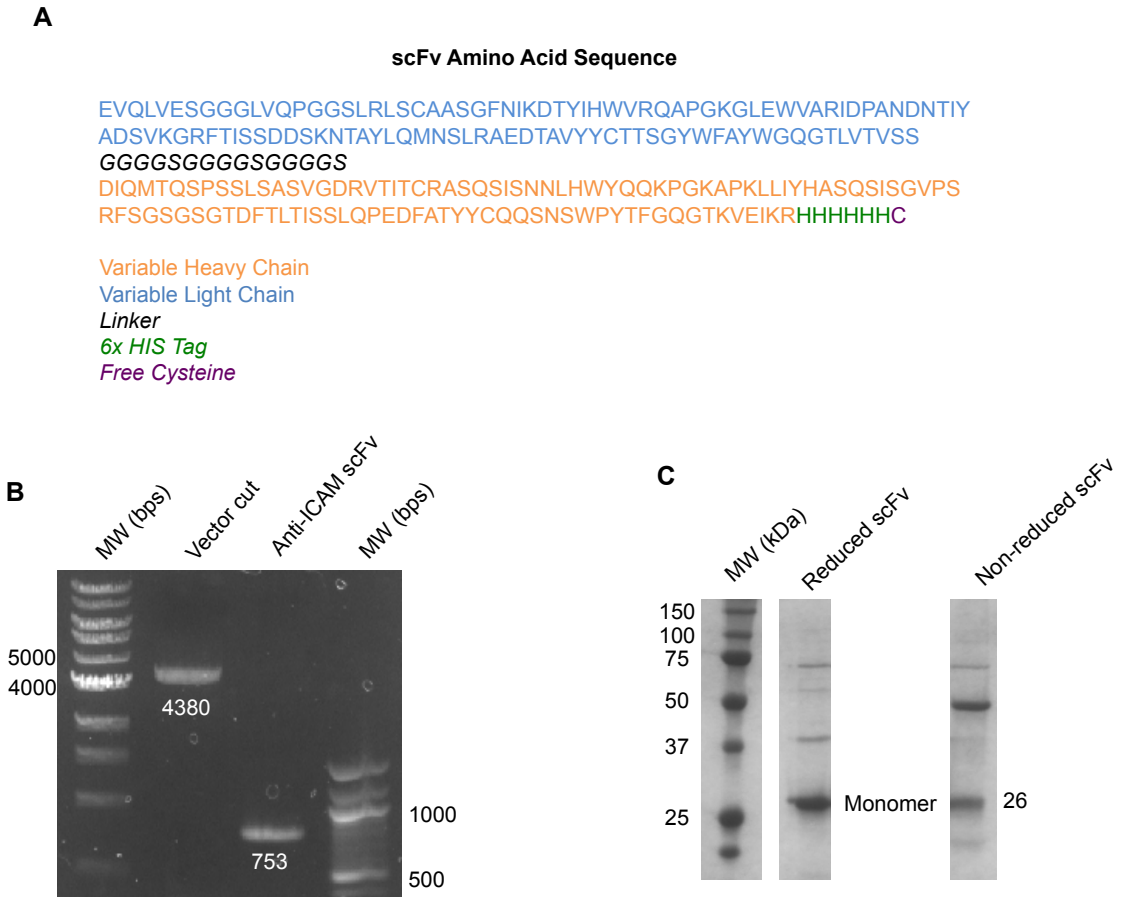

Fig. 4.4. Synthesis and Characterization of anti-ICAM-1 scFv.

(**A**) The entire amino acid sequence of the human anti-ICAM-1 scFv fragment is shown where orange represents variable light chain followed by a linker and variable heavy chain shown in blue. (**B**) Fusion construct was digested to isolate anti-ICAM-1 scFv nucleotide sequence from vector. (**C**) Western blot analysis of purified anti-ICAM-1 scFv fragment under reduced and non-reduced conditions.

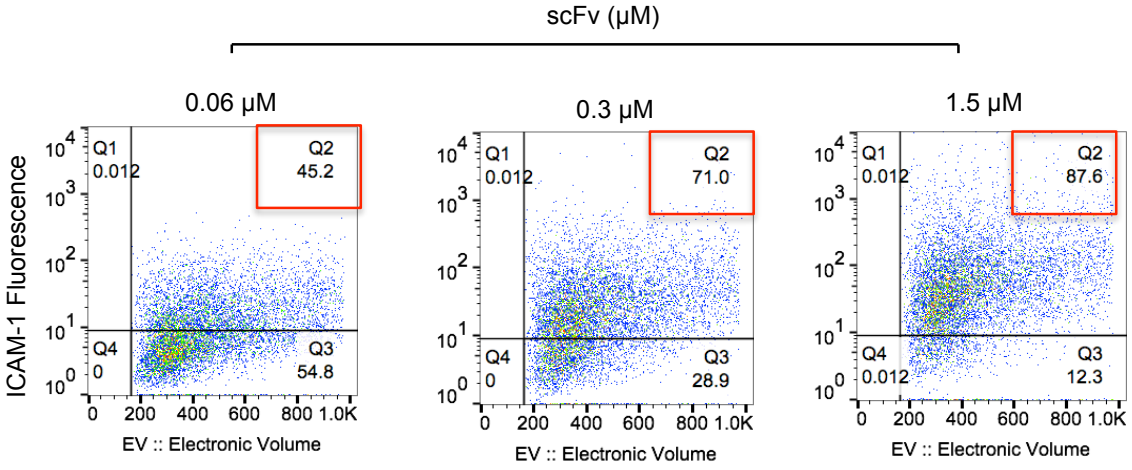

Fig. 4.5. Flow cytometry analysis of anti-ICAM-1 scFv binding to ECs.

Flow cytometry analysis reveals a dose-dependent increase in scFv binding to ECs treated with TNF-α (10 ng/ml) as quantified in the dot plots as percent population shift from IgG.

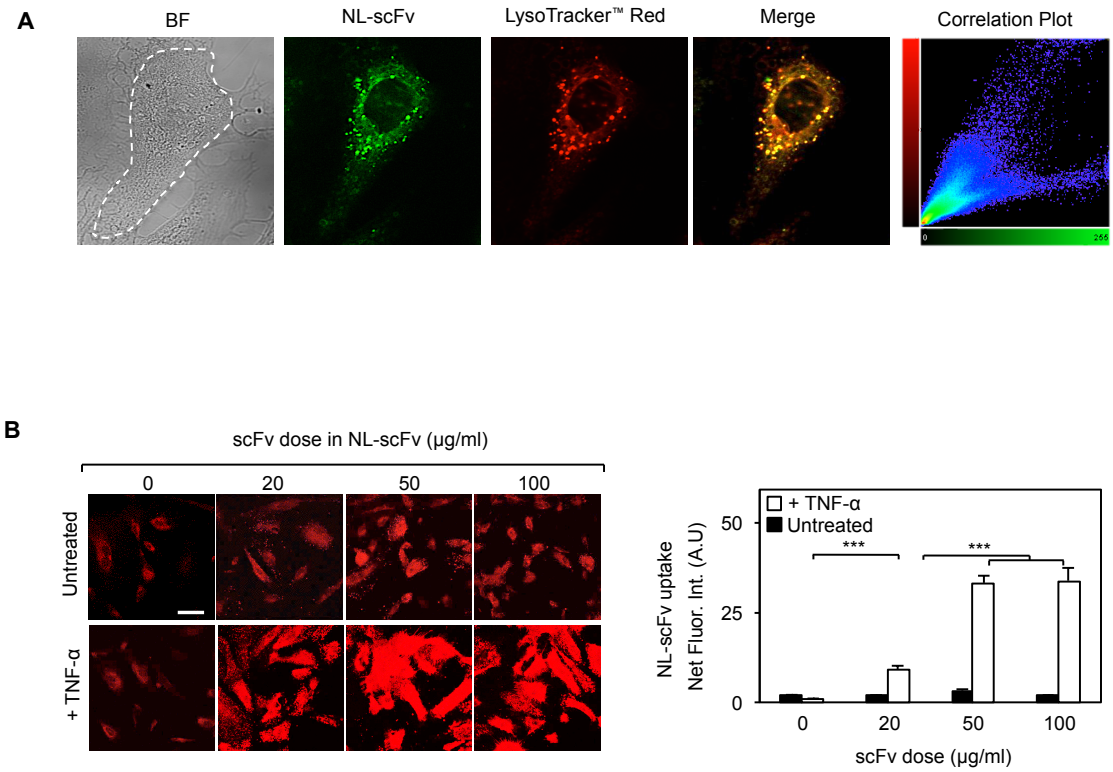

Fig. 4.6. NL-scFv Are Preferentially Uptaken by ECs Under Inflammatory Conditions.

(A) Fluorescent images of internalized NLs demonstrate strong colocalization (~95% colocalization of green and red) with LysoTracker Red™-labeled endocytic vesicles (endosomes and lysosomes). *Scale bar:* 25 µm. (**B**) Fluorescent images of internalized NL-scFv show compared to untreated ECs, ECs stimulated with TNF-α (10 ng/ml) significantly uptake NL-scFv in a dose-dependent manner as quantified in the bar graph ($n \geq 20$). ***, $p<0.001$. *Scale bar:* 100 µm.

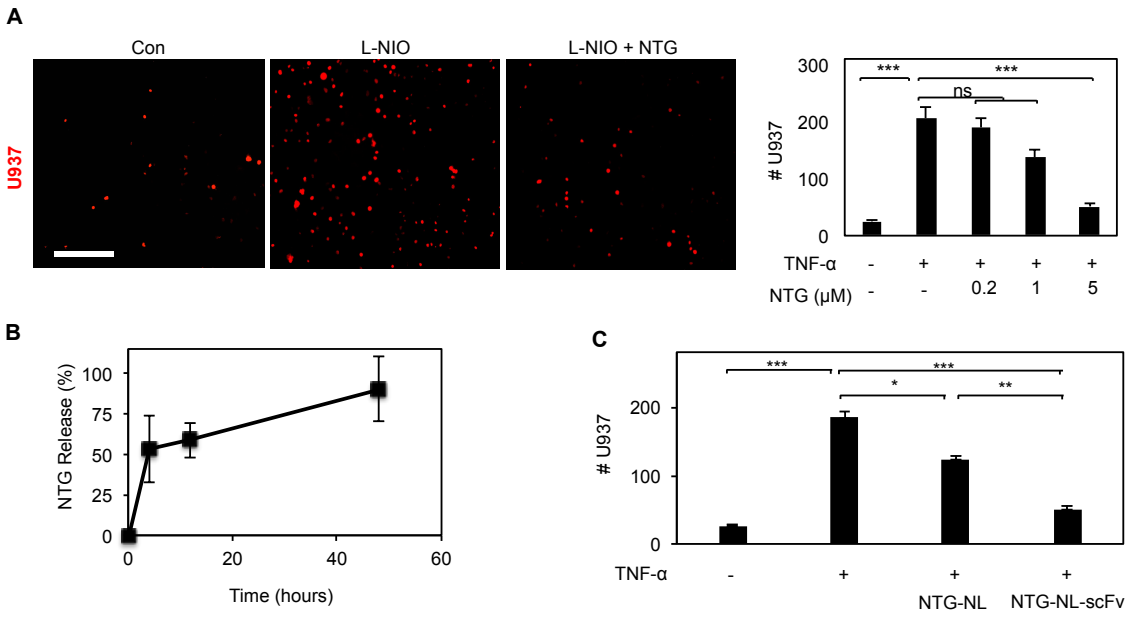

Fig. 4.7. NTG-NL-scFv Exhibits Potent Anti-Inflammatory Effects.

(**A**) NTG produces dose-dependent inhibition of U937 cell adhesion to TNF-α-treated (10 ng/ml) ECs, with significant suppression of U937 cell-EC adhesion as shown in the bar graph (n = 8 fields of view). ***, $p<0.001$. (**B**) NTG was encapsulated within nanoliposomes at 10% (w/w) and drug release measured over 48 hr using mass spectrometry. (**C**) To examine the anti-inflammatory effects of NTG-NL-scFv, PAEC monolayers were first treated with TNF-α (10 ng/ml), followed by addition of NTG-NL or NTG-NL-scFv (5 μg/ml) for 4 hr. Quantification of adherent U937 cells revealed that NTG-NL-scFv produces a 2.5-fold greater anti-inflammatory effect than non-modified NTG-NL. *, $p<0.05$ **, $p<0.01$; ***, $p<0.001$.

Chapter 5:

Conclusions

Using a combination of analytical NO measurement, microfluorimetry, vasculogenesis and monocyte-endothelial adhesion assays, immunofluorescence staining, and high-resolution confocal and phase contrast microscopy, it was demonstrated that (a) NTG significantly inhibits monocyte adhesion to NO-deficient ECs via suppression of endothelial ICAM-1 clustering, and (b) NTG prevents EC capillary regression in NO-deficient ECs by preventing the loss of actin cytoskeleton-dependent endothelial adhesion. Thus, these studies implicate NTG as a multi-purpose drug for treatment of both DR and PAH that are marked by vascular constriction, inflammation, and regression.

Further, quantitative assessment of mitochondrial superoxide formation and monocyte-EC adhesion demonstrated that NTG-NL produces a remarkable 70-fold (suppression of monocyte-EC adhesion) and 35-fold (prevention of capillary regression) increase in NTG efficacy when compared with free NTG, and as a consequence, prevents tolerance in cultured ECs treated with clinically-administered high doses of NTG. Importantly, these *in vitro* observations correlated strongly with my *ex vivo* findings that show loss of lung arterial vasorelaxation caused by high doses of free NTG was completely abolished by treatment with a similar-fold higher doses of NTG-NL. These findings indicate that NTG-NL has the potential to significantly improve the benefit/risk profile of NTG therapy.

Importantly, the benefit/risk profile of NTG therapy was further improved by delivering NTG-NL selectively to sites of vascular defect. Since both PAH and DR are marked by increased endothelial ICAM-1 expression, non-immunogenic single chain variable fragment (scFv) of ICAM-1 antibody was engineered and tethered to the surface of NTG-NL. *In vitro* studies revealed that NTG-NL modified with anti-ICAM-1 scFv exhibits 6-fold greater binding to inflamed (ICAM-1-expressing) ECs than to normal ECs and achieves superior anti-inflammatory effects *in vitro* when compared with unconjugated NTG-NL. Thus, these findings provide the rationale to examine this novel site-targeting NTG nanotherapeutic as a potentially superior therapy for various inflammation-mediated conditions.

Working Model

The findings from my studies indicate important mechanisms that can leverage NTG and NTG-NL for treatment of chronic vascular inflammation. Specifically, to recapitulate disease conditions marked by reduced eNOS/NO bioavailability, we used L-NIO, a pharmacological eNOS inhibitor, (Schematic 5.1A and B), to reduce NO production levels (Schematic 5.1C). In turn, this decrease in NO[62] likely increased Rho/ROCK activity[63] (Schematic 5.1D) causing a significant increase in actin fiber density, a key regulator of actin cytoskeletal polymerization.[96] Importantly, this increase in actin fiber formation likely contributed to ICAM-1 clustering and enhanced monocyte-EC adhesion (Schematic 5.1E and F).

Consistent with these observations, I proposed the use of Free NTG and NTG-NL to treat conditions marked by eNOS/NO deficiency. Specifically, we have shown NTG

and NTG-NL to enhance *both* eNOS expression and NO production (Schematic 5.1G and H). NTG-NL conjugated with anti-ICAM-1 scFv will selectively bind ICAM-1 and likely be uptaken via early endosomes via clathrin-mediated endocytosis (Schematic 5.1I). These NTG-NL-containing vesicles will then transport the cargo to the EC perinuclear region (Schematic 5.1K) while recycling ICAM-1 back towards the EC surface (Schematic 5.1J).[97] Importantly, once arriving to the EC perinuclear region, it is likely these NLs are degraded within these acidic organelles and NTG is released intracellularly where it can enhance eNOS expression and subsequent NO bioavailability (Schematic 5.1L) to suppress monocyte-EC adhesion. Further, my findings demonstrate that while high-dose NTG treatment enhances superoxide production, NTG-NL does not (Schematic 5.1M). Thus, the proposed therapy would allow for a new anti-inflammatory drug delivery system while addressing the limitations associated with conventional NTG therapies.

Future Directions

To further minimize phagocytic clearance, and consequently, enhance overall circulation time and site-targeting potential of the site-targeting nanotherapeutic, one can leverage the principles of nature (biomimicry) to develop nanoparticles derived from red blood cell (RBC) lipid membrane.[98,99] These 'RBC-NPs' can also be surface modified with the engineered human anti-ICAM-1 scFv and loaded with anti-inflammatory drugs for *in vitro/in vivo* studies. This nanotechnological approach, which is expected to confer superior "stealth" to these biomimetic anti-inflammatory nanoparticles, has the potential

to provide an injectable, safe, and highly effective alternative to the current clinical practice of free drug administration that produces undesirable adverse effects.

Additionally, the anti-inflammatory and pro-vasculogenic effects of the proposed site-targeting nanotherapeutic should be evaluated *in vivo*, in mice. To do so, development of an anti-ICAM-1 scFv that can target mouse ICAM-1 is essential. To address this need, collaboration with an industrial custom antibody service is ongoing to generate scFv fragments by screening a mouse ICAM-1 antigen against a proprietary naïve human scFv phage display library.

Following successful completion of the proposed studies, the production of our ICAM-1 site-targeting nanotherapeutic will be subcontracted to a Good Manufacturing Practice (GMP)-certified company to ensure high quality and reproducibility of our product. Specifically, we will target companies that manufacture NTG: Novasep, Baxter, and Pfizer and/or treat inflammatory conditions: Actellion and GSK. Next, we will evaluate its therapeutic effect in wound healing, ischemic neovascularization, vasodilation and inflammation studies in larger animals such as pigs, sheep, and/or monkeys. If successful, we aim to license this technology to pharmaceutical/biomedical companies that have an interest in diabetes, cardiovascular sciences, or nanomedicine.

Working Model

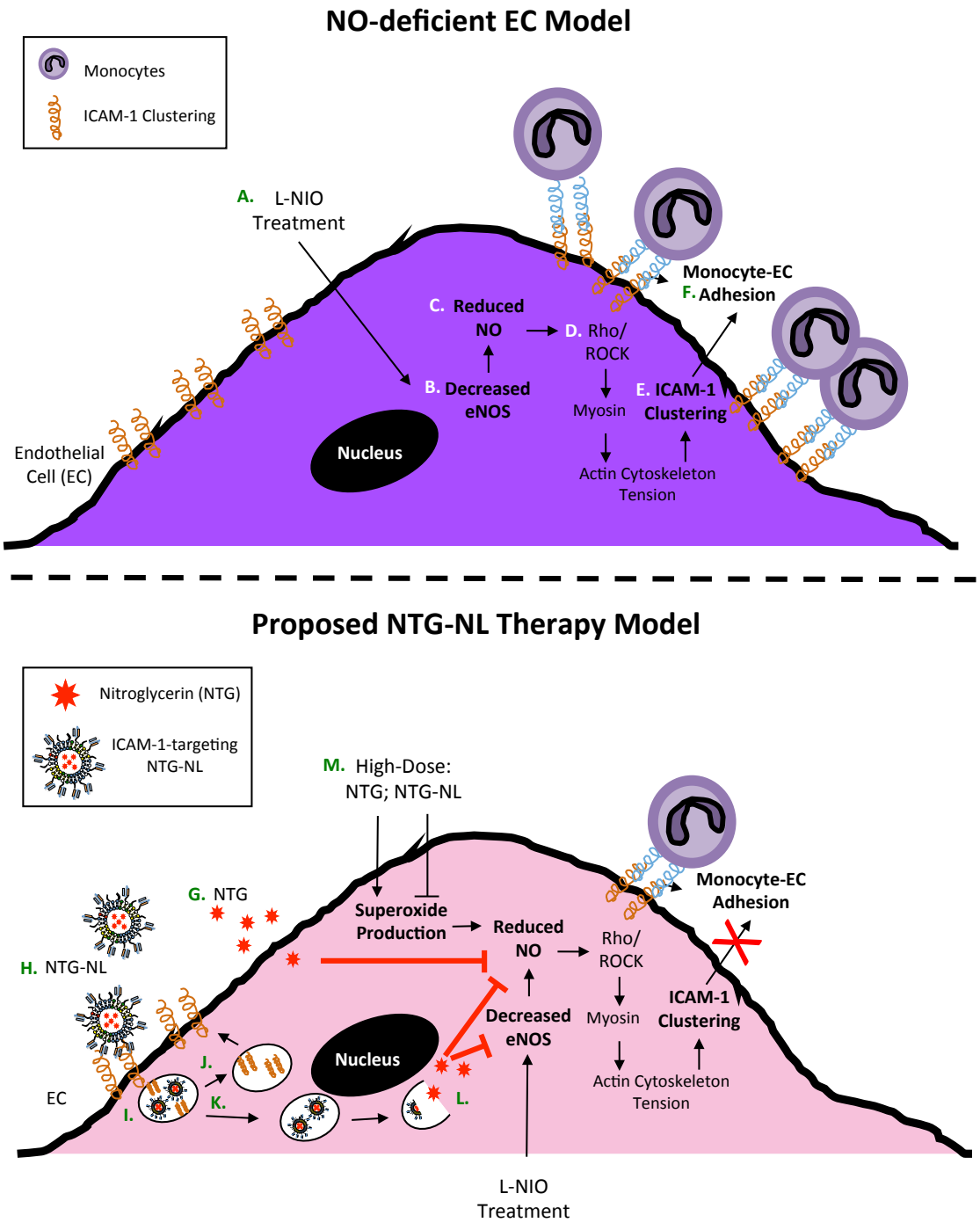

Schematic 5.1. Illustration of the mechanism behind NO-dependent vascular inflammation and therapeutic recovery using NTG and NTG-NL.

References

1 Pober, J. S. & Sessa, W. C. Evolving functions of endothelial cells in inflammation. *Nature Reviews Immunology* **7**, 803-815, doi:Doi 10.1038/Nri2171 (2007).

2 Bogdan, C. Nitric oxide and the immune response. *Nature Immunology* **2**, 907-916, doi:10.1038/ni1001-907 (2001).

3 Decaterina, R. *et al.* Nitric-Oxide Decreases Cytokine-Induced Endothelial Activation - Nitric-Oxide Selectively Reduces Endothelial Expression of Adhesion Molecules and Proinflammatory Cytokines. *J Clin Invest* **96**, 60-68, doi:Doi 10.1172/Jci118074 (1995).

4 Crosswhite, P. & Sun, Z. J. Nitric oxide, oxidative stress and inflammation in pulmonary arterial hypertension. *Journal of Hypertension* **28**, 201-212, doi:Doi 10.1097/Hjh.0b013e328332bcdb (2010).

5 Humbert, M. *et al.* Risk factors for pulmonary arterial hypertension. *Clinics in Chest Medicine* **22**, 459-475 (2001).

6 Wright, J. L., Levy, R. D. & Churg, A. Pulmonary hypertension in chronic obstructive pulmonary disease: current theories of pathogenesis and their implications for treatment. *Thorax* **60**, 605-609, doi:10.1136/thx.2005.042994 (2005).

7 Yamato, H., Sun, J. P., Churg, A. & Wright, J. L. Guinea pig pulmonary hypertension caused by cigarette smoke cannot be explained by capillary bed destruction. *J Appl Physiol (1985)* **82**, 1644-1653 (1997).

8 Hyduk, A. *et al.* Pulmonary hypertension surveillance--United States, 1980-2002. *Morbidity and mortality weekly report. Surveillance Summaries* **54**, 1-28 (2005).

9 Thenappan, T., Shah, S. J., Rich, S. & Gomberg-Maitland, M. A USA-based registry for pulmonary arterial hypertension: 1982-2006. *Eur Respir J* **30**, 1103-1110, doi:10.1183/09031936.00042107 (2007).

10 Marc Humbert, D. M., Oleg V. Evgenov, and Gaerald Simonneau. in *Handbook of Experimental Pharmacology* Vol. 218 Ch. Definition and Classification of Pulmonary Hypertension, 3-5 (2013).

11 Loscalzo, B. A. M. a. J. in *Handbook of Experimental Pharmacology* Vol. 218 Ch. Pulmonary Hypertension: Pathophysiology and Signaling Pathways, 33-37 (2013).

12 Giaid, A. & Saleh, D. Reduced expression of endothelial nitric oxide synthase in the lungs of patients with pulmonary hypertension. *The New England Journal of Medicine* **333**, 214-221, doi:10.1056/NEJM199507273330403 (1995).

13 Stenmark, K. R., Davie, N. J., Reeves, J. T. & Frid, M. G. Hypoxia, leukocytes, and the pulmonary circulation. *J Appl Physiol* **98**, 715-721, doi:Doi 10.1152/Japplphysiol.00840.2004 (2005).

14 Yau, J. W. *et al.* Global prevalence and major risk factors of diabetic retinopathy. *Diabetes Care* **35**, 556-564, doi:10.2337/dc11-1909 (2012).

15 Joussen, A. M. *et al.* A central role for inflammation in the pathogenesis of diabetic retinopathy. *Faseb J* **18**, 1450-1452, doi:10.1096/fj.03-1476fje (2004).

16 Rangasamy, S., McGuire, P. G. & Das, A. Diabetic retinopathy and inflammation: novel therapeutic targets. *Middle East African Journal of Ophthalmology* **19**, 52-59, doi:10.4103/0974-9233.92116 (2012).

17 Li, Q. *et al.* Diabetic eNOS-knockout mice develop accelerated retinopathy. *Investigative Ophthalmology & Visual Science* **51**, 5240-5246, doi:10.1167/iovs.09-5147 (2010).

18 Tang, J. & Kern, T. S. Inflammation in diabetic retinopathy. *Prog Retin Eye Res* **30**, 343-358, doi:10.1016/j.preteyeres.2011.05.002 (2011).

19 Channick, R. N. Pulmonary hypertension: Classification and treatment. *Canadian Journal of Cardiology* **26**, 5b-11b (2010).

20 Fuso, L., Baldi, F. & Di Perna, A. Therapeutic strategies in pulmonary hypertension. *Frontiers in Pharmacology* **2**, 21, doi:10.3389/fphar.2011.00021 (2011).

21 Abman, S. H. in *Handbook of experimental pharmacology* Vol. 218 Ch. Inhaled Nitric Oxide for the Treatment of Pulmonary Arterial Hypertension, 257-258 (2013).

22 Kinsella, J. P. & Abman, S. H. Inhaled nitric oxide in the premature infant: animal models and clinical experience. *Seminars in Perinatology* **21**, 418-425 (1997).

23 Gardlik, R. & Fusekova, I. Pharmacologic therapy for diabetic retinopathy. *Seminars in Ophthalmology* **30**, 252-263, doi:10.3109/08820538.2013.859280 (2015).

24 Simo, R., Sundstrom, J. M. & Antonetti, D. A. Ocular Anti-VEGF therapy for diabetic retinopathy: the role of VEGF in the pathogenesis of diabetic retinopathy. *Diabetes Care* **37**, 893-899, doi:10.2337/dc13-2002 (2014).

25 Brown, D. M. *et al.* Long-term outcomes of ranibizumab therapy for diabetic macular edema: the 36-month results from two phase III trials: RISE and RIDE. *Ophthalmology* **120**, 2013-2022, doi:10.1016/j.ophtha.2013.02.034 (2013).

26 Elman, M. J. *et al.* Randomized trial evaluating ranibizumab plus prompt or deferred laser or triamcinolone plus prompt laser for diabetic macular edema. *Ophthalmology* **117**, 1064-1077 e1035, doi:10.1016/j.ophtha.2010.02.031 (2010).

27 Elman, M. J. *et al.* Intravitreal ranibizumab for diabetic macular edema with prompt versus deferred laser treatment: three-year randomized trial results. *Ophthalmology* **119**, 2312-2318, doi:10.1016/j.ophtha.2012.08.022 (2012).

28 Das, A., McGuire, P. G. & Rangasamy, S. Diabetic Macular Edema: Pathophysiology and Novel Therapeutic Targets. *Ophthalmology* **122**, 1375-1394, doi:10.1016/j.ophtha.2015.03.024 (2015).

29 Campochiaro, P. A. *et al.* Long-term benefit of sustained-delivery fluocinolone acetonide vitreous inserts for diabetic macular edema. *Ophthalmology* **118**, 626-635 e622, doi:10.1016/j.ophtha.2010.12.028 (2011).

30 Fung, H. L. Biochemical mechanism of nitroglycerin action and tolerance: Is this old mystery solved? *Annu Rev Pharmacol* **44**, 67-85, doi:Doi 10.1146/Annurev.Pharmtox.44.101802.121646 (2004).

31 Daiber, A. *et al.* Oxidative stress and mitochondrial aldehyde dehydrogenase activity: A comparison of pentaerythritol tetranitrate with other organic nitrates. *Mol Pharmacol* **66**, 1372-1382, doi:Doi 10.1124/Mol.104.002600 (2004).

32 Bonini, M. G. *et al.* Constitutive nitric oxide synthase activation is a significant route for nitroglycerin-mediated vasodilation. *Proc Natl Acad Sci U S A* **105**, 8569-8574, doi:10.1073/pnas.0708615105 (2008).

33 El Kebir, D. *et al.* The anti-inflammatory effect of inhaled nitric oxide on pulmonary inflammation in a swine model. *Canadian Journal of Physiology and pharmacology* **83**, 252-258, doi:10.1139/y05-008 (2005).

34 Lacoste, L. L., Theroux, P., Lidon, R. M., Colucci, R. & Lam, J. Y. Antithrombotic properties of transdermal nitroglycerin in stable angina pectoris. *Am J Cardiol* **73**, 1058-1062 (1994).

35 Sydow, K. *et al.* Central role of mitochondrial aldehyde dehydrogenase and reactive oxygen species in nitroglycerin tolerance and cross-tolerance. *J Clin Invest* **113**, 482-489, doi:10.1172/JCI19267 (2004).

36 Daiber, A. *et al.* Mitochondrial aldehyde dehydrogenase (ALDH-2)--maker of and marker for nitrate tolerance in response to nitroglycerin treatment. *Chem Biol Interact* **178**, 40-47, doi:10.1016/j.cbi.2008.09.003 (2009).

37 Shi, J., Votruba, A. R., Farokhzad, O. C. & Langer, R. Nanotechnology in drug delivery and tissue engineering: from discovery to applications. *Nano Lett* **10**, 3223-3230, doi:10.1021/nl102184c (2010).

38 Peer, D. *et al.* Nanocarriers as an emerging platform for cancer therapy. *Nature Nanotechnology* **2**, 751-760 (2007).

39 Ghosh, K., Kanapathipillai, M., Korin, N., McCarthy, J. R. & Ingber, D. E. Polymeric nanomaterials for islet targeting and immunotherapeutic delivery. *Nano Lett* **12**, 203-208, doi:10.1021/nl203334c (2012).

40 Kolhar, P. *et al.* Using shape effects to target antibody-coated nanoparticles to lung and brain endothelium. *Proc Natl Acad Sci U S A* **110**, 10753-10758, doi:Doi 10.1073/Pnas.1308345110 (2013).

41 Chen, Y., Zhu, X., Zhang, X., Liu, B. & Huang, L. Nanoparticles modified with tumor-targeting scFv deliver siRNA and miRNA for cancer therapy. *Molecular therapy : the journal of the American Society of Gene Therapy* **18**, 1650-1656, doi:10.1038/mt.2010.136 (2010).

42 Chacko, A. M., Hood, E. D., Zern, B. J. & Muzykantov, V. R. Targeted Nanocarriers for Imaging and Therapy of Vascular Inflammation. *Current Opinion in Colloid & Interface Science* **16**, 215-227, doi:10.1016/j.cocis.2011.01.008 (2011).

43 Rabinovitch, M. Molecular pathogenesis of pulmonary arterial hypertension. *J Clin Invest* **122**, 4306-4313, doi:10.1172/JCI60658 (2012).

44 Tousoulis, D., Kampoli, A. M., Tentolouris, C., Papageorgiou, N. & Stefanadis, C. The role of nitric oxide on endothelial function. *Curr Vasc Pharmacol* **10**, 4-18 (2012).

45 Zhang, Y. X., Janssens, S. P., Wingler, K., Schmidt, H. H. H. W. & Moens, A. L. Modulating endothelial nitric oxide synthase: a new cardiovascular therapeutic strategy. *Am J Physiol-Heart C* **301**, H634-H646, doi:Doi 10.1152/Ajpheart.01315.2010 (2011).

46 Stokes, K. Y. *et al.* Dietary nitrite prevents hypercholesterolemic microvascular inflammation and reverses endothelial dysfunction. *Am J Physiol-Heart C* **296**, H1281-H1288, doi:Doi 10.1152/Ajpheart.01291.2008 (2009).

47 Herman, A. G. & Moncada, S. Therapeutic potential of nitric oxide donors in the prevention and treatment of atherosclerosis. *Eur Heart J* **26**, 1945-1955, doi:10.1093/eurheartj/ehi333 (2005).

48 Omar, S. A., Artime, E. & Webb, A. J. A comparison of organic and inorganic nitrates/nitrites. *Nitric Oxide* **26**, 229-240, doi:10.1016/j.niox.2012.03.008 (2012).

49 Chen, Z., Zhang, J. & Stamler, J. S. Identification of the enzymatic mechanism of nitroglycerin bioactivation. *Proc Natl Acad Sci U S A* **99**, 8306-8311, doi:10.1073/pnas.122225199 (2002).

50 Mao, M. *et al.* Nitroglycerin drives endothelial nitric oxide synthase activation via the phosphatidylinositol 3-kinase/protein kinase B pathway. *Free Radical Biology & medicine* **52**, 427-435, doi:10.1016/j.freeradbiomed.2011.09.020 (2012).

51 Farokhzad, O. C. & Langer, R. Impact of nanotechnology on drug delivery. *ACS Nano* **3**, 16-20, doi:10.1021/nn900002m (2009).

52 Ades, E. W. *et al.* HMEC-1: establishment of an immortalized human microvascular endothelial cell line. *J Invest Dermatol* **99**, 683-690 (1992).

53 Knorr, M. *et al.* Nitroglycerin-induced endothelial dysfunction and tolerance involve adverse phosphorylation and S-Glutathionylation of endothelial nitric oxide synthase: beneficial effects of therapy with the AT1 receptor blocker telmisartan. *Arteriosclerosis, Thrombosis, and Vascular Biology* **31**, 2223-2231, doi:10.1161/ATVBAHA.111.232058 (2011).

54 Yoshizumi, M., Perrella, M. A., Burnett, J. C., Jr. & Lee, M. E. Tumor necrosis factor downregulates an endothelial nitric oxide synthase mRNA by shortening its half-life. *Circulation Research* **73**, 205-209 (1993).

55 Bouzin, C., Brouet, A., De Vriese, J., DeWever, J. & Feron, O. Effects of vascular endothelial growth factor on the lymphocyte-endothelium interactions: Identification of caveolin-1 and nitric oxide as control points of endothelial cell anergy. *J Immunol* **178**, 1505-1511 (2007).

56 Parker, J. D. & Parker, J. O. Nitrate therapy for stable angina pectoris. *New Engl J Med* **338**, 520-531 (1998).

57 Uxa, A., Thomas, G. R., Gori, T. & Parker, J. D. Standard versus low-dose transdermal nitroglycerin: differential effects on the development of tolerance and

abnormalities of endothelial function. *J Cardiovasc Pharmacol* **56**, 354-359, doi:10.1097/FJC.0b013e3181ed2dae (2010).

58 Liuni, A. *et al.* Coadministration of atorvastatin prevents nitroglycerin-induced endothelial dysfunction and nitrate tolerance in healthy humans. *Journal of the American College of Cardiology* **57**, 93-98, doi:10.1016/j.jacc.2010.07.037 (2011).

59 Peschka, R., Dennehy, C. & Szoka, F. C., Jr. A simple in vitro model to study the release kinetics of liposome encapsulated material. *J Control Release* **56**, 41-51 (1998).

60 Nie, S. D. *et al.* Reversal of tolerance to nitroglycerin with vinpocetine: A role of calcitonin gene-related peptide. *Int J Cardiol* **125**, 436-438, doi:Doi 10.1016/J.Ijcard.2007.06.041 (2008).

61 Schnoor, M. Endothelial actin-binding proteins and actin dynamics in leukocyte transendothelial migration. *J Immunol* **194**, 3535-3541, doi:10.4049/jimmunol.1403250 (2015).

62 Loirand, G. & Pacaud, P. The role of Rho protein signaling in hypertension. *Nature Reviews. Cardiology* **7**, 637-647, doi:10.1038/nrcardio.2010.136 (2010).

63 Wojciak-Stothard, B., Williams, L. & Ridley, A. J. Monocyte adhesion and spreading on human endothelial cells is dependent on Rho-regulated receptor clustering. *The Journal of Cell Biology* **145**, 1293-1307 (1999).

64 Cotechini, T., Othman, M. & Graham, C. H. Nitroglycerin prevents coagulopathies and foetal death associated with abnormal maternal inflammation in rats. *Thromb Haemost* **107**, 864-874, doi:10.1160/TH11-10-0730 (2012).

65 Katzung, M. S. B. & Trevor, A. J. in *Basic and Clinical Pharmacology* Ch. 12, (2007).

66 R.Muzykantov, V. Targeted Drug Delivery to Endothelial Adhesion Molecules. *ISRN Vascular Medicine* **2013**, 1-27, doi:10.1155/2013/916254 (2013).

67 Torchilin, V. P. Recent advances with liposomes as pharmaceutical carriers. *Nature Reviews Drug Discovery* **4**, 145-160, doi:Doi 10.1038/Nrd1632 (2005).

68 Immordino, M. L., Dosio, F. & Cattel, L. Stealth liposomes: review of the basic science, rationale, and clinical applications, existing and potential. *Int J Nanomedicine* **1**, 297-315 (2006).

69 Voelkel, N. F., Gomez-Arroyo, J., Abbate, A., Bogaard, H. J. & Nicolls, M. R. Pathobiology of pulmonary arterial hypertension and right ventricular failure. *Eur Respir J* **40**, 1555-1565, doi:10.1183/09031936.00046612 (2012).

70 Kumar, D. *et al.* Chronic sodium nitrite therapy augments ischemia-induced angiogenesis and arteriogenesis. *Proc Natl Acad Sci U S A* **105**, 7540-7545, doi:Doi 10.1073/Pnas.0711480105 (2008).

71 Zhang, J., Chen, Z. Q., Cobb, F. R. & Stamler, J. S. Role of mitochondrial aldehyde dehydrogenase in nitroglycerin-induced vasodilation of coronary and systemic vessels - An intact canine model. *Circulation* **110**, 750-755, doi:Doi 10.1161/01.Cir.0000138105.17864.6b (2004).

72 Prager-Khoutorsky, M. *et al.* Fibroblast polarization is a matrix-rigidity-dependent process controlled by focal adhesion mechanosensing. *Nature Cell Biology* **13**, 1457-1465, doi:10.1038/ncb2370 (2011).

73 Bir, S. C. *et al.* Nitrite anion therapy protects against chronic ischemic tissue injury in db/db diabetic mice in a NO/VEGF-dependent manner. *Diabetes* **63**, 270-281, doi:10.2337/db13-0890 (2014).

74 Pattillo, C. B., Bir, S., Rajaram, V. & Kevil, C. G. Inorganic nitrite and chronic tissue ischaemia: a novel therapeutic modality for peripheral vascular diseases. *Cardiovasc Res* **89**, 533-541, doi:10.1093/cvr/cvq297 (2011).

75 Amin, A. *et al.* Sodium nitrite therapy rescues ischemia-induced neovascularization and blood flow recovery in hypertension. *Pflugers Archiv : European Journal of Physiology* **464**, 583-592, doi:10.1007/s00424-012-1167-y (2012).

76 Kevil, C. G., Kolluru, G. K., Pattillo, C. B. & Giordano, T. Inorganic nitrite therapy: historical perspective and future directions. *Free Radical Biology & Medicine* **51**, 576-593, doi:10.1016/j.freeradbiomed.2011.04.042 (2011).

77 Moore, K. A. *et al.* Control of basement membrane remodeling and epithelial branching morphogenesis in embryonic lung by Rho and cytoskeletal tension. *Developmental Dynamics : an official publication of the American Association of Anatomists* **232**, 268-281, doi:10.1002/dvdy.20237 (2005).

78 Davis, G. E. & Camarillo, C. W. Regulation of endothelial cell morphogenesis by integrins, mechanical forces, and matrix guidance pathways. *Experimental Cell Research* **216**, 113-123, doi:10.1006/excr.1995.1015 (1995).

79 Ingber, D. E. & Folkman, J. How does extracellular matrix control capillary morphogenesis? *Cell* **58**, 803-805 (1989).

80 Merks, R. M., Brodsky, S. V., Goligorksy, M. S., Newman, S. A. & Glazier, J. A. Cell elongation is key to in silico replication of in vitro vasculogenesis and subsequent remodeling. *Developmental Biology* **289**, 44-54, doi:10.1016/j.ydbio.2005.10.003 (2006).

81 Ghosh, K. *et al.* Tumor-derived endothelial cells exhibit aberrant Rho-mediated mechanosensing and abnormal angiogenesis in vitro. *Proc Natl Acad Sci U S A* **105**, 11305-11310, doi:10.1073/pnas.0800835105 (2008).

82 Isenberg, J. S. *et al.* Thrombospondin-1 inhibits endothelial cell responses to nitric oxide in a cGMP-dependent manner. *Proc Natl Acad Sci U S A* **102**, 13141-13146, doi:10.1073/pnas.0502977102 (2005).

83 Fukumura, D. *et al.* Predominant role of endothelial nitric oxide synthase in vascular endothelial growth factor-induced angiogenesis and vascular permeability. *Proc Natl Acad Sci U S A* **98**, 2604-2609, doi:10.1073/pnas.041359198 (2001).

84 Moghimi, S. M., Hunter, A. C. & Murray, J. C. Long-circulating and target-specific nanoparticles: theory to practice. *Pharmacol Rev* **53**, 283-318 (2001).

85 Gref, R. *et al.* Biodegradable Long-Circulating Polymeric Nanospheres. *Science* **263**, 1600-1603, doi:Doi 10.1126/Science.8128245 (1994).

86 Chapman, A. P. *et al.* Therapeutic antibody fragments with prolonged in vivo half-lives. *Nature Biotechnology* **17**, 780-783, doi:10.1038/11717 (1999).

87 Maruyama, K., Takahashi, N., Tagawa, T., Nagaike, K. & Iwatsuru, M. Immunoliposomes bearing polyethyleneglycol-coupled Fab' fragment show prolonged circulation time and high extravasation into targeted solid tumors in vivo. *FEBS letters* **413**, 177-180 (1997).

88 Ahmad, Z. A. *et al.* scFv Antibody: Principles and Clinical Application. *Clin Dev Immunol*, doi:Artn 980250
10.1155/2012/980250 (2012).

89 Nelson, A. L. Antibody fragments Hope and hype. *Mabs-Austin* **2**, 77-83 (2010).

90 Luo, G. X. *et al.* Humanization of an anti-ICAM-1 antibody with over 50-fold affinity and functional improvement. *Journal of Immunological Methods* **275**, 31-40 (2003).

91 Ardekani, S. *et al.* Nanoliposomal Nitroglycerin Exerts Potent Anti-Inflammatory Effects. *Scientific Reports* **5**, 16258, doi:10.1038/srep16258 (2015).

92 Kimura, S. *et al.* Nanoparticle-mediated delivery of nuclear factor kappaB decoy into lungs ameliorates monocrotaline-induced pulmonary arterial hypertension. *Hypertension* **53**, 877-883, doi:10.1161/HYPERTENSIONAHA.108.121418 (2009).

93 Chen, J. X., Zeng, H., Reese, J., Aschner, J. L. & Meyrick, B. Overexpression of angiopoietin-2 impairs myocardial angiogenesis and exacerbates cardiac fibrosis in the diabetic db/db mouse model. *American journal of physiology. Heart and Circulatory Physiology* **302**, H1003-1012, doi:10.1152/ajpheart.00866.2011 (2012).

94 Kanapathipillai, M. *et al.* Inhibition of Mammary Tumor Growth Using Lysyl Oxidase-Targeting Nanoparticles to Modify Extracellular Matrix. *Nano Lett* **12**, 3213-3217, doi:Doi 10.1021/Nl301206p (2012).

95 Panes, J. *et al.* Regional differences in constitutive and induced ICAM-1 expression in vivo. *Am J Physiol-Heart C* **269**, H1955-H1964 (1995).

96 Burridge, K. & Wennerberg, K. Rho and Rac take center stage. *Cell* **116**, 167-179 (2004).

97 Muro, S., Gajewski, C., Koval, M. & Muzykantov, V. R. ICAM-1 recycling in endothelial cells: a novel pathway for sustained intracellular delivery and prolonged effects of drugs. *Blood* **105**, 650-658, doi:10.1182/blood-2004-05-1714 (2005).

98 Fang, R. H. *et al.* Lipid-insertion enables targeting functionalization of erythrocyte membrane-cloaked nanoparticles. *Nanoscale* **5**, 8884-8888, doi:10.1039/c3nr03064d (2013).

99 Hu, C. M. *et al.* Erythrocyte membrane-camouflaged polymeric nanoparticles as a biomimetic delivery platform. *Proc Natl Acad Sci U S A* **108**, 10980-10985, doi:10.1073/pnas.1106634108 (2011).